A Mechanistic and Computational Analysis of Pheromone Receptor Polarity Establishment in Yeast

BY

AMBER ISMAEL
B.S., University of California, Irvine, 2004

THESIS

Submitted as partial fulfillment of the requirements
for the degree of Doctor of Philosophy in
Biological Sciences
in the Graduate College of the
University of Illinois at Chicago, 2014

Chicago, Illinois

Defense Committee:

David Stone, Advisor, Biological Sciences
Ronald Dubreuil, Chair, Biological Sciences
Jie Liang, Bioengineering
Peter Okkema, Biological Sciences
Robert Arkowitz, Université de Nice-Sophia Antipolis

This thesis is dedicated to my family and friends

who have loved and supported me and

made this possible.

“Put those hours in and look at what you get.

Nothing that you can hold, but everything that it is.

Ten thousand.”

~ Macklemore & Ryan Lewis

ACKNOWLEDGEMENTS

I would like to thank the following for their support, guidance, and contributions that have made this body of work possible:

Dr. David Stone at the University of Illinois at Chicago and current and former Stone Lab members: Dr. Reagan DeFlorio, Dmitry Suchkov, Madhushalini Sukumar, Nicholas Waszczak, Dr. Metodi Metodiev, Dr. Edward Draper III, Dr. E Li, Dr. Eli Bar, and Dr. Mary Cismowski

Dr. Robert Arkowitz at the Université de Nice-Sophia Antipolis and the Arkowitz Lab

Dr. Jie Liang at the University of Illinois at Chicago and the following Liang Lab members: Wei Tian and Dr. Youfang Cao

Dr. Metodi Metodiev at the University of Essex

My committee members: Dr. Robert Arkowitz, Dr. Ronald Dubreuil, Dr. Jie Liang, Dr. Peter Okkema, and Dr. Nava Segev

I would like to thank my family and friends who have supported me over the years and have made all of this possible:

Eveline and George Curtis, Dr. Reagan DeFlorio, Candance Denegal, Julia Eggers, Chyna Sky Gonzalez, Ben Ismael, Justin Ismael, Dr. Hsiao-Lei Lai, Madhushalini Sukumar, Xaviera Vandermay, Nicholas Waszczak, Dr. Zi Yang.

TABLE OF CONTENTS

TABLE OF CONTENTS (continued)

LIST OF TABLES

LIST OF FIGURES

LIST OF ABBREVIATIONS

α-factor	*MAT*α pheromone peptide
BiFC	Bimolecular Fluorescence Complementation
cAMP	cyclic Adenosine MonoPhosphate
cAR	cAMP Receptors
CKI	Casein Kinase type I
Gα	α subunit of the G protein heterotrimer, encoded by *GPA1*
$G\alpha^{DSD}$	α subunit of the G protein heterotrimer that cannot interact with Fus3, encoded by $gpa1^{K21E\ R22E}$
Gβ	β subunit of the G protein heterotrimer, encoded by *STE4*
$G\beta^{P-}$	β subunit of the G protein heterotrimer that cannot be phosphorylated, encoded by $ste4^{T320A\ S335A}$
Gγ	γ subunit of the G protein heterotrimer, encoded by *STE18*
GEF	Guanine nucleotide Exchange Factor
GPCR	G Protein-Coupled Receptor
LatA	Latrunculin A
LEGI	Local Excitation, Global Inhibition
MAPK	Mitogen-Activated Protein Kinase
MEK	MAP Kinase Kinase
MEKK	MAP Kinase Kinase Kinase
PAK	p21-Activated protein Kinase
PDE	Partial Differential Equation
PI	Polarity Index

LIST OF ABBREVIATIONS (continued)

PI3K	Phosphatidyl-Inositol 3-Kinase
PIP_2	Phosphatidyl-Inositol (4,5)-bisPhosphate
PIP_3	Phosphatidyl-Inositol (3,4,5)-triPhosphate
PH	Pleckstrin-Homology
PLA2A	Phospholipase A2
PM	Plasma Membrane
PMN	PolyMorphonuclear Neutrophils
RPA	Receptor Phosphorylation Assay
RT	Room Temperature
SEM	Standard Error of Mean
sGC	soluble Guanylyl Cyclase
Ste2	*MAT***a** pheromone receptor, encoded by *STE2*
VF1	Venus Fragment 1
VF2	Venus Fragment 2
WT	Wild-type
YPD	Yeast extract Peptone Dextrose

SUMMARY

Chemotaxis and chemotropism are related phenomena that play fundamental roles in many biological processes, during which, cells must interpret extracellular signaling gradients and orient in response. How cells are able to convert an extracellular gradient into a steeper intracellular signaling gradient and orient correctly remains unclear. During the chemotropic mating response of yeast, cells must interpret an extracellular pheromone gradient and orient their growth toward a potential mating partner. Pheromone binds a G protein-coupled receptor (GPCR) and induces the dissociation of Gα and Gβγ. In response to pheromone, Gβ is rapidly phosphorylated and signals through a MAP kinase cascade to the nucleus. Free Gβγ also recruits polarity proteins to the cell cortex where actin is nucleated and growth cargo is delivered for polarized growth of the mating projection. How a cell is able to polarize its growth is well understood, but how does the cell choose the direction of growth in a shallow gradient of pheromone?

In a previous paper, we proposed that activated receptor activates or recruits a downstream component that protects the receptor from phosphorylation and internalization on the up-gradient side of the cell, marking the growth site. Here we characterize the interaction between Gβ and Yck1, one of the sister yeast casein kinases required for phosphorylation and internalization of the pheromone receptor, but a mutant form of Gβ that cannot be phosphorylated has a diminished interaction with Yck1. Gβ phosphorylation and/or its interaction with Yck1 inhibits receptor phosphorylation, promotes its polarization, and is important for movement of the unphosphorylated patch to the chemotropic growth site. Cells expressing the

unphosphorylatable form of Gβ are defective in polarization of the receptor in both mating mixtures and in isotropic conditions. In response to pheromone, we were able to detect a region of receptor that persisted on the membrane longer compared to the rest of the cell. Using mathematical modeling, we showed that downstream regulation of receptor internalization by the interaction between Gβ and Yck is sufficient for a computational yeast cell to polarize the receptor correctly in a pheromone gradient. Together, these results support a novel mechanism for directional sensing.

1. Introduction

1.1 Chemotaxis versus chemotropism

Chemotaxis is directed cell movement in response to an external gradient. While chemotaxing, a cell must interpret an extracellular chemical gradient and orient its movement in response. A chemotactic cell will migrate either toward a source of chemoattractant or away from a source of chemorepellant. Chemotaxis plays an important role in a number of biological processes including embryogenesis, organogenesis, and the immune response (Jin et al., 2008, Laird et al., 2008). Collective cell migration leads to the organization of tissues and organs during the processes of embryogenesis and organogenesis, and leukocytes migrate through tissue during the immune response (Friedl and Gilmour, 2009, Friedl and Weigelin, 2008). In addition to the roles that chemotactic cells play in normal biological processes, they also play roles in many pathological conditions, including cancer metastasis and inflammatory diseases. Chemotactic cancer cells leads to cancer metastasis and excessive migration of leukocytes to sites of infection can lead to inflammatory diseases (Jin et al., 2008, Kedrin et al., 2007, Koizumi et al., 2007, Muller et al., 2001, Murphy, 2001).

The related phenomenon of chemotropism is directed cell growth in response to an external gradient. Like chemotactic cells, chemotropic cells must interpret an extracellular gradient, but instead direct their growth toward a chemoattractant or away from a chemorepellant. During the process of axon pathfinding, the growth cone must interpret extracellular gradients and direct growth over a large distance, and during the formation of new blood vessels in angiogenesis, tumor cells secrete chemokines

promoting growth leading to metastasis (Berzat and Hall, 2010, Singh, 2007). The best characterized chemotropic response is the yeast mating response in *S. cerevisiae* in which a cell orients itself in a pheromone gradient and polarizes its growth toward a potential mating partner to form a diploid cell (Arkowitz, 2009).

1.2 Models of directional sensing

Chemotactic and chemotropic cells must solve similar problems. In both cases, the cells must interpret external gradients and orient their axis of polarity accordingly. They must convert wide ranges of extracellular gradients into a steeper intracellular signaling gradient. Once the polarity site has been determined, the cells must then recruit the polarization machinery to the cell cortex to migrate or direct their growth in response to the external gradient. The study of how cells sense direction has focused on the amoebae *Dictyostelium discoideum*, mammalian neutrophils, and yeast. These cells are able to interpret signaling gradients that vary as little as 0.5-10% over the width of the cell and polarize correctly in response (Lohof et al., 1992, Mato et al., 1975, Moore et al., 2008, Segall, 1993, Zigmond, 1977). They are able to interpret the slight difference in receptor activation on the cell surface and convert it into a steep internal signaling gradient that allows the cell to grow or move in the correct direction. However, the molecular mechanisms that enable these cells to interpret shallow extracellular gradients are not fully understood.

1.2.1 Chemotactic model organisms: amoebae *Dictyostelium discoideum* and neutrophils

Attempts to understand how chemotactic cells are able to interpret shallow extracellular gradients have focused on two model systems: mammalian neutrophils

and the amoebae *D. discoideum*. These chemotactic responses are mediated by seven transmembrane G protein coupled receptors (GPCRs) distributed uniformly on the plasma membrane (PM) (Weiner et al., 2002, Xiao et al., 1997). Unlike chemotropic yeast cells, in response to an extracellular gradient, chemotactic receptors do not polarize in response to a chemical gradient, and this is thought to allow adaptation to rapidly changing directional signals (Xiao et al., 1997).

In response to starvation, *D. discoideum* amoebae signal to each other by secreting cAMP, which they migrate toward to aggregate and form a multicellular structure called a fruiting body (Jin, 2011). cAMP initiates migration through binding to the GPCR, cAR. Exposure to a gradient of cAMP is thought to create a similar gradient of activated receptor and G protein (Janetopoulos et al., 2001, Sasaki and Firtel, 2006, Ueda et al., 2001, Xu et al., 2005). Intracellular amplification of the extracellular gradient can be detected by the asymmetric localization of proteins that regulate the asymmetric distribution of PtdIns(4,5)P_2 (PIP_2) and PtdIns(3,4,5)P_3 (PIP_3) (Comer and Parent, 2002, Funamoto et al., 2002, Jin, 2011). The activated receptor releases Gβγ which activates Ras allowing it to bind to and stimulate the activation of PI3K (Jin, 2011). Activated PI3K phosphorylates PIP_2 to produce PIP_3 which results in polarization of PIP_3 (Funamoto et al., 2002, Parent et al., 1998). PIP_3 recruits pleckstrin-homology (PH) domain-containing proteins from the cytosol, and these proteins become polarized at the leading edge of the cell through their interaction with PIP_3 (Servant et al., 2000). These recruitment and polarization events are dependent on Gβ (Parent et al., 1998, Van Haastert and Devreotes, 2004). The polarization of PIP_3 and PH-domain containing proteins on the up-gradient side of the cell is

independent of actin (Parent et al., 1998, Sasaki et al., 2004, Sasaki and Firtel, 2005, Van Haastert and Devreotes, 2004). In contrast, PTEN, a PIP_3 phosphatase that converts PIP_3 to PIP_2, is localized to the rear of the cell through its interaction with PIP_2, resulting in an accumulation of PIP_2 at the rear (Funamoto et al., 2002, Van Haastert and Devreotes, 2004). This leads to an inverse gradient of PIP_3 and PIP_2, where PIP_3 is localized to the front of the cell and PIP_2 is localized at the rear of the cell. It is thought that PIP_3 localized at the leading edge of the cell recruits PH domain containing proteins to activate Ras and promote actin polymerization through interaction with the Arp2/3 regulating proteins, WASP and SCAR (Franca-Koh et al., 2006). The mechanisms involved in linking the receptor to actin are still unknown. However, when PIP_3 asymmetry is perturbed in *pten* mutants, this leads to high levels of actin and defects in chemotaxis (Iijima and Devreotes, 2002).

Further study of directional sensing in *D. discoideum* has led to the discovery of redundant pathways. It has been shown that cells mutated for all PI3Ks, and thus unable to form PIP_3, are still able to chemotax relatively normally (Hoeller and Kay, 2007). This led to the discovery of another pathway involving phospholipase A2 (PLA2A) (Chen et al., 2007). When the PIP_3 pathway and the PLA2A pathway are inhibited, cells exhibit an extreme defect in directional sensing (Chen et al., 2007). Another chemical found to regulate chemotaxis was soluble guanylyl cyclase (sGC). In response to cAMP stimulation, sGC produces cGMP, which regulates pseudopod suppression through its interactions with myosin regulatory proteins and also promotes pseudopod formation at the front (Wang et al., 2011). Ras activation has also been found to activate TORC2 and PDKA and PDKB through PI3Ks, which in turn activates

PKBA and PKBR1, found at the leading edge of the cell (Kamimura and Devreotes, 2010, Kamimura et al., 2008). A recent study has identified a PIP5 kinase responsible for the production of PIP_2 is essential for chemotaxis (Fets et al., 2014). The study of *D. discoideum* chemotaxis and its different pathways has provided much insight into the mechanisms of directional sensing.

Neutrophils use a GPCR, pertussis-toxin-sensitive formyl peptide receptor, to sense chemicals excreted by bacteria and migrate toward them (Cicchetti et al., 2002). Similar to *D. discoideum*, polarization of PIP_3 and PH domain containing proteins is independent of actin (Servant et al., 2000). Polarization of PIP_3 is coupled to a negative regulator of PIP_3, a phosphatase, SHIP1 (Nishio et al., 2007). GPCR stimulation releases free Gβγ, which activates PI3K to stimulate localization of PIP_3. PIP_3 recruits DOCK2 to the PM to initiate actin polymerization by activating Rac and Cdc42 (Nishikimi et al., 2009, Wang, 2009). Continued DOCK2 localization is dependent on a localized generation of phosphatidic acid through phospholipase D activation (Berzat and Hall, 2010). At the back of the cell, actomyosin contraction is controlled by the Rho-ROCK pathway, which is activated by $G_{12/13}$ (Wong, 2012, Xu et al., 2003).

It has been shown in neutrophils and *D. discoideum* that in response to an extracellular signal, their GPCRs are phosphorylated and internalized. In *D. discoideum* responding to cAMP, a subset of cAR1 GPCRs is rapidly internalized and this is dependent on phosphorylation of the receptor (Serge et al., 2011, Van Haastert, 1987). Mutation of the cAR1 receptor that prevented its phosphorylation, conferred defects in chemotaxis, pseudopod formation, and the localization of actin polymerization (Brzostowski et al., 2013). These observations in *D. discoideum* are similar to

observations in neutrophils mutated for the G protein-coupled receptor kinases (GRKs) responsible for GPCR agonist-induced phosphorylation and internalization. When polymorphonuclear neutrophils (PMNs) are exposed to the chemoattractant, leukotriene B4, the corresponding GPCR, BLT1, is phosphorylated and internalized in response (Kavelaars et al., 2003). PMNs mutated for GRK6 show aberrant actin dynamics and migration (Kavelaars et al., 2003). Together, these results suggest a role for GPCR phosphorylation and internalization in chemotaxis and the regulation of actin dynamics.

1.2.2 Chemotropic model organism: mating response of *S. cerevisiae*

The haploid yeast, *Saccharomyces cerevisiae*, exists as two distinct mating types, *MAT***a** and *MAT*α. Each mating type secretes a peptide pheromone that is bound by cell surface GPCRs on cells of the opposite mating type. *MAT***a** cells secrete a-factor, and *MAT*α cells secrete α-factor. Binding of pheromone to the receptor initiates a signaling cascade that results in cell cycle arrest, expression of mating specific genes, polarized growth, cell fusion, nuclear fusion, and ultimately, formation of a *MAT***a**/*MAT*α diploid cell. During the mating response, cells must interpret a gradient of pheromone and polarize their growth toward a potential mating partner. In mating mixtures consisting of both *MAT***a** and *MAT*α cells, haploid cells will preferentially mate with cells producing the highest concentration of pheromone (Jackson and Hartwell, 1990). To study the ability of haploid cells to interpret and respond to a range of pheromone concentrations and slopes, cells were exposed to varying gradients and concentrations of pheromone. It was calculated that cells can accurately respond in over a 1000-fold range of pheromone concentrations and in gradients as shallow as a 0.5% difference over the length of the cell (Moore et al., 2008, Segall, 1993). How are

cells able to convert a shallow extracellular gradient of pheromone into a steep intracellular signaling gradient and orient their growth toward the source of pheromone?

1.2.2.1 Receptor signaling to the nucleus

The mating response of yeast is mediated by two GPCRs that are uniformly distributed on the cell membrane during vegetative growth. Binding of pheromone to the receptor induces a conformational change that stimulates the activation of Gα by inducing the exchange of GDP for GTP (Fig. 1) (Bardwell, 2005, Bukusoglu and Jenness, 1996). Gβγ then dissociates from Gα-GTP and is rapidly phosphorylated in response to pheromone (Cole and Reed, 1991). Free Gβγ signals to the nucleus through its interaction with two effectors, Ste20, a p21-activated protein kinase (PAK) homolog, and Ste5, a mitogen-activated protein kinase (MAPK) scaffold protein. At the plasma membrane (PM), Gβγ recruits Ste20 and the Ste5/Ste11 complex where Ste20 phosphorylates Ste11, thereby initiating signaling to the nucleus through a MAPK cascade. The MAPK module consists of Ste11 (the MEKK), Ste7 (the MEK), and Fus3 (the MAPK). The pheromone-induced cascade of phosphorylation events results in the activation of Fus3. Most of the activated Fus3 then translocates to the nucleus where it promotes transcription of mating specific genes through Ste12 and cell cycle arrest by phosphorylation of Far1 (Bardwell, 2005).

Figure 1. Molecular mechanism of the yeast pheromone response.
(A) Pheromone binds a G protein-coupled receptor (GPCR) inducing Gα to exchange GDP for GTP and releasing free Gβγ. Gβ is rapidly phosphorylated in response to pheromone. Gβ signals to the nucleus through a MAPK cascade, resulting in the activation of the MAPK, Fus3. Fus3 translocates to the nucleus where it induces G1 arrest through Far1 and transcription of mating specific genes. Far1 bound to Cdc24 exits the nucleus and is recruited to the plasma membrane (PM) by free Gβγ. At the PM, Cdc24 activates Cdc42 and polarity proteins are recruited to the membrane where actin is nucleated. Myosin motor proteins deliver growth cargo to the PM along the actin cables resulting in formation of the mating projection. (B) Table listing components of the yeast pheromone response.

A

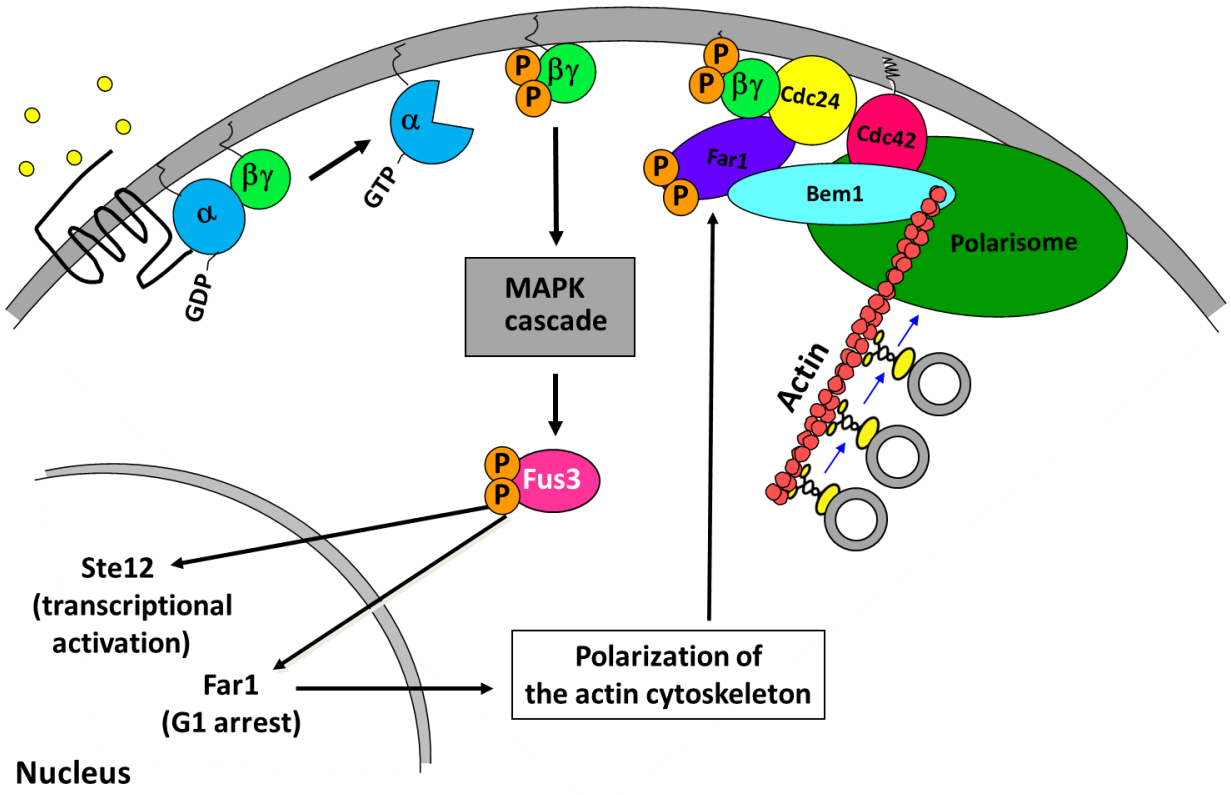

B

Gene	Protein	Function
STE2	Ste2	7 transmembrane GPCR that binds to α-factor
GPA1	Gα	Gα subunit of the G protein
STE4	Gβ	Gβ subunit of the G protein
STE18	Gγ	Gγ subunit of the G protein
FUS3	Fus3	MAPK
STE12	Ste12	substrate for MAPK, transcriptional regulator
FAR1	Far1	substrate for MAPK, progression of cell-cycle inhibitor
CDC24	Cdc24	Cdc42 GEF
CDC42	Cdc42	small Rho-like GTPase
BEM1	Bem1	Protein involved in cell polarity

1.2.2.2 Chemotropic growth

Cortical markers initiate actin polymerization at a site on the PM for polarized growth, where myosin motors deliver cargo along the polymerized actin filaments (Pruyne and Bretscher, 2000b). In vegetative cells, Bud1 acts as a cortical marker that recruits Cdc24 to the PM to activate Cdc42 for polarized growth, thereby initiating bud emergence (Park et al., 1997). Cdc24 is bound to Far1 in the nucleus. Upon entry into the cell cycle, Far1 is degraded, allowing Cdc24 to be recruited to the PM through its interaction with Bud1 (Henchoz et al., 1997, Park et al., 1997). However, during the mating response, Far1 is phosphorylated in the nucleus and stabilized by Fus3 (Gartner et al., 1998). Far1 induces cell cycle arrest and is exported out of the nucleus bound to Cdc24, the guanine nucleotide exchange factor (GEF) for Cdc42 (Chang and Herskowitz, 1990). Free Gβγ recruits the Far1-Cdc24 complex to the PM, through its interaction with Far1, where it activates Cdc42 (Butty et al., 1998). The chemotropic complex, Gβγ-Far1-Cdc24, marks the polarity site for formation of the mating projection by locally amplifying active, GTP-bound Cdc42 (Nern and Arkowitz, 1999). Active Cdc42 then recruits polarity proteins to the cell cortex for actin polymerization, and myosin motor proteins deliver growth cargo along the actin filaments to the site of growth, resulting in formation of the mating projection toward the source of pheromone (Pruyne and Bretscher, 2000a, Pruyne and Bretscher, 2000b). When a cell is exposed to a uniform concentration of pheromone and no gradient can be detected, the cell is still able to polarize its growth using Bud1 as a cortical marker (Dorer et al., 1995, Nern and Arkowitz, 1999). Therefore, the cell will form a mating projection at the incipient bud site, which is termed default shmooing.

1.2.2.3. Receptor internalization

Ste2 is the GPCR that binds α-factor. Binding of pheromone to the receptor induces a conformational change in the receptor, exposing the C-terminus to phosphorylation (Reneke et al., 1988). Receptor phosphorylation requires the activity of two sister type I casein kinases (CKI), Yck1 and Yck2 (Reneke et al., 1988). Upon phosphorylation, the receptor is ubiquitinated, internalized, and degraded in the vacuole (Hicke and Riezman, 1996, Hicke et al., 1998). Pheromone induces a 5- to 10-fold increase in receptor internalization causing it to disappear rapidly from the PM (Jenness and Spatrick, 1986). The pheromone receptor also oligomerizes, but the fraction of receptors in oligomers, as opposed to monomers, is not affected by pheromone binding (Overton and Blumer, 2000, Yesilaltay and Jenness, 2000). The endocytosis defects of pheromone receptors mutated for agonist binding or contain a C-terminal truncation are rescued by co-expression of wild-type (WT) receptors suggesting that inactive receptors are internalized with activated receptors (Yesilaltay and Jenness, 2000).

Receptor internalization has long been thought of as a means of down-regulating a signal (Dohlman et al., 1991), and more recently, receptor internalization has been proposed to also play a role in polarization. Cells defective in endocytosis are also defective in chemotropism (Suchkov et al., 2010, Vallier, 2002). Polarization of yeast proteins can be maintained by endocytosis coupled with slow diffusion (Valdez-Taubas and Pelham, 2003). Computational modeling of the yeast cell suggests that endocytosis coupled with exocytosis can stabilize polarity (Marco et al., 2007, Slaughter et al., 2009). Yeast endocytic mutants were also found to be defective in stability of polarization (Jose et al., 2013). When the pheromone receptor C-terminus is deleted

and the receptor cannot be internalized, the cells are unable to interpret pheromone gradients and orient mating projections up the gradient (Vallier, 2002). Cells defective in pheromone receptor endocytosis are defective in directional sensing and are unable to polarize the receptor in response to pheromone (Suchkov et al., 2010). Together, these observations suggest a role for receptor internalization in polarization and directional sensing.

1.2.2.4 Receptor polarization

The pheromone receptor is distributed uniformly on the PM of vegetative cells and is constitutively internalized at a low level (Jackson et al., 1991, Schandel and Jenness, 1994). Unlike in chemotactic cells, the receptor polarizes in response to an external gradient. Upon treatment with a uniform concentration of pheromone, the receptor is no longer detectable on the PM, but later reappears as a polarized crescent, and becomes more polarized as the mating projection elongates (Ayscough and Drubin, 1998, Jackson et al., 1991). In mating mixtures, the receptor crescent forms on the side of the cell closest to the potential mating partner prior to morphogenesis (Suchkov et al., 2010).

When actin-dependent directed secretion is disrupted by treating cells with LatA after pheromone treatment and global receptor internalization, initiation and maintenance of receptor polarity is impaired, but cells were still able to polarize the receptor (Ayscough and Drubin, 1998). These results suggest F-actin plays a role in the maintenance of receptor polarization, but it is not essential for the establishment of receptor polarity. Further study of receptor polarization in response to pheromone showed that actin-dependent directed secretion is not required for receptor polarization,

but receptor internalization is (Suchkov et al., 2010). Actin appears to be required to maintain receptor polarity, but not to establish receptor polarity when cells are treated with an inhibitor of actin cables (LatA) after global receptor internalization (Ayscough and Drubin, 1998).

1.3 Signal amplification mechanisms

Both chemotactic and chemotropic systems must convert a shallow extracellular gradient into a steep intracellular signaling gradient. In chemotactic cells, the receptor and G protein remain uniform on the membrane (Janetopoulos and Firtel, 2008). Activated receptor and G protein show a similar steepness as the extracellular gradient, while the internal signaling gradient becomes highly polarized (Janetopoulos et al., 2004). There appears to be amplification of the signaling gradient downstream of the G protein. During the yeast mating response, activated receptor and G protein do not show a similar steepness as the extracellular pheromone gradient, but become highly polarized. The mechanism of how cells are able to convert shallow extracellular chemical gradients into steep intracellular signaling gradients is poorly understood.

Turing first used reaction-diffusion systems to explain how spatial patterns could arise (Turing, 1990). Later, it was shown that the idea of local excitation and global inhibition (LEGI) could replicate patterns seen in biology (Gierer and Meinhardt, 1972). The LEGI mechanism couples a localized rapid excitation and a slower global inhibition. The rapid excitation, driven by receptor occupancy, at the front of the cell is able to overcome the global inhibition and over time reaches a steady-state where the cell is polarized in response to the gradient (Janetopoulos and Firtel, 2008). However, LEGI alone cannot fully explain some aspects of directional sensing during chemotaxis and

chemotropism. Variations of the LEGI model have been proposed to answer the outstanding questions. One problem with the LEGI mechanism is that once a steady-state is reached, it becomes stable. Chemotactic and chemotropic cells need to be able to respond to changes in the extracellular environment and adjust their direction of growth or movement in response. With the addition of a second, slower diffusing antagonist to the LEGI mechanism, the cells are able to track changing extracellular gradients (Meinhardt, 1999). Another variation of LEGI mechanism addresses the steepness of the intracellular signaling gradient. The two-LEGI mechanism in which two parallel, complementary LEGI mechanisms are able to amplify the shallow external gradient into a steeper internal signaling gradient (Ma et al., 2004). The balanced inactivation mechanism is similar to LEGI but with the addition of a mutually antagonistic inhibitor that is rapidly diffusing (Levine et al., 2006). The addition of the rapid diffusion inhibitor is able to account for both the steepness of the intracellular gradient and for rapid generation of asymmetry.

Evidence suggests that the LEGI mechanism is not enough to convert a shallow extracellular gradient into a steep intracellular gradient alone but requires an additional amplification step (Iglesias, 2012). In addition to LEGI, positive feedback loops can amplify a shallow intracellular gradient and convert a slight asymmetry developed by LEGI into a steeper asymmetry. Positive feedback loops can generate a greater asymmetry by autocatalysis, degradation inhibition, or delivery of a substrate (Gamba et al., 2005, Meier-Schellersheim et al., 2006, Meinhardt, 1999, Postma and Van Haastert, 2001, Skupsky et al., 2005).

1.3.1 Computational studies of polarization

Computational studies of gradient-induced cell polarization allow for insight into the spatial and temporal dynamics that occur within the cell. They have been used to highlight the important factors involved in gradient sensing, the subsequent signal amplification, and morphology. Early models proposed that pattern formation could occur using a simple mechanism consisting of a slowly diffusing activator and a fast diffusing inhibitor (Turing, 1990). Computational models focusing on pattern formation in biological systems showed that polarization could arise from a localized positive feedback loop and long range inhibition (Gierer and Meinhardt, 1972, Meinhardt, 1982, Meinhardt and Gierer, 1974). These ideas were used to develop the LEGI mechanism (described above) often used to explain the phenomenon of directional sensing. Variations of the LEGI mechanism have been used to explain the phenomenon of chemotaxis and have employed more sophisticated computational models that have identified proteins involved in signal transduction (Krishnan and Iglesias, 2004).

Computational modeling of cell polarization in yeast has primarily focused on the polarization of Cdc42 during bud site selection or symmetry breaking (Mogilner et al., 2012). The first computational model of the chemotropic pheromone induced mating response of yeast also focused on the localization of Cdc42 in a computational cell exposed to a gradient of pheromone (Yi et al., 2007). One of the main objectives of this model was to identify the interactions involved in the amplification process of gradient sensing (converting a shallow extracellular pheromone gradient into a steep intracellular signaling gradient). To do this, the authors developed a network that included local activation by both cooperative binding and positive feedback. In the model, pheromone

binds the receptor causing the G protein to dissociate into active Gα and free Gβγ. Free Gβγ recruits Cdc24 to the membrane where it can activate Cdc42. Activated Cdc42 is then able to bind to Bem1, recruiting it to the membrane, which can also bind to recruit more Cdc24 to the membrane to activate Cdc42. The main amplification step in this model is the positive feedback loop that involves Bem1 recruiting Cdc24 to the membrane to activate it, resulting in activation of Cdc42 which is then able to bind and recruit more Bem1 to the membrane. The network was able to simulate the biological process of gradient-induced cell polarization during mating and the output highlighted parameters that were important for the signal amplification process (Yi et al., 2007). However, to respond to broad ranges of pheromone concentrations and gradients, the model required a very high cooperativity value (Moore et al., 2008, Yi et al., 2007).

More recently, the same group computationally modeled pheromone-induced mating projection morphology (Chou et al., 2012). It has been observed that the shape of the mating projection is dependent on the concentration of pheromone. When the pheromone concentration is low, the mating projections are broader and longer compared to the thinner, shorter mating projections formed in high pheromone conditions. The authors hypothesized that the shape of the mating projection is due to the spatial dynamics of membrane trafficking and the net transport. Membrane trafficking (endocytosis and exocytosis) was simplified into two signaling systems controlled by Cdc42 and the heterotrimeric G protein. In high pheromone concentrations, the rate of endocytosis was increased, causing the region of the PM with more net exocytosis to be smaller resulting in thinner mating projections. Their cell

simulations were able to mimic the different mating projection morphologies observed at different pheromone concentrations (Chou et al., 2012).

Computational modeling of complex and dynamic systems can be a useful tool to study biological processes. Networks can be designed with the current experimental data, tested for their ability to replicate experimental observations, and they can generate experimentally testable predictions.

1.4 Objective of this study

How yeast cells polarize their growth in response to pheromone has been extensively studied and is well understood. Prior to actin polymerization and polarized growth, a cell must interpret a shallow gradient of pheromone and convert the shallow extracellular gradient into a steep intracellular signaling gradient. How a cell chooses which direction to polarize its growth in a gradient of pheromone remains elusive.

In response to pheromone, the most upstream component of the pheromone signaling pathway, the receptor, polarizes at the incipient shmoo site (Ayscough and Drubin, 1998, Moore et al., 2008). Receptor internalization is required for proper chemotropic growth and polarization of the receptor and G protein (Suchkov et al., 2010). Receptor and Gβ polarization at the chemotropic growth site can be detected prior to morphogenesis suggesting that it is upstream of actin-dependent directed secretion (DeFlorio et al., 2013), and actin-dependent directed secretion is not required for receptor polarization (Ayscough and Drubin, 1998, Suchkov et al., 2010). In response to pheromone, the receptor appears to be asymmetrically phosphorylated (Ballon et al., 2006, Suchkov et al., 2010). Since receptor phosphorylation induces receptor internalization, this suggests that the receptor is asymmetrically internalized.

In a genetic screen for proteins that interact with Gβγ, Yck1, one of two sister yeast casein kinases required for receptor phosphorylation, was isolated. Gβ is rapidly phosphorylated at multiple residues in response to pheromone and also contains a casein kinase type 1 (CKI) phosphorylation motif (Cole and Reed, 1991). Full phosphorylation of Gβ requires Fus3 MAPK activity and also requires Fus3 interaction with Gα (Li et al., 1998, Metodiev et al., 2002). The Fus3-Gα interaction is thought to locally amplify Gβ phosphorylation on the up-gradient side of the cell (Metodiev et al., 2002). Gβ may also be a Yck substrate that is dependent on a hierarchal phosphorylation by Fus3 prior to interaction. Together, these results and observations lead us to propose a mechanism for pheromone gradient sensing that depends on asymmetric internalization of the receptor. A gradient of pheromone leads to a similar gradient of activated receptor, free Gβγ, and activated Gα at the PM. Free Gβγ interacts with Yck, thereby protecting the receptor from Yck dependent phosphorylation. The slight asymmetry in Gβ receptor protection initiates a positive feedback loop resulting in the receptor and G protein at the back of the cell being internalized to a greater degree. This ultimately results in formation of a receptor crescent on the side of the cell closest to the gradient of pheromone, marking the site of polarization. Once the polarity site is established, polarity proteins are recruited to the membrane where actin is polymerized, and directed secretion of proteins along actin cables helps to maintain polarity. In this study, we tested the different postulates of this model to elucidate the mechanism of directional sensing and used computational modeling to provide further insight into the mechanism.

Table I: Yeast strains used in this study

Strain	Background	Genotype	Reference
AIY284	BF264-15D	*MAT***a** *bar1*Δ *ade1 his2 leu2-3,112 trp1-1a ura3*Δ YCplac111/*GAL1-STE4* YCplac22/*GAL1-myc-YCK1*	This study
AIY285	BF264-15D	*MAT***a** *bar1*Δ *ade1 his2 leu2-3,112 trp1-1a ura3*Δ YCplac111/*GAL1-ste4*$^{T320A\ S335A}$ YCplac22/*GAL1-myc-YCK1*	This study
DMY224	LRB758	*MAT***a** *his3 leu2 ura3-52 leu2*:*STE2-GFP::LEU2*	Suchkov et al., 2010
DMY222	LRB756	*MAT***a** *his3 leu2 ura3-52 yck1-D1::ura3 yck2-2*^{ts} *leu2*:*STE2-GFP::LEU2*	Suchkov et al., 2010
AIY100	YDB111	*MAT***a** *SST2-GFP-KanMX6 Ste2*^{7XR}*-mCherry-caURA3 Gpa1*^{G302S}-HisMX6 YCplac111	This study
AIY101	YDB111	*MAT***a** *SST2-GFP-KanMX6 Ste2*^{7XR}*-mCherry-caURA3 Gpa1*^{G302S}*-HisMX6* YCplac111/*GAL1-STE4*	This study
AIY221	YDB111	*MAT***a** *SST2-GFP-KanMX6 Ste2*^{7XR}*-mCherry-caURA3 Gpa1*^{G302S}*-HisMX6* YCplac111/*GAL1-ste4*$^{T320A\ S335A}$	This study
YDB111	BY4741	*MAT***a** *SST2-GFP-KanMX6 Ste2*^{7XR}*-mCherry-caURA3 Gpa1*^{G302S}*-HisMX6*	Ballon et al., 2006
AIY109	YDB111	*MAT***a** *SST2-GFP-KanMX6 Ste2*^{7XR}*-mCherry-caURA3 Gpa1*^{G302S}*-HisMX6 ste4*$^{T320A\ S335A}$*::LEU2*	This study

Table I: Yeast strains used in this study (continued)

Strain	Background	Genotype	Reference
DMY169	BF264-15D	*MAT***a** *bar1*Δ *ade1 his2 leu2-3,112 trp1-1a ura3*Δ *leu2:STE2-GFP::LEU2*	Suchkov et al., 2010
AIY197	RDY114	*MAT***a** *ste4*$^{T320A\ S335A}$ *bar1*Δ *ade1 his2 leu2-3,112 trp1-1a ura3*Δ *leu2:STE2-GFP::LEU2*	This study
RDY114	BF264-15D	*MAT***a** *ste4*$^{T320A\ S335A}$ *bar1*Δ *ade1 his2 leu2-3,112 trp1-1a ura3*Δ	DeFlorio et al., 2013
DSY246	BF264-15D	*MAT*α *bar1*Δ *ade1 his2 leu2-3,112 trp1-1a ura3*Δ	Stone lab
AIY273	Stone lab 220	*MAT***a** *bar1*Δ *ade1 his2 leu2-3,112 trp1-1a ura3*Δ *STE7*Δ*::KanMX* YCplac22/*GAL1-STE7* pRS416/*ADH1-VF1-YCK1* pRS415/*ADH1-STE4-VF2*	This study
AIY276	Stone lab 220	*MAT***a** *bar1*Δ *ade1 his2 leu2-3,112 trp1-1a ura3*Δ *STE7*Δ*::KanMX* YCplac22/*GAL1-STE7* pRS416/*ADH1-VF1-YCK1* pRS415/*ADH1-VF2*	This study
AIY275	Stone lab 220	*MAT***a** *bar1*Δ *ade1 his2 leu2-3,112 trp1-1a ura3*Δ *STE7*Δ*::KanMX* YCplac22/*GAL1-STE7* pRS415/*ADH1-STE4-VF2* pRS416/*ADH1-VF1*	This study
RDY126	BF264-15D	*MAT***a** *ste4::URA3 GFP-STE4::ura3 bar1*Δ *ade1 his2 leu2-3,112 trp1 ura3*Δ	DeFlorio et al., 2013

Table I: Yeast strains used in this study (continued)

Strain	Background	Genotype	Reference
NWY069	BF264-15D	*MAT***a** *bar*Δ *ste4*$^{T320A\ S335A}$ Δ*ste18::URA3* Δ*arg5/6::G418* Δ*lys1::hph* YCplac22/*GAL1-3xHA-STE18* YCplac111/*GAL1-ste4*$^{T320A\ S335A}$	This study
NWY068	BF264-15D	*MAT***a** *bar*Δ Δ*ste18::URA3* Δ*arg5/6::G418* Δ*lys1::hph* YCplac22/*GAL1-3xHA-STE18* YCplac111/*GAL1-STE4*	This study
NWY071	BF264-15D	*MAT***a** *bar*Δ Δ*ste18::URA3* Δ*arg5/6::G418* Δ*lys1::hph* YCplac22 YCplac111	This study
NWY074	BF264-15D	*MAT***a** *bar*Δ *ste4*$^{T320A\ S335A}$ Δ*ste18::URA3* Δ*arg5/6::G418* Δ*lys1::hph* YCplac22 YCplac111	This study
NWY073	BF264-15D	*MAT***a** *bar1*Δ *ade1 his2 leu2-3,112 trp1-1a ura3*Δ pESC-LEU/*GAL1-myc-YCK1*	This study
NWY052	BF264-15D	*MAT***a** *bar1*Δ Δ*ste18::URA3* Δ*lys1::hph* Δ*arg5/6::G418* YCplac22/*GAL1-His6x-STE18* YCplac111/*GAL1-STE4*	This study
EDY208	BF264-15D	*MAT***a** *bar1*Δ *ade1 his2 leu2-3,112 trp1-1a ura3*Δ *ste2*Δ::*KanMX* #1a	Stone lab
DSY257	BF264-15D	*MAT***a** *bar1*Δ *ade1 his2 leu2-3,112 trp1-1a ura3*Δ	Stone lab

Table II: Plasmids used in this study

Plasmid #	Plasmid name	Plasmid marker/type	Reference
MCB26	YCplac111/*GAL1-STE4*	LEU2/CEN	Cismowski et al., 2001
DMB115	YCplac22-*GAL1-myc-YCK1*	TRP1/CEN	This study
DMB114	pESC-LEU/*GAL1-myc-YCK1*	LEU2/2µm	This study
RDB131	YCplac111/*GAL1-ste4*$^{T320A\ S335A}$	LEU2/CEN	DeFlorio et al., 2013
NWB032	YCplac22/*GAL1-3xHA-STE18*	TRP1/CEN	This study
AIB130	YIplac128/*ste4*$^{T320A\ S335A}$	LEU2/INT	This study
DSB155	YCplac111	LEU2/CEN	Gietz and Sugino, 1988
DSB156	YCplac33	URA3/CEN	Gietz and Sugino, 1988
DSB157	YCplac22	TRP1/CEN	Gietz and Sugino, 1988
LHP1921	*STE2*$^{1-419}$*-GFP*	LEU2/INT	Dunn et al., 2004
p416-VF1	pRS416/*ADH1-Venus Fragment 1*	URA3/2µm	Remy et al., 2004
p415-VF2	pRS415/*ADH1-Venus Fragment 2*	LEU2/2µm	Remy et al., 2004
pPC2	pRS416/*ADH1-VF1-YCK1*	URA3/2µm	Paquin et al., 2007
AIB201	pRS415/*ADH1-STE4-VF2*	LEU2/2µm	This study
MCB40	YCplac22/*GAL1-His6x-STE18*	TRP1/CEN	Cismowski et al., 2001

2. MANUSCRIPT: Gβ PROMOTES POLARIZATION OF THE PHEROMONE RECEPTOR BY INHIBITING ITS PHOSPHORYLATION

A. Ismael[1], W. Tian[2†], N. Waszczak[1†], M. Metodiev[3], Y. Cao[2], J. Liang[2], D. Suchkov[1], E. Bar[1], R. Arkowitz[4], and D. Stone[1]

[1]Laboratory for Molecular Biology, Department of Biological Sciences, University of Illinois at Chicago, Chicago, IL 60607, USA.

[2]Department of Bioengineering, University of Illinois at Chicago, Chicago, IL 60607.

[3]School of Biological Sciences, University of Essex, Essex, UK.

[4]CNRS UMR7277 / INSERM UMR1091 / Université de Nice - Sophia Antipolis, Institute of Biology Valrose, Nice, France.

[†]These authors equally contributed to this work.

Manuscript contributions:

Amber Ismael: Figures 4A,C-D, 6A-D, 7A-D, 8A-B

Wei Tian: Figures 2A,B, 3A-G, 8C-H, 9B-G; Tables III, IV, V, VI

Nicholas Waszczak: Figures 4B, 5A-B

Dr. Eli Bar: Figure 4A, top – identified interaction in a screen for Gβγ interactors published in Bar et al., 2003

Dmitry Suchkov: Figures 4B – preliminary experiment showing myc-Yck1 binding to a Gβγ column, 7A, top – observation published in Suchkov et al., 2010

2.1 Introduction

The phenomenon of chemotaxis, directed cell migration in response to an external chemical gradient plays an important role in a number of biological processes including embryogenesis, organogenesis, and the immune response (Friedl and Gilmour, 2009, Jin et al., 2008, Laird et al., 2008). Chemotaxis also plays a role in many pathological conditions including cancer metastasis and inflammatory diseases (Kedrin et al., 2007, Koizumi et al., 2007, Muller et al., 2001). The related phenomenon of chemotropism, directed cell growth in response to an external chemical gradient, plays an important role in axon guidance and angiogenesis (Berzat and Hall, 2010, Biber et al., 2002, Rubel and Cramer, 2002, Singh, 2007).

Both chemotactic and chemotropic cells must interpret an extracellular chemical gradient and polarize their movement or growth in response. Directional sensing is mediated by agonists binding to G protein-coupled receptors (GPCRs) on the cell surface (Jin, 2013). These cells are able to orient correctly in shallow gradients that vary as little as 0.5-10% over their width (Lohof et al., 1992, Mato et al., 1975, Moore et al., 2008, Segall, 1993). The shallow extracellular chemical gradient is mirrored by a shallow gradient in receptor occupancy on the cell surface (Janetopoulos and Firtel, 2008). This means that the cell must interpret a slight difference in receptor occupancy and activation and convert this into a steep intracellular signaling gradient. How cells do this remains unclear. One widely proposed explanation for this phenomenon is the local excitation, global inhibition (LEGI) model (Janetopoulos and Firtel, 2008). This mechanism couples rapid localized excitation with a slower global inhibition to explain the phenomenon of directional sensing in shallow extracellular gradients. Once the cell

has established a polarity site, polarity proteins are recruited to the cell cortex where actin is polymerized to direct its growth and maintain cell polarity.

Chemotactic cells direct their movement and must respond quickly to rapidly changing extracellular gradients. The receptors remain uniformly distributed on the membrane during the chemotactic response (Comer and Parent, 2002), and it is thought it is to enable fast adjustments in polarity. Instead of polarizing the receptor, the shallow gradient of activated receptor is converted into steep intracellular signaling gradients that direct the cell to orient its movement in the correct direction (Berzat and Hall, 2010, Janetopoulos and Firtel, 2008). Actin is not required for directional sensing but is required for motility (Jin et al., 2000, Parent et al., 1998, Servant et al., 2000, Van Haastert and Devreotes, 2004). Although chemotactic cells do not redistribute their receptors in response to an extracellular gradient, several studies have suggested that receptor phosphorylation and internalization are required for proper actin dynamics and chemotaxis (Brzostowski et al., 2013, Kavelaars et al., 2003).

In contrast, the mating response of *S. cerevisiae* is chemotropic. In the haploid phase of the yeast life cycle, cells exist as two distinct mating types, *MAT***a** and *MAT*α. Each mating type secretes a peptide pheromone that is bound by cell surface GPCRs on cells of the opposite mating type. Receptor activation initiates a signaling cascade that results in cell cycle arrest and polarized growth up the pheromone gradient toward a potential mating partner (Fig. 1) (Jackson and Hartwell, 1990). In vegetative cells, the pheromone receptor is distributed uniformly on the plasma membrane (PM). Pheromone binding induces the receptor to undergo a conformational switch that stimulates Gα to exchange GDP for GTP, after which activated Gα dissociates from

Gβγ. In response to pheromone, Gβγ is rapidly phosphorylated (Cole and Reed, 1991). Free Gβγ signals to the nucleus through a mitogen activated protein kinase (MAPK) cascade resulting in phosphorylation and activation of the MAPK, Fus3 (Bardwell, 2005). Activated Fus3 translocates to the nucleus where it induces G1 arrest and transcription of mating specific genes (Bardwell, 2005). Free Gβγ also acts as a positional determinate and recruits Far1 bound to Cdc24, the guanine nucleotide exchange factor (GEF) for Cdc42, to the cell cortex (Butty et al., 1998). The chemotropic complex, Gβγ-Far1-Cdc24, marks the polarity site for formation of the mating projection by locally amplifying active, GTP-bound Cdc42 (Nern and Arkowitz, 1999). Activated Cdc42 recruits polarity proteins to the cell cortex to facilitate actin polymerization, and myosin motor proteins deliver growth cargo along the actin filaments to the site of growth for formation of the mating projection (Pruyne and Bretscher, 2000a, Pruyne and Bretscher, 2000b). In vegetative cells, the cortical protein Bud1 interacts directly with Cdc24, recruiting it to the PM to activate Cdc42 for actin polymerization and bud emergence (Park et al., 1997, Pruyne and Bretscher, 2000b). When a cell is exposed to isotropic pheromone, it will form its mating projection where it would have formed the next bud; the cell uses Bud1 as the positional determinate when it cannot detect a gradient of pheromone (Dorer et al., 1995, Nern and Arkowitz, 1999). This is termed default shmooing.

Similar to chemotactic cells, vegetative yeast cells have their receptors distributed uniformly on the PM. In response to pheromone, however, there is a dramatic redistribution of the receptors on the PM. The pheromone receptor is rapidly internalized, and after falling below our detection on the PM, it reappears as a stable

polarized crescent on the PM of the mating projection (Ayscough and Drubin, 1998, Moore et al., 2008, Suchkov et al., 2010). The mechanism of pheromone-induced receptor internalization, which results in 5- to 10-fold increase in receptor internalization and causes it to disappear rapidly from the PM, is well understood (Jenness and Spatrick, 1986). Pheromone binding to the receptor induces a conformational change that exposes its C-terminus to phosphorylation. Receptor phosphorylation requires the activity of two sister type I casein kinases (CKI), Yck1 and Yck2 (Hicke et al., 1998). Upon phosphorylation, the receptor is ubiquitinated, internalized, and degraded (Hicke and Riezman, 1996, Hicke et al., 1998). Receptor internalization has long been thought of primarily as a way of down-regulating a signal (Dohlman et al., 1991). More recently, studies of receptor phosphorylation and internalization have suggested new roles for receptor internalization in polarization and direction sensing (Brzostowski et al., 2013, Kavelaars et al., 2003, Suchkov et al., 2010, Vallier, 2002). We previously reported that pheromone-induced receptor internalization is required for receptor polarization and directional sensing (Suchkov et al., 2010).

How yeast cells polarize their growth in response to pheromone has been extensively studied and is well understood, but how the cell senses the direction of the pheromone gradient is still unclear. It has been calculated that yeast cells can orient accurately in a gradient that varies as little as 0.5% over their width (Moore et al., 2008). How does the cell interpret a shallow gradient of pheromone and convert the shallow extracellular gradient into a steep intracellular signaling gradient prior to actin dependent directed secretion? In a genetic screen for proteins that interact with Gβ, Yck1 was identified. The discovery of this interaction led us to propose a model that

explains how receptor polarization occurs upstream of actin-dependent directed secretion. We postulate that asymmetric internalization of the receptor establishes the polarity site resulting in formation of a receptor crescent on the up-gradient side of the cell.

Here we show that Gβ inhibits receptor phosphorylation and promotes receptor polarization, and that these events are dependent on Gβ phosphorylation. A mutant form of Gβ that cannot be phosphorylated, $G\beta^{P-}$, is also defective in its interaction with Yck1, one of the sister casein kinases required for receptor phosphorylation and internalization. These results are consistent with our proposed mechanism for receptor polarity establishment by asymmetric internalization. We were also able to detect a region on the PM where α-factor bound receptor persisted longer compared to the rest of the cell. Taken together, our results support a novel mechanism for receptor polarization upstream of actin-dependent directed secretion in pheromone gradients.

2.2 Materials and Methods

Yeast strain construction

The yeast strains used in this study are listed in Table I. *MAT***a** (DSY257) cells were transformed with YCplac111/*GAL1-STE4* (MCB26) (Cismowski et al., 2001) and YCplac22/*GAL1-myc-YCK1* (DMB115) or YCplac111/*GAL1-ste4*$^{T320A\ S335A}$ (RDB131) (DeFlorio et al., 2013) and YCplac22/*GAL1-myc-YCK1* (DMB115) to create the genetic interaction assay strains, AIY284 and AIY285, respectively. The Gβγ and $G\beta^{P-}\gamma$ column strains used in this study were knocked out for *ARG5/6* by transplacement with a fragment containing KanMX4 G418 amplified from pFA6-kanMX4, flanked with ends homologous to *ARG5/6* using the following primers: 5'-TCCAAATTCCAAAAATTTG

TGTCTTCATTAAACAAATCCACCATAGCAGGCGTACGCTGCAGGTCGAC-3' and 5'-TCAGGGATACCAGCATACTCTCCATAACCCATAGCAAGATTAATATTTTGATCGA TGAATTCGAGCTCG-3'. Integrants were selected for on medium containing 200 mg/L Geneticin G418. *LYS1* was knocked out by transplacement by creating a TEF promoter-hph-TEF terminator fragment amplified from pAG32 plasmid and flanked by ends homologous to *LYS1* using the following primers: 5'-GCTGCCGTCACATTAC ATCTAAGAGCTGAAACTAAACCCCTAGAGGCTCTGTTTAGCTTGCCTTGTC-3' and 5'-GTACCAGAACGGTAGGTTTGTTAAACACAGTAGCCACAGTGTATATGCTC GTTTTCGACACTGGAT-3'. Integrants were selected for on medium containing Hygromycin B. MCY46 (*ste18*Δ*::URA3*) (Cismowski et al., 2001) was knocked out for *ARG5/6* and *LYS1* (as described above), and transformed with either YCplac22/*GAL1-3xHA-STE18* (NWB032) and YCplac111/*GAL1-STE4* (MCB26) (Cismowski et al., 2001) or YCplac22 and YCplac111 (Gietz and Sugino, 1988), to create NWY068 and NWY071, respectively. RDY114 (*ste4*$^{T320A\ S335A}$) (DeFlorio et al., 2013) was knocked out for *ARG5/6* and *LYS1* (as described above) and for *STE18* by transplacement with a fragment containing *URA3* amplified from DSB156, flanked with ends homologous to *STE18* using the following primers: 5'CTAAGAATGACATCAGTTCAAAACTCTCC ACGCTTACAACAACCTCAGGACACATTTCCCCGAAAAGTGC-3' and 5'-GAATAAGAT ATGAACGGAGCCAAAATTAGAAGAAAAAAAAAGATAGGGTGTTGCCACGACTCATC TCCAT-3'. The resulting strain was transformed with YCplac22/*GAL1-3xHA-STE18* (NWB032) and YCplac111/*GAL1-ste4*$^{T320A\ S335A}$ (RDB131) (DeFlorio et al., 2013) to create NWY069. The strain used to overexpress N-terminally myc-tagged Yck1 was generated by transforming DSY257 with pESC-LEU/*GAL1-myc-YCK1* (DMB114) to

create NWY073. The strain used for analysis of Gβ phosphorylation was made by knocking out *LYS1* and *ARG5/6* (as described above) in MCY46 (*ste18*Δ*::URA3*) (Cismowski et al., 2001) and then the resulting strain was transformed with YCplac111/*GAL1-STE4* (MCB26) (Cismowski et al., 2001) and YCplac22/*GAL1-His6x-STE18* (MCB40) (Cismowski et al., 2001) to create NWY052. The strains used for the bimolecular fluorescence complementation assays were created by transforming *MAT***a** *bar1*Δ *ade1 his2 leu2-3,112 trp1-1a ura3*Δ *STE7*Δ*::KanMX* YCplac22/*GAL1-STE7* cells with pRS416/*ADH1-VF1-YCK1* (pPC2) (Paquin et al., 2007) and pRS415/*ADH1-STE4-VF2* (AIB201), pRS416/*ADH1-VF1-YCK1* (pPC2) (Paquin et al., 2007) and pRS415/*ADH1-VF2* (p415-VF2) (Remy et al., 2004), or pRS415/*ADH1-STE4-VF2* (AIB201) and pRS416/*ADH1-VF1* (p416-VF1) (Remy et al., 2004) to create AIY273, AIY276, and AIY275, respectively. The strains used to visualize Sst2-GFP localization in G1-synchronized cells were created by transforming *MAT***a** *SST2-GFP-KanMX6* *Ste2*^{7XR}*-mCherry-caURA3 Gpa1*^{G302S}*-HisMX6* (YDB111) (Ballon et al., 2006) cells with YCplac111 (Gietz and Sugino, 1988), YCplac111/*GAL1-STE4* (MCB26) (Cismowski et al., 2001), or YCplac111/*GAL1-ste4*$^{T320A\ S335A}$ (RDB131), to create AIY100, AIY101, and AIY201, respectively. *ste4*$^{T320A\ S335A}$ was integrated into YDB111 (Ballon et al., 2006) *in situ*, using Msc1-cut YIplac128/*ste4*$^{T320A\ S335A}$ (AIB130, see below) to create AIY109. To visualize Ste2-GFP localization, AIY197 was created by integrating Hpa1-cut LHP1921 (Dunn et al., 2004) into RDY114 (DeFlorio et al., 2013).

Plasmid construction

The plasmids used in this study are listed in Table II. YCplac22/*GAL1-3xHA-STE18* was constructed by PCR amplifying *STE18* from pGEX-KG-*STE18* (MCB35) with the following primers: Forward primer was 5'-TGCTATCCAGTCGACATGTACCCATACGA CGTCCCAGACTACGCTTACCCATACGACGTCCCAGACTACGCTTACCCATACGAC GTCCCAGACTACGCTATGACATCAGTTCAAAACTC-3' and reverse primer was 5'-TGGACCGCCAAGCTTTTACATAAGCGTACAACAAA-3'. The forward primer included a sequence for N-terminal 3x-HA tagging of Ste18. The SalI-HindIII cut PCR product was inserted into YCplac22/*GAL1* (Cismowski et al., 2001). YIplac128/*ste4*$^{T320A\ S335A}$ was constructed by PCR amplifying *ste4*$^{T320A\ S335A}$ from RDY120 (DeFlorio et al., 2013) lacking the first 112 bases using the oligomers 5'-CGCGAATTCTGCGCTTCCACAGAACTAATG-3' and 5'-CGCGGATCCAAATA GAGGCCGCCAGACAAG-3'. The PCR fragment cut with EcoRI and BamHI was subcloned into YIplac128 (Gietz and Sugino, 1988) to create AIB130. pRS415/*ADH1-STE4-VF2* was constructed by PCR amplifying genomic *STE4* lacking the stop codon using the oligomers 5'-GCAGGATCCGATGGCAGCACATCAGATGG-3' and 5'-GCTGGATCCTTGATAACCTGGAGACCAT-3'. The BamHI-cut PCR fragment was subcloned into p415-*VF2* (Remy et al., 2004) in frame with the C-terminal Split-Venus fragment under the control of the *ADH1* promoter to create AIB201.

Yck1-Gβ genetic interaction assay

*MAT***a** cells transformed with YCplac111/*GAL1-STE4* and YCplac22/*GAL1-myc-YCK1* (AIY284) or YCplac111/*GAL1-ste4*$^{T320A\ S335A}$ and YCplac22/*GAL1-myc-YCK1* (AIY285) were grown to mid-log phase in selective synthetic medium containing 2%

sucrose and 10-fold dilutions were spotted on selective synthetic medium containing 2% dextrose (no expression) or 2% galactose to induce expression. The plates were incubated at 30°C for 2 overnights.

Yck1-Gβ Split-Venus bimolecular fluorescence complementation (BiFC) assay

*MAT***a** *STE7*Δ*::KanMX* YCplac22/*GAL1-STE7* cells transformed with pRS416/*ADH1-VF1-YCK1* and pRS415/*ADH1-STE4-VF2* (AIY273), pRS416/*ADH1-VF1-YCK1* and pRS415/*ADH1-VF2* (AIY276), or pRS415/*ADH1-STE4-VF2* and pRS416/*ADH1-VF1* (AIY275) were grown to mid-log phase in selective synthetic liquid medium containing 2% sucrose and induced with 2% galactose for 1 hour before being treated with 150nM α-factor. Images were acquired 2.5 hours after pheromone treatment using an ANDOR Revolution XD spinning disk laser confocal system with a motorized Olympus IX-81 microscope, a Yokogawa CSU-X1 spinning disk unit, motorized XYZ control (piezo) and an iXon897 EMCCD camera, controlled by Andor iQ2 software. A UplanSApo NA 1.4x100 objective was used with a laser excitation of 488-nm. Signal above background was quantified using ImageJ by obtaining the mean PM signal using the segmented line tool, and the cytoplasmic mean fluorescence using the selection brush tool. PM localization was quantified by calculating the PM mean/cytoplasmic mean ratio.

Gβ immunoblotting

DMY222 (*MAT***a** *his3 leu2 ura3-52 yck1-D1::ura3 yck2-2^{ts} leu2*:*STE2-GFP::LEU2*) and the isogenic strain DMY224 (*MAT***a** *his3 leu2 ura3-52 leu2*:*STE2-GFP::LEU2*) were grown to mid-log phase at room temperature (RT) in YPD, shifted to 37°C (restrictive temperature) or maintained at RT, and treated with either 150 nM

α-factor or 1.2 uM α-factor for 1 hour. After 1 hour, cell equivalents were collected from all cultures and immunoblotting was performed essentially as described in (Li et al., 1998).

Gβγ/Gβ^{P-}γ columns

NWY069, NWY068, and NWY071 cells were grown to mid-log phase in selective medium containing 2% sucrose and 0.1% dextrose, induced with 2% galactose for 5 hours, and then treated with 150 nM α-factor for 1 hour. Cells were harvested at 5,000 rpm at RT, washed once with cold deionized water, and frozen in an ice/ethanol bath. Cells were lysed at 4 degrees Celsius with glass beads in 1X TBS buffer (150mM NaCl, 10mM Tris pH 8, 100mM PMSF, 2mM aprotinin, 2mM pepstatin, 2mM leupeptin). Crude lysates were centrifuged at 13,200 rpm at 4 degrees Celsius for 20 minutes and protein concentrations were obtained using the Pierce 660nm assay kit. 7.3mg of each protein lysate was mixed with 30µL Thermo anti-HA agarose beads, volume was adjusted to 1.25mL with 1X TBS buffer, and incubated for 2 hours at 4 degrees Celsius with over end rotation. After incubation, beads were washed 3x with 1X TBS-T buffer (150mM NaCl, 10mM Tris pH 8, Tween-20 0.1%). NWY073 cells were grown to mid-log phase in selective medium containing 2% sucrose and 0.1% dextrose, and induced with 2% galactose. Lysis was conducted and protein concentration was obtained as described above. 900µg (H) or 225µg (L) of NWY073 lysate was added to beads, volume was adjusted to 1.25mL with 1X TBS buffer, and incubated at 4 degrees Celsius for 1 hour with over end rotation. Beads were washed 3x with 1X TBS-T buffer, and then 50uL 1X TBS buffer, 5X SDS sample buffer to a 1X final concentration. A Western blot was performed using α-HA primary (1:900) and α-mouse IgGI HRP (1:400,000).

Myc-Yck1 binding was determined by subtracting the signal from the negative control strain (NWY071). Mass spec analysis was performed as previously described in Alldridge et al., 2008 and Metodiev, 2001. Mixed equal volumes were eluted and run out on 5/10% SDS-PAGE. ~70-55kDa and ~55-45kDa regions were excised out, trypsinized, and analyzed by nanoscale LC-MS/MS as previously described in Metodieva et al., 2013.

Mass spectrometry analysis of Gβ phosphorylation

NWY052 cells were grown to mid-log phase in selective synthetic medium with 2% sucrose and induced with 2% galactose for 5.5 hours. The heavy labeled culture had L-lysine:2HCL, U-13C6 and L-Arginine: HCL U13C6, U-15N2 (Cambridge Isotope Labs) and was treated with 150 nM α-factor for 1 hour after galactose induction. The non-heavy labeled culture was not treated with α-factor. Cells were harvested, beads were lysed, and pull-down was performed as previously described (Cismowski et al., 2001). Lysates were incubated overnight on Ni-NTA (25mg of total input for each culture). Elution was performed as previously described (Metodiev, 2011), equal volumes were mixed, and ran out on a 5/10% PAGE gel. The 45-50 kDa region was excised out, trypsinized, and peptides were extracted. Protein preps were vacuum concentrated and TiO_2 phospho-peptide enrichment was performed using a Pierce kit. Protein preps were analyzed by nanoscale LC-MS/MS as previously described in Metodieva et al., 2013.

Sst2-GFP localization in G1-synchronized cells

G1-synchronized cells from *MAT***a** *SST2-GFP-KanMX6 Ste2*^{7XR}*-mCherry-caURA3 Gpa1*^{G302S}*-HisMX6* (YDB111) cells transformed with YCplac111 (AIY100),

YCplac111/*GAL1-STE4* (AIY101), or YCplac111/*GAL1-ste4*$^{T320A\ S335A}$ (AIY221) were obtained as previously described (Suchkov et al., 2010), incubated on ice for 3 hours, centrifuged and resuspended in selective synthetic medium containing 2% galactose for 1 hour at 30°C, and treated with 1.2 µM α-factor and 200 µM of lactrunculin A (LatA) (0'). Images were acquired using an Axioskop 2 microscope (Carl Zeiss, Jena, Germany) with a 100x oil immersion objective with a laser excitation of 488-nm and a digital AxioCam camera at 15-minute intervals and were processed with Zeiss AxioVision software (Carl Zeiss). PM/Cyto ratio was quantified as described above. Polarity Index (PI) was quantified as described in the figure legend (Suchkov et al., 2010).

Sst2-GFP time-lapse localization in mating mixtures

*MAT*α cells and *MAT***a** *SST2-GFP* cells expressing Gβ (YDB111) or Gβ^{P-} (AIY109) were grown to mid-log phase in synthetic medium containing 2% dextrose and mixed 1:1. Images from 6 fields were acquired at 15-minute intervals on synthetic agar pads containing 2% dextrose using the spinning disk microscope described above. Twenty one z-sections were acquired over 6 µm using a laser excitation of 488-nm or DIC. Mating mixtures were maintained at 30°C using an Okolab chamber. Images were sum projected using ImageJ and the switch angle was quantified as described in the figure legend.

Ste2-GFP localization in G1-synchronized cells

G1-synchronized *MAT***a** Gβ (DMY169) and Gβ^{P-} (AIY197) cells expressing *STE2-GFP* were obtained essentially as previously described (Suchkov et al., 2010), centrifuged and resuspended in synthetic medium containing 1.5% sucrose and 0.5%

dextrose, treated with 9 nM α-factor (0'), and 200 µm of LatA was added after 15 minutes. Images were acquired at 15 minute intervals using the Zeiss Axioskop 2 previously described with a laser excitation of 488-nm. The polarity index (PI) was quantified as described in the figure legend (Suchkov et al., 2010).

Ste2-GFP time-lapse localization in mating mixtures

*MAT*α cells and MAT**a** *STE2-GFP* cells expressing Gβ (DMY169) or $G\beta^{P-}$ (AIY197) were grown to mid-log phase in synthetic medium containing 2% dextrose and mixed 1:1. Images were acquired at 15-minute intervals on synthetic agar pads containing 2% dextrose using the spinning disk microscope described above. Fifteen z-sections were acquired over 4.2 µm using a laser excitation of 488-nm or DIC. Mating mixtures were maintained at 30°C using an Okolab chamber. Images were sum projected using ImageJ and the signal intensity along the insipient long axis of the cell was quantified using BudPolarity (Vernay et al., 2012). Receptor polarization was quantified as described in the figure legend.

Visualization of membrane receptor

DMY169 G1-synchronized cells were obtained essentially as previously described (Suchkov et al., 2010), and treated with 6 nM α-factor at 30°C in YPD. Aliquots were taken at 5 minute increments after pheromone treatment and treated with 10 mM Sodium Azide, and PM receptor was bound with Alexa Fluor 594-conjugated α-factor essentially as previously described (Toshima et al., 2006). Images were acquired using an ANDOR Revolution WD spinning disk laser confocal system with a motorized Olympus IX-81 microscope, a Yokogawa CSU-W1 spinning disk unit, a Prior motorized stage and a neo sCMOS camera, controlled by Andor iQ2 software. A

UPLSAPO 60x Silicon immersion objective (NA 1.3) was used and 9 z-sections were acquired over 4.8 µm using a laser excitation of 561-nm and 1 center slice was imaged with DIC. Images were sum projected using ImageJ.

*MAT***a** WT cells (DSY257) and *MAT***a** *ste2*Δ cells (EDY208) were both grown to mid-log phase in YPD medium and PM receptor was bound with Alexa Fluor 594-conjugated α-factor essentially as previously described (Toshima et al., 2006) to confirm receptor binding specificity. Images were acquired using the spinning disk laser confocal system described above taking a center slice using a laser excitation of 561-nm and a center slice with DIC.

Membrane receptor time-lapse

*MAT***a** cells (RDY126) were grown to mid-log phase in YPD medium and PM receptor was bound with Alexa Fluor 594-conjugated α-factor essentially as previously described (Toshima et al., 2006). Images were acquired at 1-minute intervals at RT using an ANDOR Revolution WD spinning disk laser confocal system with a motorized Olympus IX-81 microscope, a Yokogawa CSU-W1 spinning disk unit, a Prior motorized stage and a neo sCMOS camera, controlled by Andor iQ2 software. A UPLSAPO 60x Silicon immersion objective (NA 1.3) was used and 9 z-sections were acquired over 5.6 µm using a laser excitation of 561-nm and 1 center slice was imaged with DIC. Images were sum projected and membrane fluorescence was obtained using the segmented line tool in ImageJ.

To filter out the noise in the data (Fig. 2A), we used a moving average function. For a position on the membrane at a time point, we calculated its fluorescence intensity by averaging the fluorescence intensity of the region around that position with the

window size of the region equal to 1/10 of membrane perimeter. For the position *x* at time *t* in cell *c* with a window size *w*, the fluorescence intensity is calculated by the following formula:

$$\mathrm{FI_n}(x,t,c) = \mathrm{avg}(\mathrm{FI_o}\left(x-\frac{w}{2},t,c\right),\ldots,\mathrm{FI_o}\left(x+\frac{w}{2},t,c\right)),$$

where $\mathrm{FI_n}$ denotes the new value after filtering, $\mathrm{FI_o}$ the original raw value. After sliding the average window over the cell membrane, the high frequency noise is removed (Fig. 2B). To make data from different cells comparable with each other, we then removed the background from each cell by subtracting the minimum value of the cell, and rescaled the range of data to [0,1] by dividing all data points by the current maximum value of the cell.

Figure 2. Computational cell data smoothing

(A) Raw values for PM fluorescence. (B) High frequency PM noise was filtered out using a sliding average by averaging the fluorescence intensity of the region around a position with the window size of the region equal to $1/10^{th}$ of the membrane perimeter. Background was removed by subtracting the minimum value from each data set, and the relative decrease in intensity for each data point at each time point was determined by dividing each value by the maximal value.

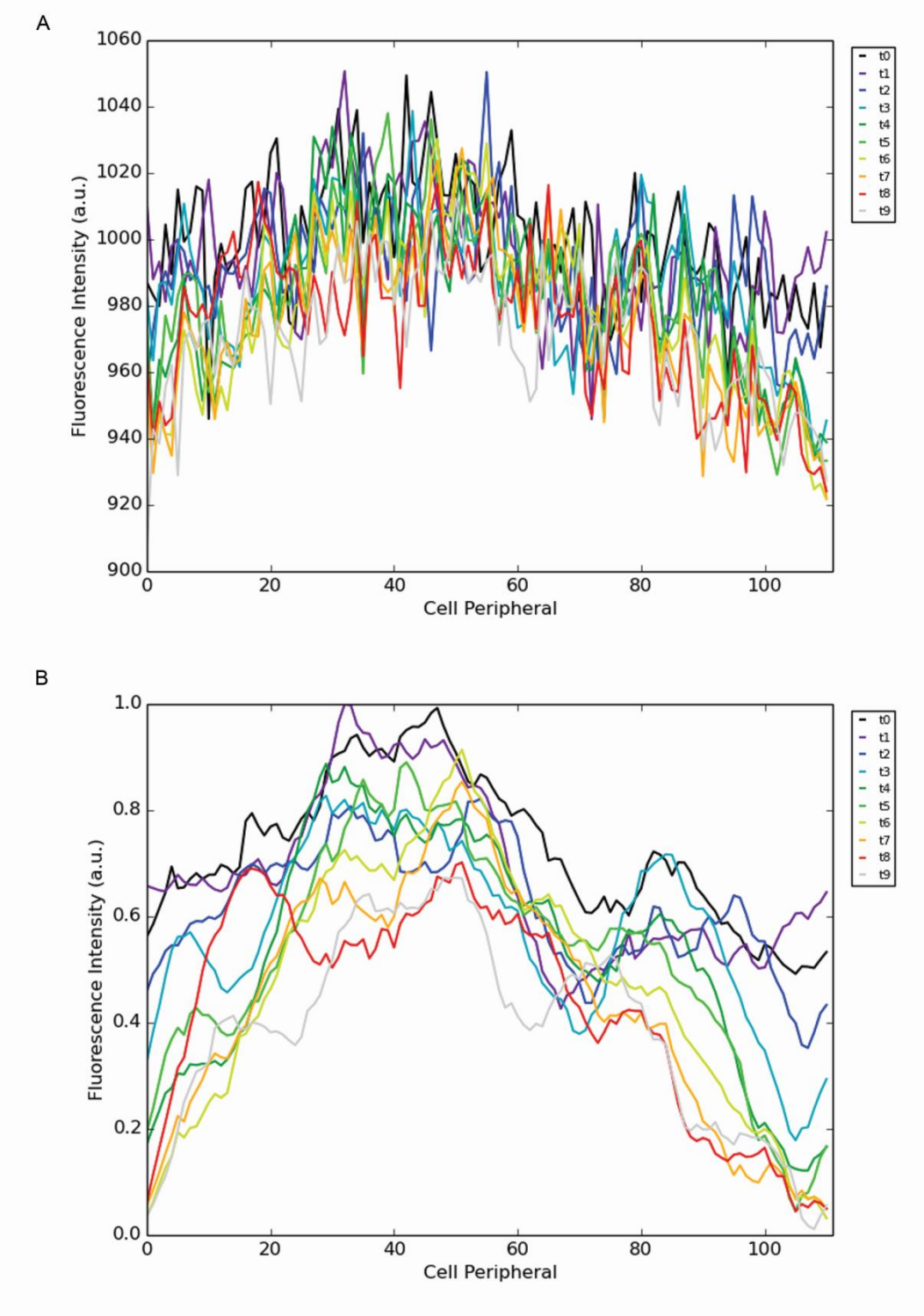
A
Fluorescence Intensity (a.u.)
Cell Peripheral
t0
t1
t2
t3
t4
t5
t6
t7
t8
t9
B
Fluorescence Intensity (a.u.)
Cell Peripheral

Assuming the kinetics of internalization resemble a 1st order chemical reaction, we calculated the relative fluorescence intensity of time point *t* compared to time point 0 to calculate how membrane receptor density changes with time using the following formula:

$$\mathrm{FI}_r(x,t,c) = \mathrm{FL}_n(x,t,c)/\mathrm{FL}_n(x,0,c)$$

The result FI_r of an example cell is plotted as a heat map, where the *y*-axis is the time point, and the *x*-axis represents the pixel position in the trace around the PM.

Next, we determined the protected region of a cell by fitting the values of a pixel at different time points using the exponential decay formula:

$$FI(t) = FI(0)exp(-\lambda t)$$

where λ is the decay rate. The threshold for receptor protection was set as the pixels with the slowest 30% decay rates. We calculated the average FI of the protected regions at different time points and compared it to the average of the rest of the cell. In some cases the protected regions were fragmented. If the distance between two protected regions was less than 1/10 of the perimeter of the cell and the average rate of region after connecting was still above the threshold, the two regions were connected.

Computational modeling

To model the PM of yeast, we used a three-dimensional sphere with the membrane discretized in a latitude-longitudinal way. Uniformly spaced patches were partitioned by the 16 *n* latitude bands (pole to pole) (Fig. 3A) and the 40 *m* longitude lines (Fig. 3B). The center of each patch was used to represent its position (Fig. 3C). The latitudinal spacing and longitudinal spacing, Table III, Eq.1 and Table III Eq.2,

respectively, give the surface distance between two neighboring patches. The *j*-th patch in the *i*-th band is denoted by an index pair (*i,j*) and the position of the (*i,j*) patch, (x_{ij}, y_{ij}, z_{ij}), is given by Table III, Eq.3. The pheromone gradient change is linear along the *x*-axis and, thus, only x_{ij} is needed to determine the local pheromone concentration of the (*i,j*) patch given by Table III Eq.4. In each patch, we simulated the reaction network model with the pheromone concentration appropriate to its center position with the pheromone concentration at the front of the cell being 10 nM and the back being 5 nM (Fig. 3G). All proteins were assumed to diffuse laterally, as only the PM was modeled in this analysis. Molecules in one patch can diffuse to the 4 neighboring patches (Fig. 3E,F), except for those in the “pizza slices” ringing each pole, which can only diffuse to the three neighboring patches (Fig. 3D,F). If the effect of surface curvature on diffusion is ignored, the diffusion of each molecular species can be obtained from Table III, Eq.5-7.

Figure 3: Spatial model of a yeast cell.
(A) The cell radius, *r*, was discretized into *n* latitude bands. (B) Each latitude band was cut into *m* patches. (C) The latitude bands were globally uniformly spaced with a surface distance of *hv*, which in the *i*-th band the patches were spaced uniformly with a surface distance of *hjh*.
(D) Molecules in a "pizza slice" around one pole diffuse among the three neighbor patches of it. (E) Molecules in other patches diffuse among the four neighboring patches. Effect of curvature is ignored in diffusion calculation. (F) "pizza slice" patches with three neighboring patches are around the poles, and patches with four neighbors comprise the rest of the patches in the computational yeast cell. (G) A copy of the reaction network model with proper local pheromone concentration was placed in each patch.

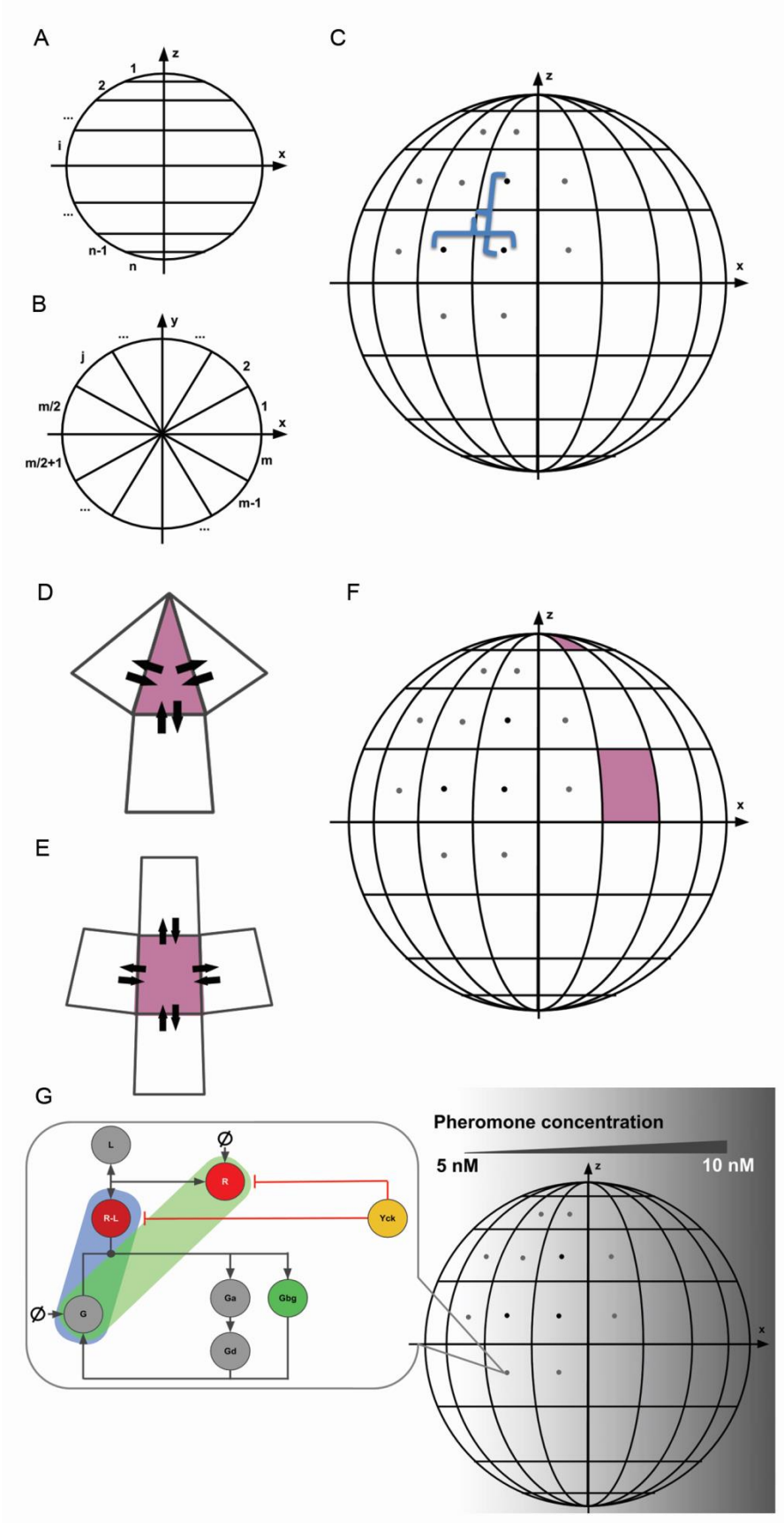
A
z
1
2
...
i
...
n-1
n
x
B
y
...
...
j
2
m/2
1
x
m/2+1
m
m-1
...
...
C
z
x
D
E
F
z
x
G
L
Ø
R
R-L
Yck
Ga
Gbg
Ø
G
Gd
Pheromone concentration
5 nM
10 nM
z
x

Table III. Equations used for spatial model of yeast cell.

Eq #	Equation	Comments
1	$h_v = \frac{\pi r}{n}$	Latitudinal patch spacing
2	$h_{ih} = r\sqrt{1-\cos^2(\frac{2i+1}{2n}\pi)}$	Longitudinal patch spacing
3	$x_{ij} = \sqrt{r^2 - z_{ij}^2}\cos(\frac{2j+1}{2m}2\pi)$, $y_{ij} = \sqrt{r^2 - z_{ij}^2}\sin(\frac{2j+1}{2m}2\pi)$ and $z_{ij} = r\cos(\frac{2i+1}{2n}\pi)$	The position of the $\{i,j\}$-patch, (x_{ij}, y_{ij}, z_{ij})
4	$[\mathrm{L}(x_{ij})] = [\mathrm{L}(r)] + (x_{ij} - r)\cdot\psi$	pheromone concentration of the $\{i,j\}$-patch; $\psi = 1.25nM/\mu m$
5	$D\nabla^2[S_k(i,j)] = D(\frac{[S_k(i-1,j)] + [S_k(i+1,j)] - 2[S_k(i,j)]}{h_v^2} + \frac{[S_k(i,j-1)] + [S_k(i,j+1)] - 2[S_k(i,j)]}{h_{ih}^2})$	Diffusion of the k-th molecular species Sk in the $\{i,j\}$-patch[a]
6	$D\nabla^2[S_k(1,j)] = D(\frac{[S_k(1,j)] + [S_k(3,j)] - 2[S_k(2,j)]}{h_v^2} + \frac{[S_k(1,j-1)] + [S_k(1,j+1)] - 2[S_k(1,j)]}{h_{1h}^2})$	Diffusion of the k-th molecular species Sk in the patches ringing the north pole[a]
7	$D\nabla^2[S_k(n,j)] = D(\frac{[S_k(n,j)] + [S_k(n-2,j)] - 2[S_k(n-1,j)]}{h_v^2} + \frac{[S_k(n,j-1)] + [S_k(n,j+1)] - 2[S_k(n,j)]}{h_{nh}^2})$	Diffusion of the k-th molecular species Sk in the patches ringing the south pole[a]

[a]D = 0.001μm^2/s was used for all molecular species.

To mathematically model pheromone-induced receptor polarization upstream of actin-dependent directed secretion, and to evaluate how our proposed model affects receptor polarity, we created 3 networks. The initial values and reaction rates are given in Table IV. The reactions are described in Table V. Network 1 models only the most basic and best characterized components and comprises of the receptor-pheromone interactions, G protein cycle, and Yck-dependent internalization of the receptor and G protein (Table V, Reactions 1-12) with no downstream regulation of receptor internalization. Reactions 1 and 2 (Table V) represent the synthesis of receptors (R), and the association and disassociation of receptors (R) and pheromone (L). Reactions 3-6 (Table V) comprise the G protein cycle. Reaction 3 (Table V) is the synthesis of the heterotrimeric G protein (G). In reaction 4 (Table V), the heterotrimeric G protein (G) is activated by active receptor (RL) to dissociate into free Gβγ (Gbg) and free active Gα (Ga), which is then deactivated to the inactive form of Gα (Gd) in reaction 5 (Table V). Free inactive Gα (Gd) and free Gβγ (Gbg) reassociate to form the heterotrimeric G protein (G) given by reaction 6 (Table V). Reactions 7 and 8 (Table V) represent the interaction of Yck1 and Yck2 (Yck) with inactive (R) and active receptors (RL), respectively, which trigger the process of receptor internalization. Internalization of the G protein (G) with receptor (R) is also represented by reactions 7 and 8 (Table V). When either active (RL) or inactive (R) receptors are internalized, they also take away nearby heterotrimer G proteins (G) from the membrane with a stoichiometry of 1:1. In this model, we did not incorporate explicitly the binding of pheromone receptor (R) and the G protein heterotrimer (G). Network 2 adds the $G\beta^{P}\gamma$-Yck interaction represented by the addition of reactions 9 and 10 (Table V). Reaction 9 and 10 (Table V) represent

the phosphorylation of $G\beta^{P}\gamma$ (GbgP) and its binding to Yck (YckGbgP), respectively. Network 3 adds the Gα-Fus3 interactions represented by the addition of reactions 11-14 (Table V). In reaction 11 (Table V), phosphorylated Gβγ (GbgP) activates Fus3 (Fus3A), which can also be deactivated into Fus3 given by reaction 12 (Table V). Active Fus3 (Fus3A), in turn, accelerates the phosphorylation of Gβγ (GbgP), given by reaction 13 (Table V). Moreover, active Gα (Ga) can recruit active Fus3 (Fus3A) to phosphorylated Gβγ (GbgP) to make the reaction even faster, given by reaction 14 (Table V). A common set of coupled partial differential equations (PDEs) was derived from their corresponding reaction formulae (Table VI). Each PDE describes how the concentration of a given molecule changes over time and space. Differences in the topology of the three networks were accounted for by varying the initial values of the relevant parameters (color-coded in Table IV).

Table IV: Definitions and parameters.

Parameter	Description	Initial Value	Reaction Rate [a]	Value
r	Cell radius	2μm	k_{rs}	$7.96 \times 10^{-2}\mu m^{-2}s^{-1}$ (45)
sa	Cell surface area	$50.27\mu m^2$	k_{rl}	$3.32 \times 10^{-3}\mu m^3 s^{-1}$ (45)
v	Cell volume	$33.51\mu m^3$	k_{rlm}	$0.01 s^{-1}$ (45)
L(r)	Pheromone at cell front	10nM	k_{gs}	$7.96 \times 10^{-2}\mu m^{-2}s^{-1}$
L(-r)	pheromone at cell back	5nM	k_{ga}	$5.03 \times 10^{-4}\mu m^2 s^{-1}$ (45)
R	Inactive receptor	10,000/sa (7)	k_{gad}	$0.11 s^{-1}$ (45)
RL	Active receptor	0	k_{gd}	$50.3\mu m^2\ s^{-1}$ (45)
G	Heterotrimeric G protein	10,000/sa (7)	k_{i0}	$5.03 \times 10^{-6}\mu m^2 s^{-1}$ (45)
Ga	Active G_α	0	k_{i1}	$2.51 \times 10^{-5}\mu m^2 s^{-1}$ (46)
Gd	Inactive G_α	0	D	$0.001\mu m^2 s^{-1}$ (47)
Gbg	$G_{\beta\gamma}$	0	k_{bp0}	0; $5.8 \times 10^{-3}s^{-1}$; $5.8 \times 10^{-3}s^{-1}$
GbgP	$G_{\beta^P\gamma}$	0	k_{bpd}	0; $1 \times 0^{-3}s^{-1}$; $1 \times 10^{-3}s^{-1}$
Yck	Yck1/2	[b]4,000/sa	k_{bp1}	0; 0; $1 \times 10^{-5}\mu m^2 s^{-1}$
YckGbgP	Yck1/2-$G_{\beta^P\gamma}$ complex	0	k_{bp2}	0; 0; $1 \times 10^{-7}\mu m^4 s^{-1}$
Fus3	Inactive Fus3	[c]2,130/v	k_{yi}	0; $5 \times 10^{-3}\mu m^2\ s^{-1}$; $5 \times 10^{-3}\ \mu m^2 s^{-1}$
Fus3P	Active Fus3	0	k_{ya}	0; $3 \times 10^{-3}\ s^{-1}$; $3 \times 10^{-3}s^{-1}$
			k_{fa}	0; 0; [d]3 $\mu m^2 s^{-1}$
			k_{fd}	0; 0; $1\ s^{-1}$ (48)

[a]Rate constants from Table V. [b]The total number of Yck molecules per cell was reported to be 7,790 (Ghaemmaghami et al., 2003). We assumed 4,000 Yck molecules on the cell surface. [c]The total number of Fus3 molecules per cell was reported to be 8,480 (Ghaemmaghami et al., 2003), with about 25% in the cytoplasm (Maeder et al., 2007). [d]We set Fus3 phosphorylation at 3X faster than its dephosphorylation based on Maeder et al., 2007. Parameter values are color-coded according to network. Those in black are used in all three networks. Blue values correspond specifically to network 1, while those in green and red correspond to networks 2 and 3, respectively.

Table V. Reaction formulae.

Rx #	Reaction	Comments
1	$\emptyset \xrightarrow{k_{rs}} \mathrm{R}$	Synthesis of receptor
2	$\mathrm{R} + \mathrm{L} \underset{k_{rlm}}{\overset{k_{rl}}{\rightleftharpoons}} \mathrm{RL}$	Association/disassociation of receptor & pheromone
3	$\emptyset \xrightarrow{k_{gs}} \mathrm{G}$	Synthesis of heterotrimeric G protein
4	$\mathrm{RL} + \mathrm{G} \xrightarrow{k_{ga}} \mathrm{RL} + \mathrm{Ga} + \mathrm{Gbg}$	Activation of G protein by liganded-receptor
5	$\mathrm{Ga} \xrightarrow{k_{gad}} \mathrm{Gd}$	Inactivation of Gα
6	$\mathrm{Gd} + \mathrm{Gbg} \xrightarrow{k_{gd}} \mathrm{G}$	Reassociation of Gα & Gβγ
7	$\mathrm{Yck} + \mathrm{R} + (\mathrm{G}) \xrightarrow{k_{i0}} \mathrm{Yck}$	Yck1/2-stimulated internalization of inactive receptors and heterotrimeric G protein[a]
8	$\mathrm{Yck} + \mathrm{RL} + (\mathrm{G}) \xrightarrow{k_{i1}} \mathrm{Yck}$	Yck1/2-stimulated internalization of active receptors and heterotrimeric G protein[a]
9	$\mathrm{Gbg} \underset{k_{bpd}}{\overset{k_{bp0}}{\rightleftharpoons}} \mathrm{GbgP}$	Phosphorylation & dephosphorylation of Gβγ
10	$\mathrm{GbgP} + \mathrm{Yck} \underset{k_{ya}}{\overset{k_{yi}}{\rightleftharpoons}} \mathrm{YckGb}$	Association/disassociation of $G\beta^{P}\gamma$ and Yck1
11	$\mathrm{GbgP} + \mathrm{Fus3} \xrightarrow{k_{fa}} \mathrm{GbgP} + \mathrm{Fus3A}$	Activation of Fus3 by $G\beta^{P}\gamma$
12	$\mathrm{Fus3A} \xrightarrow{k_{fd}} \mathrm{Fus3}$	Deactivation of Fus3
13	$\mathrm{Fus3A} + \mathrm{Gbg} \xrightarrow{k_{bp1}} \mathrm{Fus3A} + \mathrm{GbgP}$	Phosphorylation of Gβ by active Fus3
14	$\mathrm{Ga} + \mathrm{Fus3A} + \mathrm{Gbg} \xrightarrow{k_{bp2}} \mathrm{Ga} + \mathrm{Fus3A} + \mathrm{GbgP}$	Gα recruitment of active Fus3 to phosphorylate Gβ

[a]The stoichiometry of the internalized receptor and heterotrimeric G protein is assumed to be 1:1.

Table VI: Partial differential equations.

Eq #	Equation
1	$\frac{\partial[\mathrm{R}]}{\partial t} = D\nabla^2[\mathrm{R}] + k_{rs} - k_{rl}[\mathrm{R}][\mathrm{L}] + k_{rlm}[\mathrm{RL}] - k_{i0}[\mathrm{Yck}][\mathrm{R}]$
2	$\frac{\partial[\mathrm{RL}]}{\partial t} = D\nabla^2[\mathrm{RL}] + k_{rl}[\mathrm{R}][\mathrm{L}] - k_{rlm}[\mathrm{RL}] + k_{i1}[\mathrm{Yck}][\mathrm{RL}]$
3	$\frac{\partial[\mathrm{G}]}{\partial t} = D\nabla^2[\mathrm{G}] + k_{gs} + k_{gd}[\mathrm{Gd}][\mathrm{Gbg}] - k_{ga}[\mathrm{G}][\mathrm{RL}] - k_{i0}[\mathrm{Yck}][R] - k_{i1}[\mathrm{Yck}][\mathrm{RL}]$
4	$\frac{\partial[\mathrm{Ga}]}{\partial t} = D\nabla^2[\mathrm{Ga}] + k_{ga}[\mathrm{G}][\mathrm{RL}] - k_{gad}[\mathrm{Ga}]$
5	$\frac{\partial[\mathrm{Gd}]}{\partial t} = D\nabla^2[\mathrm{Gd}] + k_{gad}[\mathrm{Ga}] - k_{gd}[\mathrm{Gd}][\mathrm{Gbg}]$
6	$\frac{\partial[\mathrm{Gbg}]}{\partial t} = D\nabla^2[\mathrm{Gbg}] + k_{ga}[\mathrm{G}][\mathrm{RL}] - k_{gd}[\mathrm{Gd}][\mathrm{Gbg}] + k_{bpd}[\mathrm{GbgP}] - k_{bp0}[\mathrm{Gbg}] - k_{bp1}[\mathrm{Fus3A}][\mathrm{Gbg}] - k_{bp2}[\mathrm{Ga}][\mathrm{Fus3A}][\mathrm{Gbg}]$
7	$\frac{\partial[\mathrm{GbgP}]}{\partial t} = D\nabla^2[\mathrm{GbgP}] - k_{bpd}[\mathrm{GbgP}] + k_{bp0}[\mathrm{Gbg}] + k_{bp1}[\mathrm{Fus3A}][\mathrm{Gbg}] + k_{bp2}[\mathrm{Ga}][\mathrm{Fus3A}][\mathrm{Gbg}] - k_{yi}[\mathrm{Yck}][\mathrm{GbgP}] + k_{ya}[\mathrm{YckGbgP}]$
8	$\frac{\partial[\mathrm{Yck}]}{\partial t} = D\nabla^2[\mathrm{Yck}] - k_{yi}[\mathrm{Yck}][\mathrm{GbgP}] + k_{ya}[\mathrm{YckGbgP}]$
9	$\frac{\partial[\mathrm{YckGbgP}]}{\partial t} = D\nabla^2[\mathrm{YckGbgP}] + k_{yi}[\mathrm{Yck}][\mathrm{GbgP}] - k_{ya}[\mathrm{YckGbgP}]$
10	$\frac{\partial[\mathrm{Fus3}]}{\partial t} = D\nabla^2[\mathrm{Fus3}] + k_{fd}[\mathrm{Fus3A}] - k_{fa}[\mathrm{GbgP}][\mathrm{Fus3}]$
11	$\frac{\partial[\mathrm{Fus3A}]}{\partial t} = D\nabla^2[\mathrm{Fus3A}] - k_{fd}[\mathrm{Fus3A}] + k_{fa}[\mathrm{GbgP}][\mathrm{Fus3}]$

2.3 Results

2.3.1 Yck1 interacts with Gβ but has a lesser interaction with $G\beta^{P-}$

In Suchkov et al., 2010, we proposed that the receptor polarizes by activating a downstream component that protects it from internalization. This results in differential internalization of the receptor in response to pheromone, and establishes a polarity site on the PM marked by receptors protected from internalization. A possible candidate for the downstream component is Gβ, which we have found interacts with Yck1. Here we characterized the interaction between Gβ and Yck1.

The Gβ-Yck1 interaction was identified in an allele-specific genetic screen for proteins that interact directly with Gβ (Bar et al., 2003). We overexpressed Gβ and looked for proteins that, when co-overexpressed with Gβ, are able to rescue the lethality of Gβ overexpression, but not a mutated form of Gβ (Bar et al., 2003). In the genetic screen, co-overexpression of Yck1 was found to rescue lethality, indicating a genetic interaction (Fig. 4A, top).

Figure 4. Gβ interacts with Yck1 at the plasma membrane and is a potential Yck substrate.

(A) Cells induced to co-overexpress Gβ and Yck1 (top) or $G\beta^{P-}$ and Yck1 (bottom) were spotted in 10-fold serial dilutions and assayed for growth. (B) Myc-Yck1 binds to a Gβγ column (NWY068) 10.3- (L) and 2.4-fold (H) more than the negative control column (NWY071). Myc-Yck1 binds to a Gβγ column (NWY068) 1.9- (L) and 2.3-fold (H) more than to a $G\beta^{P-}\gamma$ column (NWY069). Myc-Yck1 binding was determined by subtracting the background binding in the negative control column (NWY071). H indicates high (900µg) myc-Yck1 input and L indicates low (225µg) myc-Yck1 input. (C) Localization of Gβ-Yck1 interaction was visualized *in vivo* using BiFC. Membrane localization of fluorescence in pheromone-treated cells prior to morphogenesis (top) and after shmoo formation (bottom). PM localization was quantified by dividing the mean PM fluorescence by the mean cytoplasmic fluorescence to obtain the mean PM/mean Cyto ratio (PM/Cyto ratio). Cells co-expressing Gβ-VF2 and VF1-Yck1 had a significantly higher PM fluorescence localization compared to the control strain co-expressing Gβ-VF2 and empty-VF1 (The average mean PM/mean Cyto ratios ± SEM for cells co-expressing Gβ-VF2 and VF1-Yck1 and cells co-expressing Gβ-VF2 and empty-VF1 were 1.46 ± 0.09 and 0.95 ± 0.03, respectively. $p < 0.0001$; $n \geq 19$). (D) Western blot analysis of *yck1*Δ *yck2*^{ts} cells assayed for pheromone-induced phosphorylation of Gβ at the permissive (RT) and restrictive (37°C) temperatures. – , L, H indicates no α-factor, 150 nM α-factor, and 1.2 µM α-factor, respectively. (E) Phospho-map of Gβ 317-337 region. Blue indicates sites identified by mass spec analysis only (T318); Red indicates sites identified by both genetic analysis and mass spec analysis (T320, T335); Green indicates sites identified by genetic analysis only (T322). Arrows indicate putative MAPK and CKI (YCK) sites.

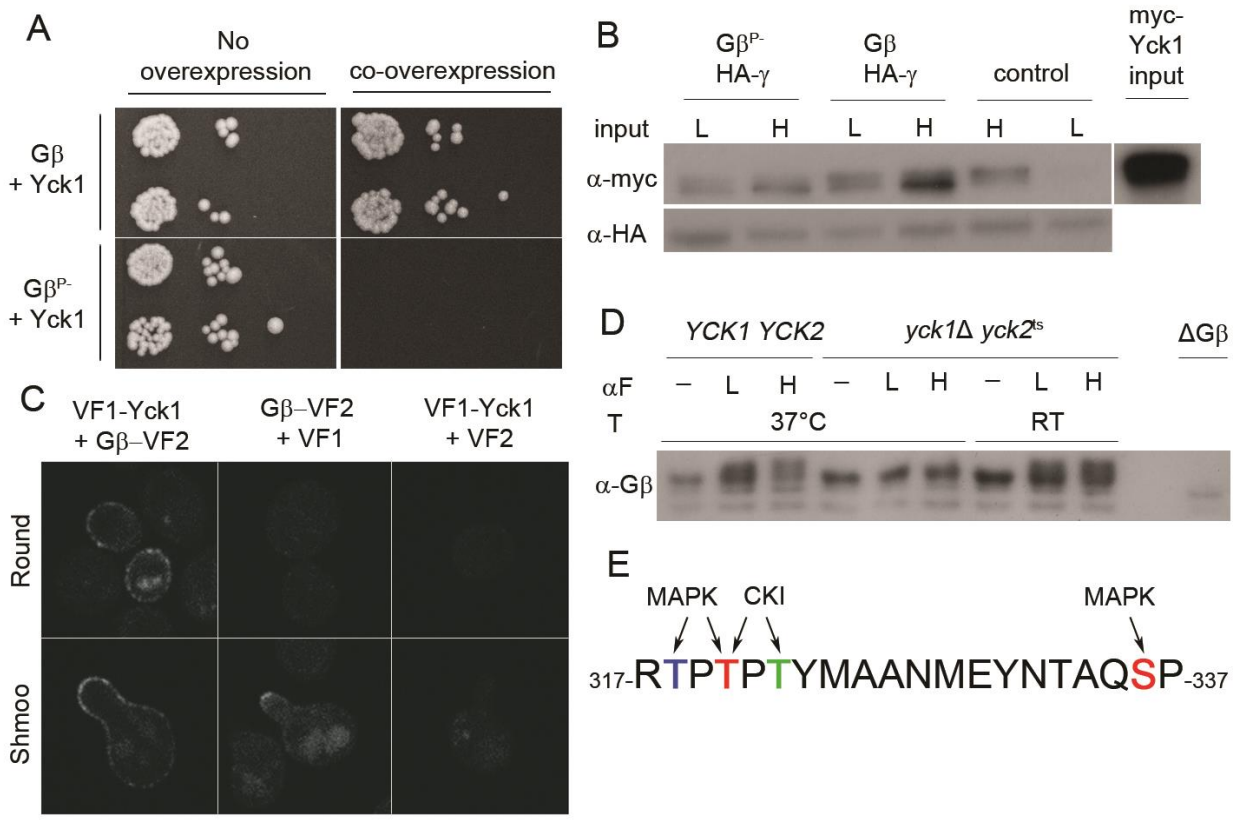
A
No overexpression
co-overexpression
Gβ + Yck1
GβP- + Yck1
B
GβP- HA-γ
Gβ HA-γ
control
myc-Yck1 input
input
L
H
L
H
H
L
α-myc
α-HA
C
VF1-Yck1 + Gβ–VF2
Gβ–VF2 + VF1
VF1-Yck1 + VF2
Round
Shmoo
D
YCK1 YCK2
yck1Δ yck2ts
ΔGβ
αF
–
L
H
–
L
H
–
L
H
T
37°C
RT
α-Gβ
E
MAPK
CKI
MAPK
317-RTPTPTYMAANMEYNTAQSP-337

To test for interaction between Gβ and Yck1, we assayed the ability of myc-Yck1 to bind to a Gβγ column (Fig. 4B). Lysate from cells overexpressing 3xHA-tagged Gγ and Gβ was bound to anti-HA beads to form the Gβγ column. Lysate from cells overexpressing myc-Yck1 was incubated with the Gβγ-bound beads and myc-Yck1 binding was confirmed by immunoblotting. Approximately 10.3- (L) and 2.4-fold (H) more myc-Yck1 bound the Gβγ column than the negative control column. These results support the interaction between Gβ and Yck1 identified in the genetic interaction assay.

To determine where and when Gβ and Yck1 interact in pheromone-treated cells, we used the Split-Venus BiFC assay (Remy et al., 2004) (Fig. 4C). Venus Fragment 1 (VF1) was fused to the N-terminus of Yck1 and Venus Fragment 2 (VF2) was fused to the C-terminus of Ste4, both under the control of the *ADH1* promoter. Because constitutive overexpression of Gβ induces permanent cell cycle arrest by activating the mating response, we assayed the Gβ-VF2 and VF1-Yck1 Split-Venus interaction in *ste7*Δ::*KanMX* YCplac22/*GAL1-STE7* cells, which allows for conditional activation of the mating pathway. Cells were cultured in glucose medium to repress Ste7-dependent signaling, and switched to galactose medium to induce Ste7 expression shortly before pheromone treatment. The Gβ-VF2 + VF1-Yck1 BiFC signal was detectable on the PM of isotropic pheromone-treated cells prior to morphogenesis (Fig. 4C, top) and concentrated on the PM of mating projections in shmooing cells (Fig. 4C, bottom). Although some fluorescence was detected at the tips of shmooing cells expressing only Gβ-VF2 + VF1 (Fig. 4C, middle column), it was qualitatively and quantitatively distinguishable from the signal generated by Gβ-VF2 + VF1-Yck1 interaction (Table VII). When the PM signal of Gβ-VF2 + VF1-Yck1 cells was normalized to the

cytoplasmic signal (PM/Cyto), they had a significantly higher ratio compared to Gβ-VF2 + VF1 cells (Table VII). Additionally, when the fraction of the PM containing a 25% greater signal compared to the cytoplasmic mean was quantified, the Gβ-VF2 + VF1-Yck1 cells had significantly more fluorescence on the PM compared to Gβ-VF2 + VF1 cells (Table VII). This background fluorescence in the Gβ-VF2 + VF1 negative control strain is attributable to high expression from the *ADH1* promoter coupled with highly localized secretion to the tip of the mating projection.

Table VII: Quantification of BiFC results

	% cells with PM signal[a]		PM/Cyto ± SEM[b]		% PM ± SEM ≥ 1.25X Cyto[c]	
	Pre-shmoo	Shmooed	Pre-shmoo	Shmooed	Pre-shmoo	Shmooed
Gβ-VF2 + VF1-Yck1	28.5	15.2	n.d.	1.46 ± 0.09	n.d.	50.5 ± 5.4
Gβ-VF2 + VF1	3.4	27.4	n.d.	0.95 ± 0.03	n.d.	17.0 ± 1.9
Statistical comparison	$n \geq 72$	$n \geq 45$		$p < 0.0001$; $n \geq 19$		$p < 0.0001$; $n \geq 19$

No background signal was seen in the Gβ-VF2+VF1 negative control cells. Detectable fluorescence was observed on the tips of a significant fraction of the shmooing Gβ-VF2 +VF1-Yck1 negative control cells. This is attributable to the direct, irreversible interaction between the VF1 and VF2 fragments (Bendezu and Martin, 2011), where they are concentrated together by directed secretion, and is clearly distinguishable from the Gβ-VF2/VF1-Yck1 interaction signal by the measures shown here. [a]Cells with clear PM signal were scored by eye. [b]The PM signal was normalized to the cytoplasmic signal in each cell by dividing the mean PM fluorescence by the mean cytoplasmic fluorescence. [c]The fraction of the PM showing a signal at least 25% greater than the mean cytoplasmic signal in each cell was determined.

Gβ is rapidly phosphorylated in response to pheromone (Cole and Reed, 1991), and full phosphorylation of Gβ requires the activity of the MAPK, Fus3 (Li et al., 1998). It was previously shown that GβΔ$^{310\text{-}346}$ (*ste4*Δ$^{310\text{-}346}$) abolished pheromone-induced Gβ phosphorylation (Cole and Reed, 1991). In a directed screen, within the Ste4 310-346 region to isolate mutant forms of Ste4 that cannot be phosphorylated, *ste4*$^{T320A\ S335A}$ was identified, and analysis of strains carrying this mutation suggested that Gβ phosphorylation did not affect signaling to the nucleus or adaptation (Li et al., 1998). It has been shown that some CKI proteins prefer substrates that have already been phosphorylated within the consensus sequence (Flotow et al., 1990, Flotow and Roach, 1989, Meggio et al., 1979). The CKI recognition motif for hierarchal substrate phosphorylation is –S(P)/T(P)-$X_{n(1\text{-}3)}$-S/T- (Flotow et al., 1990, Flotow and Roach, 1989, Meggio et al., 1979). Analysis of the Gβ 310-346 region revealed that Gβ contains a CKI consensus sequence. Because CKI proteins prefer to have their substrates phosphorylated, we asked whether Gβ phosphorylation affected the interaction with Yck1 using the double mutant form of Gβ that cannot be phosphorylated, *ste4*$^{T320A\ S335A}$ (hereafter, Gβ^{P-}). We tested the ability of Gβ^{P-} to interact with Yck1 in the genetic interaction assay and found that co-overexpression of Yck1 with Gβ^{P-} did not rescue the lethality of Gβ^{P-} overexpression (Fig. 4A, bottom), consistent with the idea that Gβ^{P-} interacts less well with Yck1. We also tested the ability of myc-Yck1 to bind to a Gβ^{P-}γ column, and as suggested by the genetic data, we found that myc-Yck1 had a 1.9- (L) and 2.4-fold (H) lower binding to the Gβ^{P-}γ column compared to the Gβγ column (Fig. 4B). Together, these results suggest that Gβ^{P-} interacts less well with Yck1 than does Gβ.

2.3.2 Full Gβ phosphorylation requires Yck activity, and Gβ is phosphorylated within the CKI motif

Because Gβ is rapidly phosphorylated in response to pheromone (Cole and Reed, 1991), contains a CKI phosphorylation motif within the phosphorylation domain, and interacts directly with Yck1, we asked whether Yck activity is required for Gβ phosphorylation. Pheromone-induced Gβ phosphorylation can be detected on immunoblots. In vegetative cells, Gβ is predominately in the unphosphorylated form (Fig. 4D). Upon treatment with pheromone, Gβ shifts to multiple slower migrating bands corresponding to different phospho-species of the protein (Fig. 4D). To determine whether full phosphorylation of Gβ requires Yck activity, we used the *yck1*Δ*yck2-2*^{ts} temperature sensitive strain and assayed the Gβ shift in response to pheromone. We were able to detect full phosphorylation of Gβ at the permissive temperature (RT) (Fig. 4D) but not the restrictive temperature (37°C) (Fig. 4D). The Gβ kinases are not inhibited by high temperature, as pheromone induced full phosphorylation of Gβ in the isogenic *YCK1YCK2* strain at 37°C (Fig. 4D). These data indicate that Yck activity is required for full phosphorylation of Gβ.

Because full phosphorylation of Gβ requires Yck activity, we asked whether pheromone induces phosphorylation of the residues in the CKI motif (-S(P)/T(P)-$X_{n(1-3)}$-S/T-) (Flotow et al., 1990, Flotow and Roach, 1989, Meggio et al., 1979). Genetic analyses suggested that Gβ residues T320, T322, and S335 are phosphorylated (Fig. 4E) and that full Gβ phosphorylation is dependent on the pheromone-responsive MAPK, Fus3 (Li et al., 1998). Mass spec analysis of Gβ phospho-peptides purified from pheromone-treated cells overexpressing Gβγ confirmed

T320 and S335 as phosphorylation sites (Fig. 5) and revealed one more, T318 (Fig. 4E,5A-D). These data are consistent with Gβ being a CKI substrate, as both T320 and T322 are potential CKI phosphorylation sites.

Figure 5. Gβ phosphorylation analysis by mass spectrometry.
Heavy-labeled cells overexpressing Gβγ were treated with 150 nM of α-factor for 1 hour, harvested, and analyzed by mass spectrometry to identify sites of pheromone-induced phosphorylation. (A) CID spectrum of a doubly-phosphorylated peptide locating the phosphates at S335 (for certain) and either of T318 or T320: diagnostic fragment ions for S335 are y_5 and y_6, and for S318/S320 is b_3 (indicated with arrowheads). Andromeda score is 110. (B) High-resolution HCD (high-collision energy dissociation) spectrum of the singly-phosphorylated peptide locating the phosphates at T320: diagnostic ions are b_2 and b_3 (indicated with arrowheads). The Andromeda score is 116. (C) CID spectrum of a doubly-phosphorylated peptide locating the phosphates at T318 and T320: diagnostic fragment ions are b_5, b_6, and b_8 (indicated with arrowheads). The Andromeda score is 115. (D) High-resolution HCD (high-collision energy dissociation) spectrum of the singly-phosphorylated peptide locating the phosphates at T320: diagnostic fragment ions are b_2 and b_3 (indicated with arrowheads). The Andromeda score is 81.

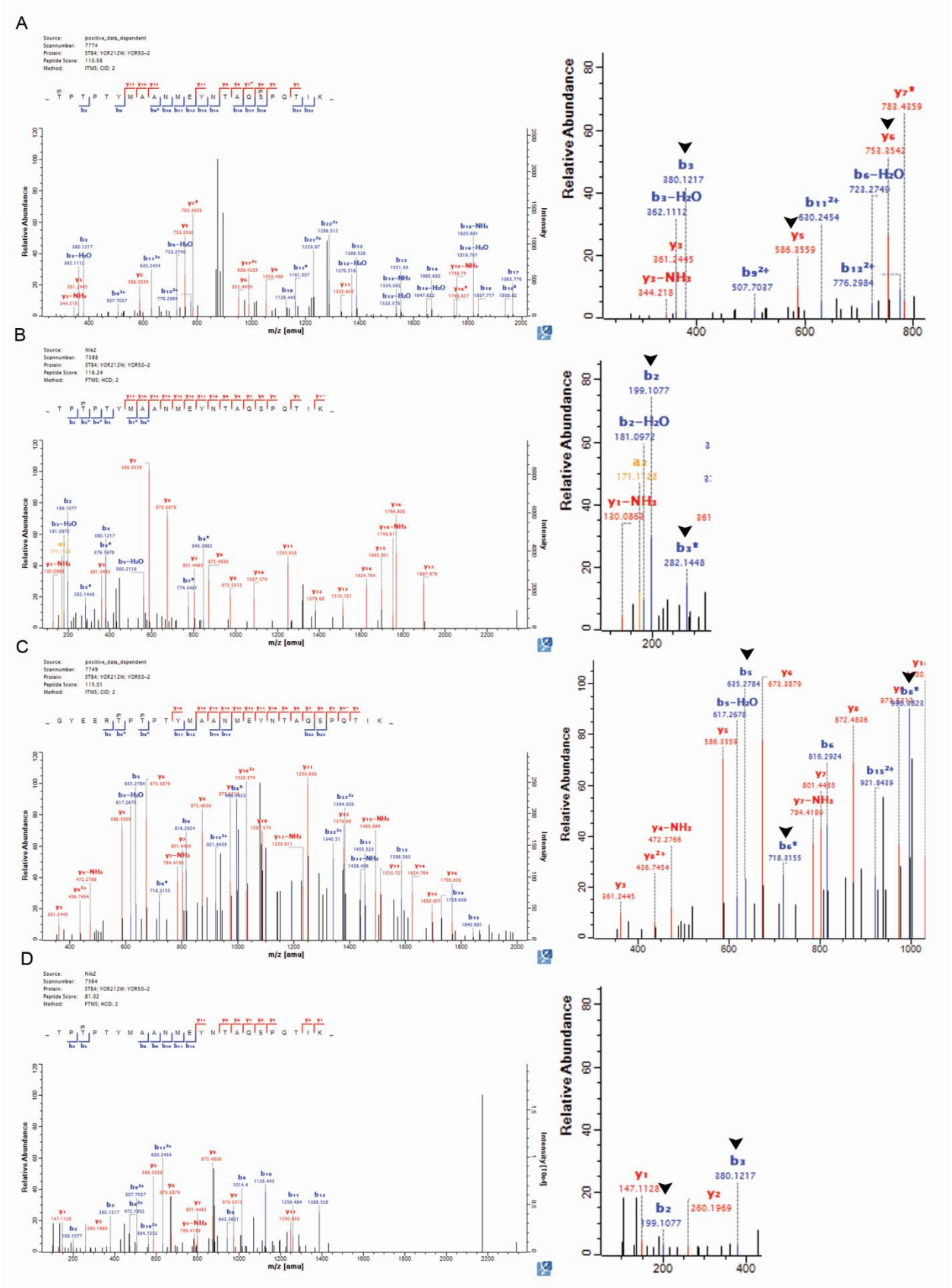
A
B
C
D
Relative Abundance
m/z [amu]
Intensity

2.3.3 Gβ, but not $G\beta^{P-}$, increases the proportion and polarity of unphosphorylated receptor in the absence of F-actin

Pheromone binding induces a conformational change in the receptor that exposes its C-terminus to Yck-dependent phosphorylation (Hicke et al., 1998). C-terminal phosphorylation of the receptor triggers its subsequent ubiquitination and internalization (Hicke et al., 1998). In the absence of Yck activity, the receptor is not phosphorylated (Hicke et al., 1998) and therefore, is not internalized, which means it cannot polarize (Suchkov et al., 2010). It has been shown that the DEP domains of Sst2 bind specifically to the C-terminal cytosolic tail of the unphosphorylated receptor (Ballon et al., 2006). Sst2 is a regulator of G protein signaling (RGS) protein and is a GAP for Gα (Apanovitch et al., 1998, Dohlman et al., 1996, Dohlman and Thorner, 1997, Ross and Wilkie, 2000). In this study, the authors constructed a strain with a receptor that is mutated such that it is unable to be internalized (*Ste2*^{7XR}) and, therefore, the receptor does not polarize in response to pheromone (Ballon et al., 2006). Because they showed that Sst2-GFP binds specifically to unphosphorylated receptor (Ballon et al., 2006), this allows us to use the strain as a receptor phosphorylation assay (RPA) strain to visualize unphosphorylated receptor. Consistent with our model, in response to pheromone, Sst2-GFP polarized to the PM of the mating projection (Ballon et al., 2006). In Ballon et al., 2006, they attributed Sst2-GFP localization in the mating projection to newly synthesized receptor that hadn't yet been phosphorylated (Ballon et al., 2006). However, in a recently published paper, we showed that in the absence of actin-dependent directed secretion, Sst2-GFP is still able to polarize (Fig. 6A, top) (Suchkov et al., 2010). This suggests that the receptor is asymmetrically

phosphorylated in response to pheromone, which would lead to asymmetric receptor internalization. Because Gβ polarizes at the growth site prior to morphogenesis (DeFlorio et al., 2013), this lead us to postulate that Gβ interacts with Yck1 to locally inhibit receptor phosphorylation.

To determine if Gβ plays a role in the phosphorylation state of the receptor in response to pheromone, we overexpressed Gβ in the RPA strain and used Sst2-GFP as a reporter of unphosphorylated receptor. We induced Gβ or $G\beta^{P-}$ overexpression in G1-synchronized cells for 1 hour, then treated the cells with isotropic pheromone and LatA (0'), and followed Sst2-GFP localization over time (Fig. 6A, middle and bottom). Because Sst2 is a negative regulator of the pheromone response (Apanovitch et al., 1998, Dohlman et al., 1996), overexpression of both Gβ and $G\beta^{P-}$ induces expression of Sst2-GFP. To control for pheromone induced Sst2 expression, we normalized Sst2-GFP by dividing the mean PM Sst2-GFP signal by the mean cytoplasmic Sst2-GFP signal (PM/Cyto ratio). In response to pheromone, cells overexpressing Gβ had significantly more PM localized Sst2-GFP (Fig. 6B) and were significantly more polarized (Fig. 6C) compared to cells not overexpressing Gβ and cells overexpressing $G\beta^{P-}$ (Fig. 6B,C). The observed increase in polarity may be due to the cell cycle localization of Gβ at the presumptive default shmoo site (DeFlorio et al., 2013). Using Sst2-GFP as a reporter for unphosphorylated receptor, this suggests that Gβ expression leads to polarization of unphosphorylated receptor and more unphosphorylated receptor on the PM, but $G\beta^{P-}$ expression does not. This is consistent with Gβ protecting the receptor from phosphorylation at a discrete region on the PM, and this protection is dependent on the interaction between Gβ and Yck1.

Figure 6. Local inhibition of receptor phosphorylation by Gβγ helps establish the chemotropic growth site.

(A to C) Gβ overexpression inhibits receptor phosphorylation and augments its polarity in pheromone- and LatA-treated cells.
(A) Representative images of cells expressing the native level of Gβ, excess Gβ, or excess $G\beta^{P-}$, treated with pheromone and LatA at time 0. The intensity of the Sst2-GFP signal on the PM corresponds to the location and quantity of unphosphorylated receptor. Arrowheads indicate polarized Sst2-GFP crescents. ↑↑ indicates overexpression. (B) Sst2-GFP localization to the PM was normalized to reporter expression by dividing the mean PM by the mean cytoplasm fluorescence in each cell. The graph shows the mean PM/cytoplasmic ratios ± SEM at the indicated time points. *p* values were calculated relative to Gβ↑↑. **p* < 0.04; ** *p* < 0.01; † *p* ≤ 0.0001; *n* ≥ 20 for each strain and time point. (C) The degree of Sst2-GFP polarization on the PM of each cell is indicated by the Polarity Index (PI), which was determined by dividing the mean fluorescence on the brightest 1/3rd of the PM by the mean signal on the rest of the PM. The graph shows the mean PIs ± SEM. *p* values were calculated relative to Gβ↑↑. * *p* < 0.02; ** *p* = 0.0016; †*p* = 0.0003; *n* ≥ 20 for each strain and time point. In (B) and (C), the graphs represent two trials for the control strain, and three trials for the Gβ↑↑ and $G\beta^{P-}$↑↑ strains. (D) Time-lapse images of mating cells showing the Sst2-GFP reporter moving from the presumptive default polarity site to the chemotropic site, where cell fusion ultimately occurs. The degree of movement is described by the switch angle (yellow arc). Mean switch angles ± SEM were 82.6 ± 8.2 for the control cells and 52.2 ± 7.9 for $G\beta^{P-}$ cells in two trials of each. *p* < 0.01; *n* ≥ 34.

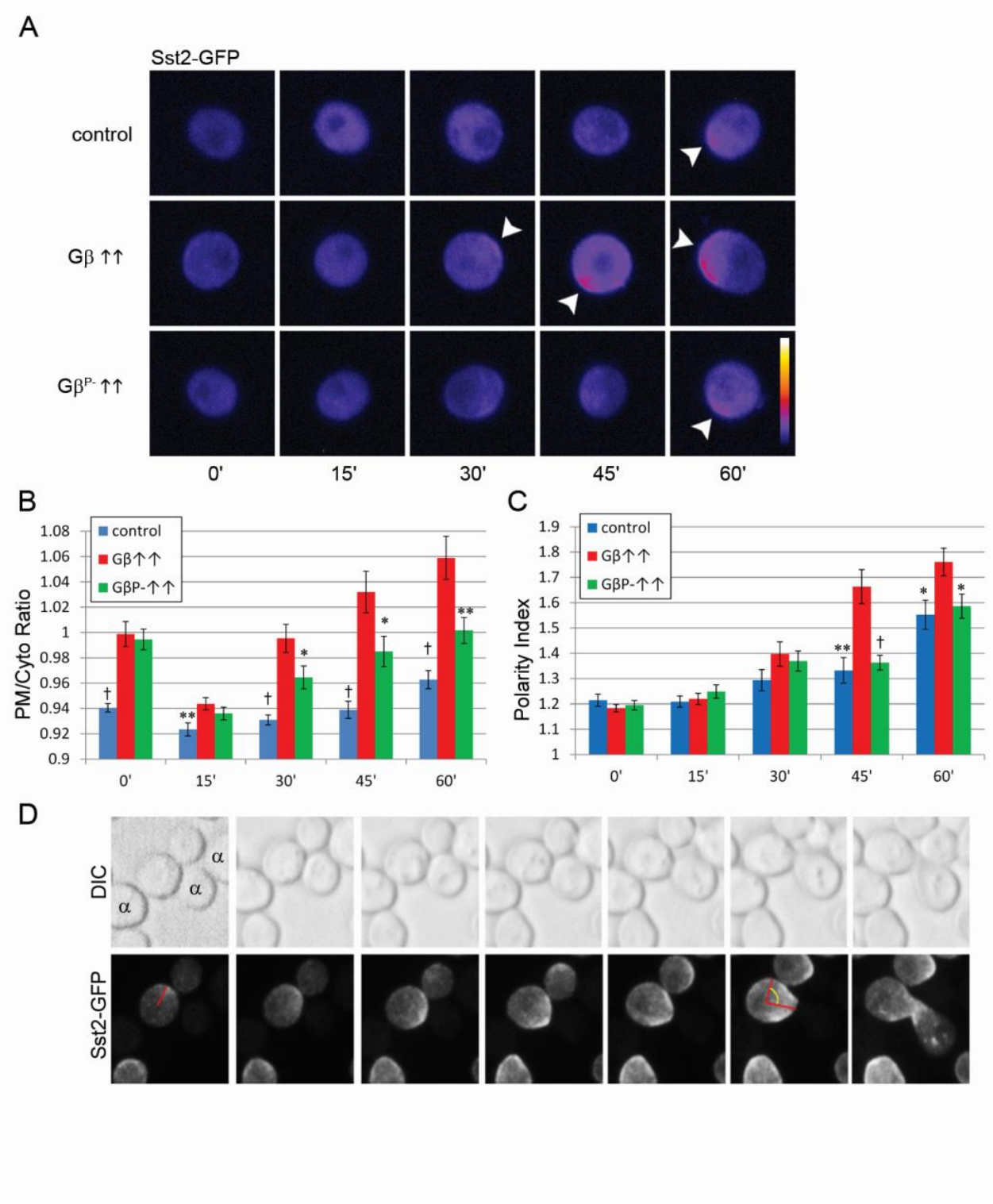
A
Sst2-GFP
control
Gβ ↑↑
Gβ^P- ↑↑
0'
15'
30'
45'
60'
B
PM/Cyto Ratio
control
Gβ↑↑
GβP-↑↑
C
Polarity Index
control
Gβ↑↑
GβP-↑↑
D
DIC
Sst2-GFP

2.3.4 Unphosphorylated receptor crescents localize where Gβ cells will form the mating projection in mating mixtures, but $G\beta^{P-}$ cells are defective

We are able to visualize polarization of the patch of unphosphorylated receptor in the absence of actin-dependent directed secretion in cells exposed to a uniform concentration of pheromone (Fig. 6A, top) (Suchkov et al., 2010). This led us to ask whether the localization of the unphosphorylated receptor patch is directional. To examine receptor phosphorylation in cells responding to a gradient of pheromone, we used the RPA strain and followed Sst2-GFP in mating mixtures when the cells are exposed to natural pheromone gradients from *MAT*α cells (Fig. 6D). In mating mixtures, RPA cells had a patch of concentrated Sst2-GFP at the presumptive default shmoo site (Fig. 6D). Over time, the patch appears to relocate or 'move' from the initial site to the chemotropic growth site where the mating projection formed (Fig. 6D). Pheromone binding the receptor induces the receptor to change its conformation exposing the receptor C-terminus to Yck-dependent phosphorylation. Therefore, we would expect to see more phosphorylation on the side of the cell closest to the pheromone gradient where there is more activated receptor. Instead, we see a concentration of unphosphorylated receptor at the incipient growth site. In contrast, RPA cells expressing $G\beta^{P-}$ were defective in 'moving' the initial patch of Sst2-GFP from the presumptive default site to the chemotropic site. The degree of Sst2-GFP 'movement' was quantified by measuring the angle between the initial Sst2-GFP site to where it 'moved' along the PM to form the mating projection (switch angle). Cells expressing $G\beta^{P-}$ had a significantly smaller average switch angle compared to cells expressing Gβ (52.2 ± 7.9 and 82.6 ± 8.2, respectively; $p < 0.01$; $n \geq 34$). These results suggest that

the interaction between Gβ and Yck1 is important for establishment of the chemotropic growth site.

2.3.5 $G\beta^{P-}$ cells are defective in receptor polarization in the absence of F-actin

In vegetative cells, the receptor is distributed uniformly on the membrane. In response to isotropic pheromone treatment, the receptor is rapidly internalized and disappears from the PM, later reappearing as a polarized crescent and remains polarized within the mating projection (Ayscough and Drubin, 1998, Moore et al., 2008, Suchkov et al., 2010). It was initially thought that receptor polarization in response to pheromone was due to actin-dependent directed secretion of the receptor to the growth site. However, we showed that the receptor can polarize in the absence of actin-dependent directed secretion but that receptor polarization requires receptor internalization (Suchkov et al., 2010). In Suchkov et al., 2010, we showed that if you treat cells with isotropic pheromone for 15 minutes and allow the receptor to internalize and then block actin-dependent directed secretion by the addition of LatA, the receptor is still able to polarize (Fig. 7A, top). It was proposed that during the first 15 minutes of pheromone treatment, when the majority of the receptor is being internalized, a polarity landmark is established. Sahin et al., 2008 proposed that in the absence of F-actin, a pre-existing polarity landmark can be amplified by biased docking and fusion of secretory vesicles to that site. Therefore, in the absence of F-actin, Ste2-GFP may polarize by amplifying a pre-existing polarity landmark that was established during global receptor internalization, resulting in polarization of the receptor over time.

Figure 7. $G\beta^{P-}$ cells are defective in receptor polarization.
(A and B) Isotropic conditions. Gβ and $G\beta^{P-}$ cells expressing the receptor reporter, Ste2-GFP, were treated with pheromone at time 0 and with LatA after global receptor internalization (15'). (A) Representative images. Arrowheads indicate Ste2-GFP crescents. (B) Polarity Indices were measured as in Fig. 2C. The graph shows mean PIs ± SEM representing three trials for each strain. p values represent the comparison of Gβ and $G\beta^{P-}$ cells within the time point. * $p < 0.03$; $n \geq 30$ for each strain and time point. (C and D) Mating mixtures. (C) Time-lapse images of mating Gβ and $G\beta^{P-}$ cells showing Ste2-GFP localization. Insets show BudPolarity output (Vernay et al., 2012). BudPolarity uses the sum projection to find the long axis of the cell and quantifies fluorescence intensity along the long axis of the cell. (D) Receptor polarization was quantified using BudPolarity by dividing the peak PM fluorescence by the cell's threshold prior to apparent morphogenesis. The BudPolarity output shown is for the Gβ cell depicted in Fig. 7C, top. The mean polarization values ± SEM were 1.76 ± 0.14 and 1.28 ± 0.07 for Gβ and $G\beta^{P-}$ cells, respectively. $p < 0.007$; $n \geq 17$. Two trials were conducted with each strain.

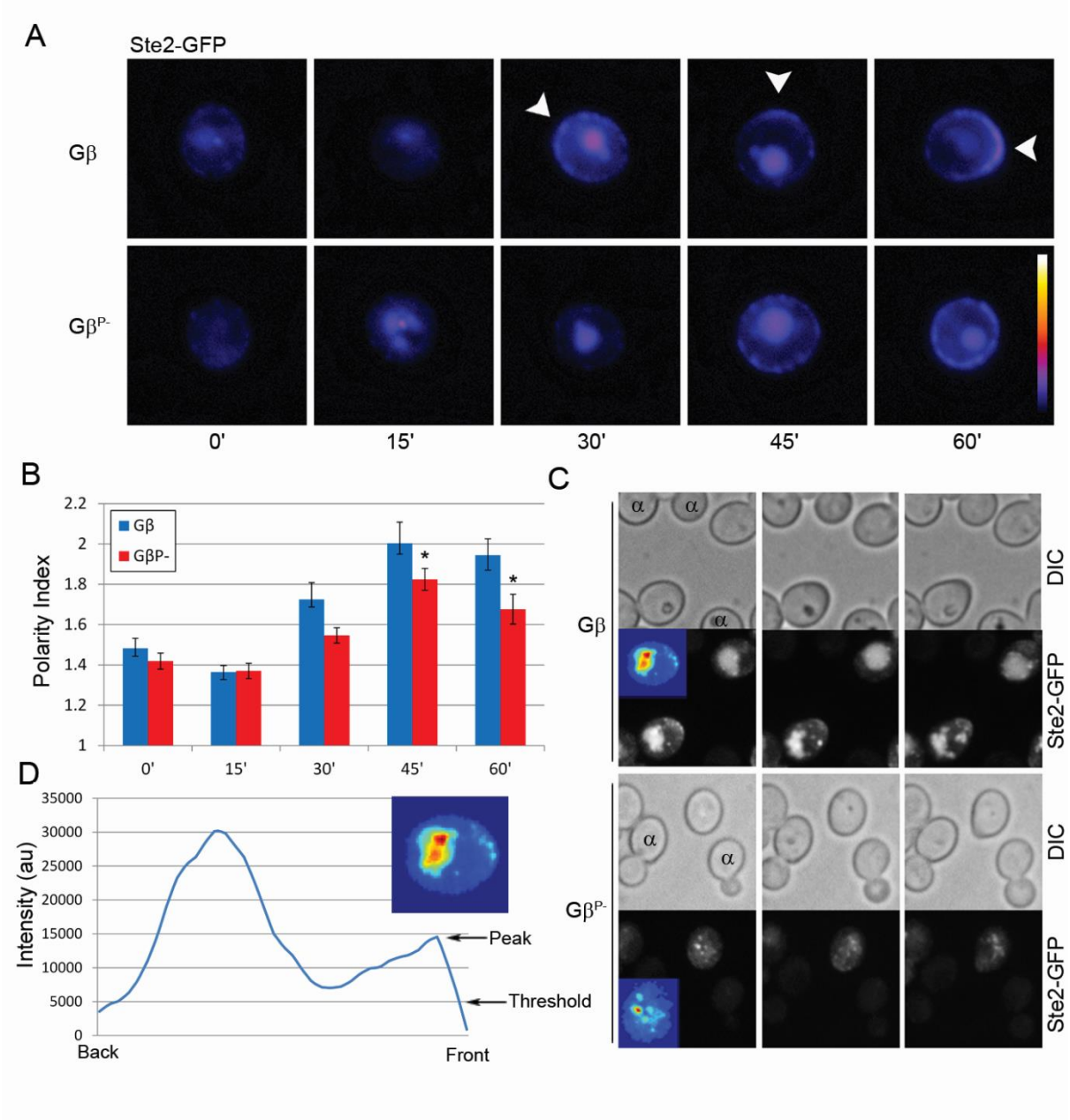
A
Ste2-GFP
Gβ
GβP-
0'
15'
30'
45'
60'
B
Polarity Index
Gβ
GβP-
2.2
2
1.8
1.6
1.4
1.2
1
0'
15'
30'
45'
60'
*
*
C
Gβ
GβP-
α
DIC
Ste2-GFP
D
Intensity (au)
35000
30000
25000
20000
15000
10000
5000
0
Peak
Threshold
Back
Front

To determine if the interaction between Gβ and Yck1 is important for establishment of receptor polarity, we tested the ability of cells expressing $G\beta^{P-}$ to polarize Ste2-GFP in the absence of F-actin. Gβ and $G\beta^{P-}$ G1-synchronized cells were treated with LatA 15 minutes after isotropic pheromone treatment, and Ste2-GFP localization was followed over time (Fig. 7A). To quantify Ste2-GFP polarization on the PM, we measured the PI, which is determined by dividing the mean fluorescence on the brightest 1/3rd of the PM by the mean signal on the rest of the PM (Fig. 7B) (Suchkov et al., 2010). Cells expressing $G\beta^{P-}$ did not polarize Ste2-GFP on the PM in the absence of F-actin as well as Gβ cells, suggesting that the interaction between Gβ and Yck is important for receptor polarity.

2.3.6 In mating mixtures, $G\beta^{P-}$ cells are defective in receptor polarization prior to apparent morphogenesis

In mating mixtures, the receptor polarizes prior to morphogenesis at the incipient mating projection on the side of the cell closest to the potential mating partner (Fig. 7C, top) (Suchkov et al., 2010). Cells expressing $G\beta^{P-}$ have previously been shown to be defective in directional sensing (DeFlorio et al., 2013) and were defective in receptor polarization when treated with isotropic pheromone in the absence of F-actin (Fig. 7A, bottom), so we asked whether Gβ phosphorylation is important for receptor polarization prior to apparent morphogenesis in mating mixtures where the cells are exposed to a natural pheromone gradient from *MAT*α cells. To test this, we imaged Ste2-GFP in cells expressing Gβ and $G\beta^{P-}$ mixed with wild-type *MAT*α cells (Fig. 7C). We quantified Ste2-GFP polarization prior to apparent morphogenesis using BudPolarity (Vernay et al., 2012). BudPolarity uses the sum projection to find the long

axis of the cell and quantifies fluorescence intensity along the long axis of the cell. We divided the peak PM fluorescence by the threshold fluorescence to determine the polarization ratio (Fig. 7D). Cells expressing $G\beta^{P-}$ had a significantly lower average peak ratio compared to cells expressing Gβ. The polarization ratios were 1.76 ± 0.14 (mean ± SEM) and 1.28 ± 0.07 for Gβ and $G\beta^{P-}$ cells, respectively ($p < 0.007$; $n \geq 17$). These results suggest that Gβ phosphorylation is important for receptor polarization prior to morphogenesis in mating mixtures and are consistent with the interaction between Gβ and Yck1 being important for the polarization.

2.3.7 PM receptor can be detected at all time points

Our observation that the receptor is asymmetrically phosphorylated in the absence of actin-dependent directed secretion is consistent with the receptor being asymmetrically internalized. The protected receptor on the PM marks the polarity site where the mating projection will later form. In this case, we would expect to see polarized receptor on the PM at all times during the early pheromone response. However, in response to pheromone, using Ste2-GFP to visualize the receptor, the receptor is rapidly internalized and disappears from the membrane, later reappearing as a polarized crescent. GFP has a 15 minute maturation time (Gordon et al., 2007); therefore, even though we are unable to detect fluorescent receptor at the membrane, there may be newly synthesized receptor on the membrane that hasn't matured, or the receptor fluorescence could be below our ability to detect with GFP. To test whether there was receptor present on the PM during the first 20 minutes of pheromone response, when we are unable to detect Ste2-GFP, we used Alexa Fluor 594-conjugated α-factor to visualize receptor on the PM. Pheromone treated

G1-synchronized cells expressing Ste2-GFP were arrested with Sodium Azide at 5 minute intervals, and cell surface receptors were bound with the fluorescent α-factor. The fluorescent α-factor appears to bind specifically to the receptor as no binding was detected in *ste2*Δ cells (Fig. 8).

Figure 8. Receptor binding of Alexa Fluor 594-conjugated α-factor. Cells expressing *STE2* (DSY257) and *ste2*Δ (EDY208) were incubated with Alexa Fluor 594-conjugated α-factor and imaged for binding.

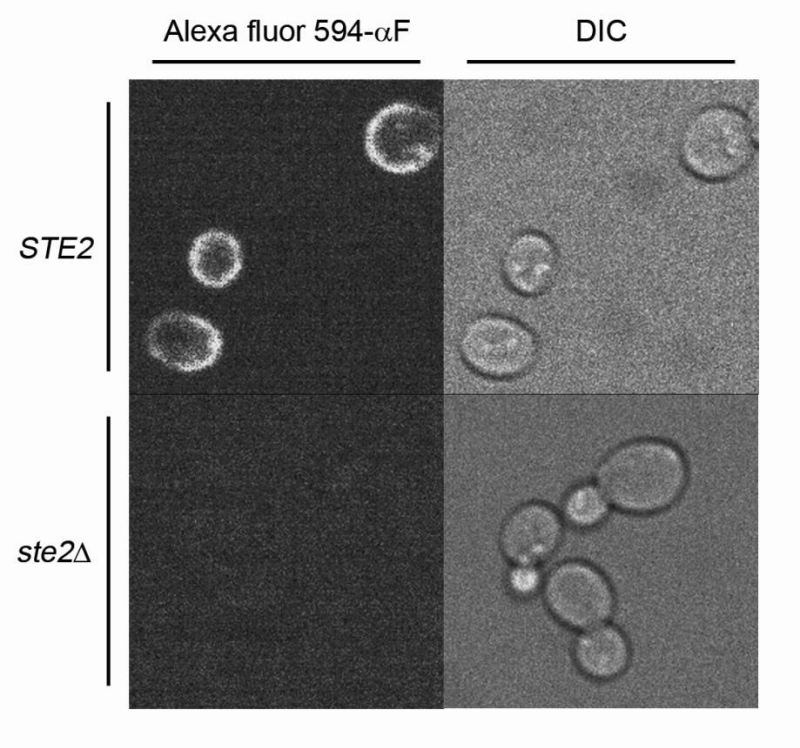
Alexa fluor 594-αF
DIC
STE2
ste2Δ

Prior to pheromone treatment, we were able to detect receptor on the PM with both GFP and Alexa Fluor 594. After pheromone treatment, when the receptor is rapidly internalized, we were unable to detect GFP tagged receptor on the PM (Fig. 9, top). Using Alexa Fluor 594, however, we were able to visualize polarized receptor on the PM at all time points during the first 20 minutes of pheromone treatment (Fig. 9, bottom). Alexa Fluor 594 staining of receptor on the PM after pheromone treatment suggests that the receptor is not completely internalized in response.

Figure 9. Visualization of PM receptor in response to pheromone.
Cells expressing *STE2-GFP* (DMY169) were treated with pheromone and aliquots were incubated with Alexa Fluor 594-conjugated α-factor to visualize PM receptor.

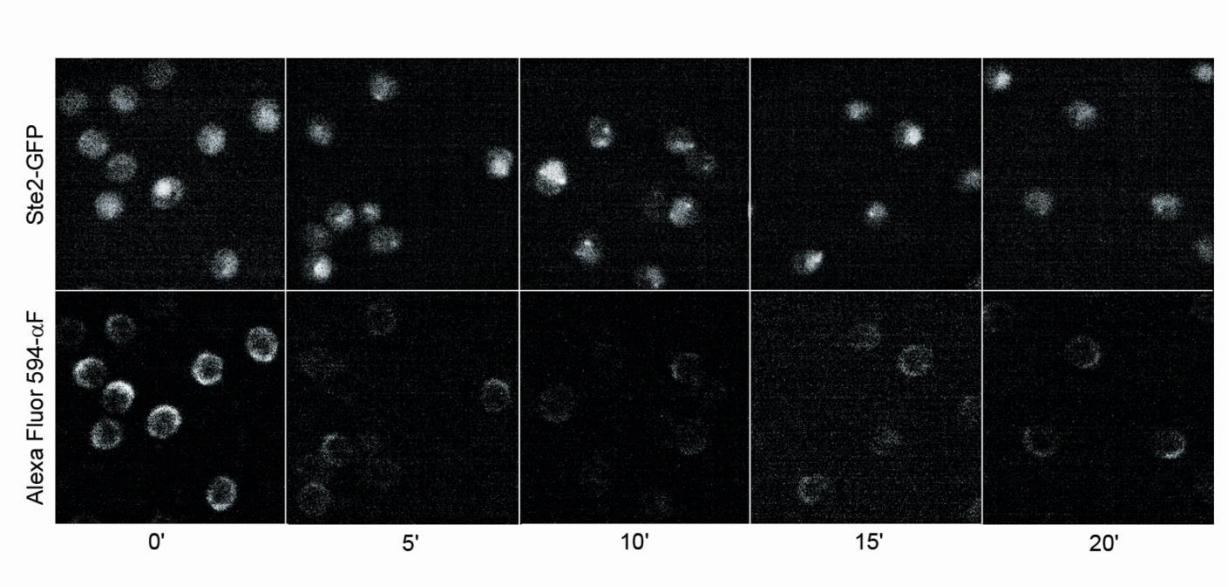
Ste2-GFP
Alexa Fluor 594-αF
0'
5'
10'
15'
20'

2.3.8 A region of receptor on the PM persists longer compared to the rest of the cell in response to pheromone

In response to pheromone, we are able to visualize asymmetric receptor phosphorylation in the absence of actin-dependent directed secretion (Suchkov et al., 2010), which would lead to asymmetric receptor internalization. When cells are treated with pheromone and allowed to internalize the receptor for 15 minutes and then treated with LatA to inhibit actin-dependent directed secretion, the cells are able to form receptor crescents over time (Suchkov et al., 2010). We postulate that during the first 15 minutes when the receptor is being globally internalized, a polarity landmark is established by differential receptor internalization. Using a more sensitive way to visualize receptor on the PM, we were able to detect polarized receptor crescents immediately after pheromone treatment (Fig. 9, bottom). These observations are consistent with the receptor being asymmetrically internalized in response to pheromone. To test this, we bound cell surface receptors with Alexa Fluor 594-conjugated α-factor and followed receptor internalization over time (Fig. 10A). After data smoothing (previously described) (Fig. 10B), loss of PM fluorescence (decay) was determined for every pixel at every time point (Fig. 10C). The protected region was determined by identifying the pixels with the 30% slowest rate of PM fluorescence loss after connecting (previously described) (Fig. 10C, black bar). In 30 out of 49 cells, the loss of PM fluorescence appeared to be asymmetric. When we compared the PM fluorescence loss of the slowest 30% (after connecting) (protected) to the PM fluorescence loss of the rest of the cell (unprotected), the protected region appears to remain constant and the unprotected region appears to decrease (Fig. 10D). These

observations are consistent with the receptor being asymmetrically internalized in response to pheromone.

Figure 10. Receptor distribution in response to pheromone.
(A) Time-lapse of Alexa Fluor 594-conjugated α-factor bound to cell surface receptors. (B) PM fluorescence intensity for all time points after the noise was filtered out by data smoothing as described previously (Fig. 2) for the cell in panel B. (C) The change in PM fluorescence intensity over time compared to time point 0' for the cell in panel B. The blue color denotes there is a net decrease in the position at that time point compared to time point 0, whereas red denotes a net increase. The black bar indicates the protected regions (after connecting). (D) The graph represents the average rate of PM fluorescence loss over time in the pixels with the 30% slowest rate of loss (protected region) and the rest of the cell (unprotected region) of 30 cells. Error bars = SEM (E) Network 1. Without downstream regulation, the rate of receptor internalization decreases uniformly as the number of receptors on the PM decreases. (F) Network 2. Receptor interaction starts off faster at the front of the cell, but this difference inverts within 10 minutes as $G\beta^{P}\gamma$ inhibits Yck. (G) Network 3. Receptor internalization becomes slower at the front of the cell within 5 minutes as Gα recruitment of Fus3 locally enhances phosphorylation of Gβ.

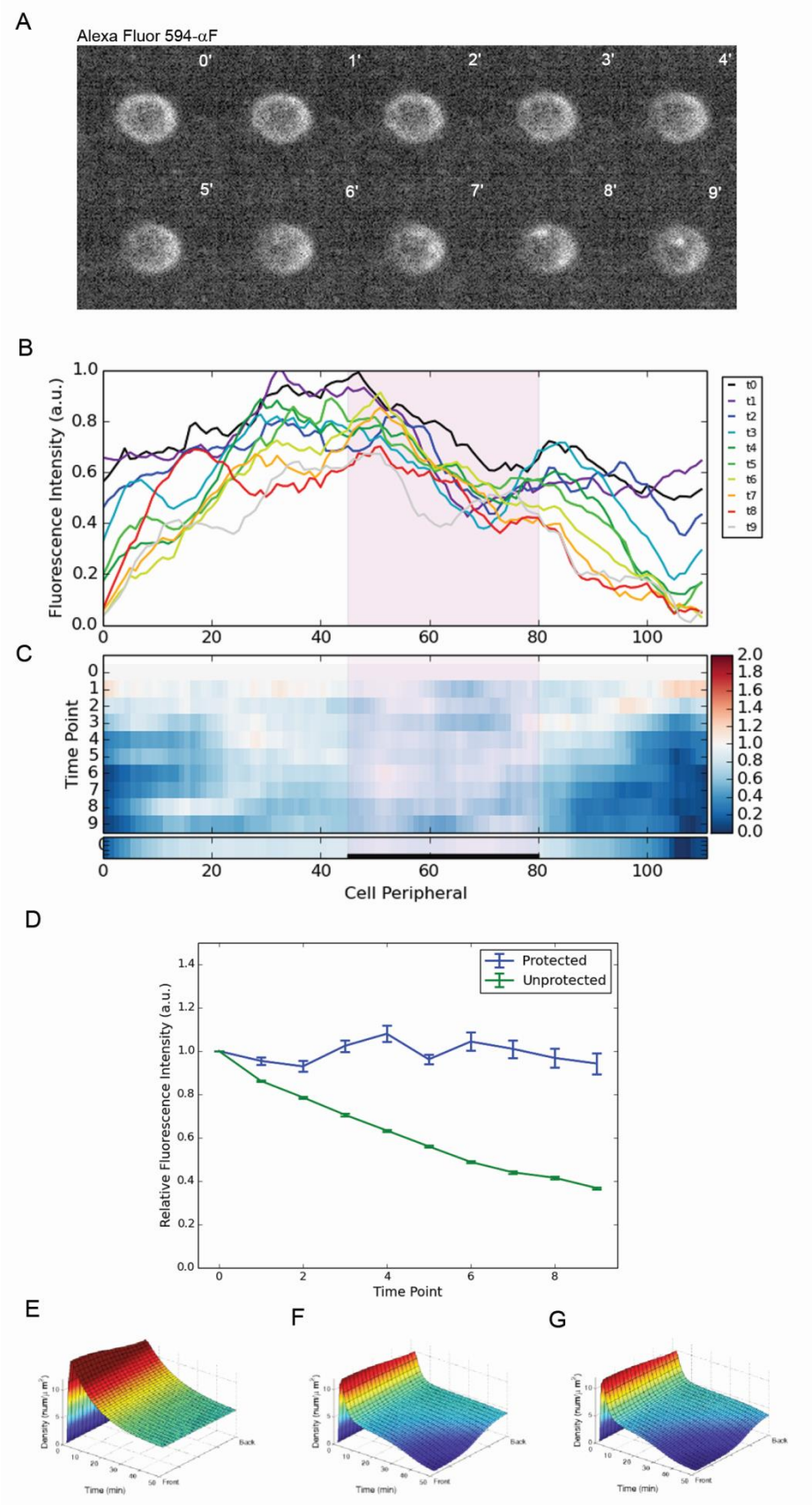
A
Alexa Fluor 594-αF
0'
1'
2'
3'
4'
5'
6'
7'
8'
9'
B
Fluorescence Intensity (a.u.)
t0
t1
t2
t3
t4
t5
t6
t7
t8
t9
C
Time Point
Cell Peripheral
D
Protected
Unprotected
Relative Fluorescence Intensity (a.u.)
Time Point
E
F
G
Time (min)
Front
Back

2.3.9 Mathematical modeling of receptor polarization

Here we have presented results supporting a novel mechanism by which the receptor can polarize upstream of actin-dependent directed secretion up the pheromone gradient (Fig. 11A). Yeast polarization in response to a pheromone gradient has been modeled, but these models have included regulators of actin polymerization (Yi et al., 2007). We are interested in pheromone-induced polarization upstream of actin-dependent directed secretion and its regulators. Using PDEs to computationally model the yeast pheromone response, we asked whether the Gβ-Yck interaction described in our model is sufficient to polarize the receptor up a pheromone gradient upstream of actin.

In a recently published paper, we presented results that suggest that pheromone-induced receptor polarization can occur in the absence of actin-dependent directed secretion (Suchkov et al., 2010). In the absence of downstream regulation of receptor internalization (Network 1) (Fig. 11B), the receptor is unable to polarize toward the pheromone gradient (Fig. 11E). The spatio-temporal distribution of the total concentration of the receptors, including both active and inactive forms, is shown in Figure 11E. Prior to introduction of the pheromone gradient, the receptors are distributed uniformly on the membrane. After 10 minutes of pheromone treatment, most receptors on the cell surface have disappeared due to a uniform internalization rate (Fig. 10E). We have proposed a model here where phosphorylated Gβ interacts with Yck and protects the receptor from internalization, resulting in polarization of the receptor in response to a pheromone gradient. To determine whether the addition of downstream regulation of receptor internalization (Gβ-Yck interaction) is sufficient to

polarize the receptor, we asked whether Network 2 (Fig. 11C) can polarize the receptor in response to a pheromone gradient. Our results show that Network 2 is able to polarize the pheromone receptors prior to actin-dependent directed secretion (Fig. 11F). Upon treatment with pheromone, the amount of receptor on the membrane decreases; however, they are not completely lost, and the polarity is gradually established at approximately 30 minutes. During the first 5 minutes, the concentration of the receptor at the front of the cell is lower compared to the back. After 15 minutes, the cell starts to polarize the receptor toward the pheromone gradient as a significant fraction of Yck was already repressed through its interaction with phosphorylated Gβ. This also corresponds to an asymmetry in the rate of receptor internalization and the receptor at the front of the cell is internalized at a slower rate (Fig. 10F). It was previously reported that full phosphorylation of Gβ is dependent on Fus3 and its interaction with Gα (Li et al., 1998, Metodiev et al., 2002). It was proposed that Gα recruits Fus3 to the membrane to phosphorylate Gβ, leading to an amplification of Gβ phosphorylation at the front of the cell (Metodiev et al., 2002). Since phosphorylated Gβ interacts with Yck, we asked what effect this additional positive feedback loop would have on receptor polarization and rate of receptor internalization (Network 3) (Fig. 11G, 10G). We found that the addition of the Gα-Fus3 interaction, which leads to amplification of Gβ phosphorylation, makes the pheromone response of Network 3 faster than that of Network 2 (Fig. 11G). With the positive feedback loop formed by the Gα-Fus3 interaction, Network 3 polarizes more efficiently and more robustly than Network 2.

Figure 11. Postulated feedback loops underlying directional sensing in yeast. (A) Cartoon model of polarity establishment. We propose that the establishment of pheromone-induced cell polarity prior to the initiation of actin-cable directed secretion depends on two interconnected positive feedback loops. Initially, a shallow gradient of pheromone is mirrored by a similarly shallow gradient of occupied receptor across the cell. This slight differential in activated receptor leads to a corresponding differential in activated G protein. As Gβγ inhibits receptor internalization by interacting with Yck1/2, the signaling apparatus preferentially accumulates on the up-gradient side of the cell. At the same time, Gα recruits the Fus3 MAPK to phosphorylate Gβ, which augments its interaction with Yck1/2 while preventing its interaction with Gα. The two loops act synergistically to promote local signaling while protecting Gβγ from internalization, thereby generating a concentration gradient of free $G\beta^{P}\gamma$. Ultimately, the localized increase in Gβγ is sufficient to trigger the nucleation of actin cables. Directed secretion then reinforces the spatial signal and drives mating projection formation. (B) Network 1. Yck1/2 (Yck) triggers the internalization of inactive and active receptors (R, RL), represented by the blue and green bars, respectively. One heterotrimeric G protein is removed along with each receptor. (C) Network 2. Phosphorylation of Gβ is included. The binding of $G\beta^{P}\gamma$ (GbgP) to Yck inhibits receptor and G protein internalization. (D) Network 3. The Gα-Fus3 feedback loop is included. Active Gα recruits active Fus3 to phosphorylate Gβ, which augments the interaction of Gβ with Yck and Gβγ-activation of Fus3 through the MAPK cascade (not shown). (E) Network 1. Without downstream regulation, the pheromone gradient induces complete removal of the receptor from the membrane; no polarity is generated. (F) Network 2. With the addition of $G\beta^{P}\gamma$-Yck interaction, which slows receptor and G protein internalization, the pheromone gradient induces receptor polarity. (G) Network 3. Gα recruitment of Fus3 leads to locally enhanced phosphorylation of Gβ, and consequently, faster receptor polarization.

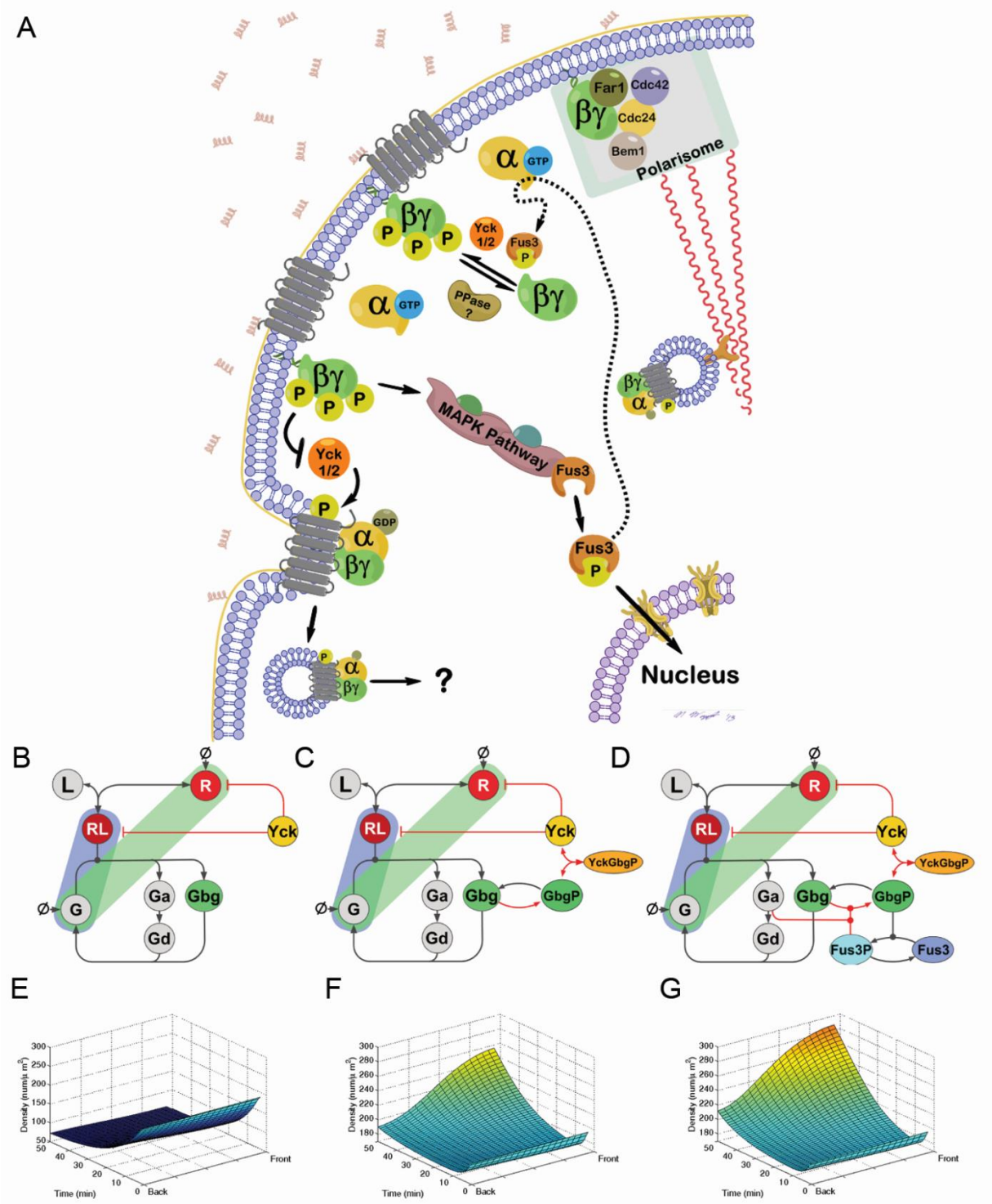
A
Far1
Cdc42
βγ
Cdc24
Bem1
Polarisome
α GTP
P
βγ
P
P
Yck 1/2
Fus3 P
α GTP
PPase ?
βγ
P
βγ
P
P
MAPK Pathway
Fus3
Yck 1/2
P
GDP
α
βγ
Fus3 P
P
α
βγ
?
Nucleus
B
L
R
RL
Yck
G
Ga
Gbg
Gd
C
L
R
RL
Yck
YckGbgP
G
Ga
Gbg
GbgP
Gd
D
L
R
RL
Yck
YckGbgP
G
Ga
Gbg
GbgP
Gd
Fus3P
Fus3
E
F
G
Density (numb m²)
Time (min)
Front
Back

2.4 Discussion

In response to pheromone, the receptor is rapidly internalized, later reappears as a polarized crescent, and remains polarized within the mating projection (Ayscough and Drubin, 1998, Jackson et al., 1991). It was thought that receptor polarization was due to secretion of the receptor along actin cables (Dohlman et al., 1991). But how does the cell interpret a shallow pheromone gradient and choose the direction of growth? It has been shown that the receptor is able to polarize prior to the detection of polarized actin cables and in the absence of actin-dependent directed secretion (Ayscough and Drubin, 1998, Suchkov et al., 2010). In a previous study, we proposed that the receptor is asymmetrically internalized and that activated receptor activates or recruits a downstream component that protects it from phosphorylation and internalization (Suchkov et al., 2010). In this study, we sought to identify this downstream factor. The Gβ-Yck1 interaction was isolated in a Gβ allele-specific genetic screen (Bar et al., 2003). Here, we characterized the interaction between Gβ and Yck1 and found that a mutant form of Gβ that cannot be phosphorylated, $G\beta^{P-}$ (Li et al., 1998), has a diminished interaction with Yck1 (Fig. 4A,B). The data presented here suggest that Gβ and Yck1 interact at the PM (Fig. 4C) and that Gβ is a potential Yck substrate (Fig. 4D). Gβ inhibits receptor phosphorylation (Fig. 6A,B) and promotes its polarization (Fig. 6A,C), whereas $G\beta^{P-}$ is defective in inhibition of receptor phosphorylation (Fig. 6A,B), polarization of unphosphorylated receptor (Fig. 6A,C), and movement of the unphosphorylated patch to the chemotropic growth site in mating mixtures (Fig. 6D). Cells expressing $G\beta^{P-}$ are also defective in polarization of the receptor in both mating mixtures (Fig. 7C) and in isotropic conditions in the absence of actin-dependent directed

secretion (Fig. 7A,B). In response to pheromone, we were able to detect a region of receptor on the PM that persisted longer compared to the rest (Fig. 10A-D). Our results suggest that the interaction between Gβ and Yck1 is important for asymmetric receptor phosphorylation and receptor polarization and are consistent with a novel mechanism for receptor polarization in response to a pheromone gradient.

2.4.1 Gβ interacts with Yck to establish the growth site

When a cell is exposed to a gradient of pheromone, this leads to a gradient of activated receptor and a corresponding gradient of free Gα and free Gβγ. Free Gβ is rapidly phosphorylated in response to pheromone. Partially phosphorylated Gβ interacts with Yck, protecting the receptor from Yck-dependent phosphorylation and internalization, thereby preventing internalization of the G protein as well (Suchkov et al., 2010). On the up-gradient side of the cell there is slightly more free Gβγ and thus, slightly more protection of the receptor and G protein. On the down-gradient side of the cell, there is slightly less protection of the receptor and G protein. This asymmetric internalization of the receptor and G protein initiates a positive feedback loop that amplifies the shallow external gradient of pheromone and converts it into a steep intracellular signaling gradient marking the polarity site. Once the polarity site is established, actin is nucleated and receptor polarization is maintained by secretion of the receptor to the growth site. This proposed model is consistent with our observations that when the interaction between Gβ and Yck1 is diminished, the cells are defective in asymmetric phosphorylation (Fig. 6A,C), receptor polarization (Fig. 6A-D), and also a previously published result showing that cells expressing $G\beta^{P-}$ are defective in chemotropism (DeFlorio et al., 2013).

2.4.2 Gβ phosphorylation and amplification

Our data suggest that Gβ is a Yck substrate (Fig. 4D). Full phosphorylation of Gβ requires the activity of the two yeast casein kinases, Yck1 and Yck2 (Hicke et al., 1998). Previous studies have reported that some CKI proteins prefer to have their substrates phosphorylated within the CKI motif (–S(P)/T(P)-$X_{n(1-3)}$-S/T-) and that makes for a better CKI substrate (Flotow et al., 1990, Flotow and Roach, 1989, Meggio et al., 1979). A good candidate for the kinase responsible for the initial phosphorylation is the MAPK, Fus3. Full phosphorylation of Gβ requires the activity of Fus3, and also the interaction of Fus3 with Gα (Li et al., 1998, Metodiev et al., 2002). It was previously proposed that Gα recruits Fus3 to the membrane to phosphorylate Gβ (Metodiev et al., 2002). Our mass spectrometry data are consistent with the initial phosphorylation at residue 318 in the CKI motif also being a MAPK phosphorylation site. This initial Gβ phosphorylation within the CKI recognition motif could make Gβ a recognized Yck substrate and result in phosphorylation at either 320 or 322 (Fig. 4E). This would lead to an amplification of Gβ phosphorylation on the up-gradient side of the cell initiating a second positive feedback loop and thus an amplification of the receptor protective element on the up-gradient side of the cell resulting in more protection of the receptor and G protein at the front of the cell. Together these two positive feedback loops would result in a more robust polarization of the receptor as suggested by more robust polarization of the receptor in Network 3 (Fig. 11G).

2.4.3 $G\beta^{P-}$ defects

Although $G\beta^{P-}$ cells were not completely defective in protection of the receptor from phosphorylation (PM/Cyto ratio) in the absence of F-actin (Fig. 6A,B) and ‘moving’

the patch of Sst2-GFP in the RPA strain (Fig. 6D), the cells were defective compared to Gβ cells. Additionally, $G\beta^{P-}$ cells were not completely defective in polarization of the receptor in the absence of F-actin (Fig. 7A,B) and in mating mixtures (Fig. 7C,D), but were defective compared to Gβ cells. The observations that $G\beta^{P-}$ cells are not completely defective in both the RPA strain experiments and receptor polarization is consistent with our data that suggests that $G\beta^{P-}$ only has a ~50% binding defect with Yck1/2 compared to Gβ. However, the defects seen in $G\beta^{P-}$ cells is consistent with the idea that its interaction with Yck is important for protection of the receptor from phosphorylation, receptor polarization, and establishment of the chemotropic growth site.

2.4.4 Receptor internalization assay

In ~61% of the cells, we were able to detect a region of receptor on the membrane that had a slower rate of internalization compared to the rest of the cell (Fig. 10A-D). One possible reason we were not able to detect differential internalization in a larger fraction of the population is because the cells were treated with an isotropic concentration of pheromone and not with a gradient of pheromone. In the case where there is no external pheromone gradient, the cell must default shmoo at a site marked internally by Bud1 (Dorer et al., 1995, Nern and Arkowitz, 1999). Gβ localization has been shown to be cell cycle dependent shown to polarize at the G1/S transition (DeFlorio et al., 2013). Additionally, Gβ may also polarize during apical bud growth when proteins are being secreted to the tip of the growing daughter cell (Pruyne and Bretscher, 2000a, Pruyne and Bretscher, 2000b). In isotropic conditions, our model would predict that we would only be able to detect a region of protected receptor where

Gβ is localized. Therefore, during the other stages of the cell cycle when Gβ is not polarized, we may not be able to detect differential internalization.

2.4.5 Receptor internalization and directional sensing

Receptor internalization has been thought to be mainly for down-regulation of signaling. However, studies have linked receptor internalization to directional sensing, cell migration, and chemotropism (Brzostowski et al., 2013, Kavelaars et al., 2003). Chemotactic cells do not polarize their receptors in response to a chemical gradient, and it is thought that they keep them distributed uniformly on the membrane because they need the ability to continually sense rapidly changing environments during migration. Although chemotactic cells don't polarize their receptors, cells defective in receptor endocytosis have been found to exhibit aberrant actin polymerization and chemotaxis (Brzostowski et al., 2013, Kavelaars et al., 2003). In contrast, chemotropic cells polarize their receptors in response to an external gradient. When the pheromone receptor C-terminus is deleted and cannot be internalized, the cells are defective in formation of the mating projection toward the source of pheromone (Vallier, 2002). In a recent study, we showed that receptor internalization is required for receptor polarization and directional sensing (Suchkov et al., 2010).

2.4.6 Role of Gβ in chemotropism

The role of Gβ in actin polymerization during formation of the mating projection has been well characterized. Free Gβγ signals through the MAPK cascade activating the MAPK, Fus3. Free Gβγ also recruits the Far1-Cdc24 complex to the cell cortex where it can activate Cdc42, which recruits Bni1, resulting in actin polymerization (Butty et al., 1998, Pruyne and Bretscher, 2000a, Pruyne and Bretscher, 2000b). In this study,

we have presented evidence for a new role of Gβ in establishment of a polarity site within a gradient of pheromone through its interaction with the yeast casein kinases. Our results also suggest that Gβ is a Yck substrate. What is the function of Gβ phosphorylation? We recently reported that Gβ phosphorylation is required for proper localization of Gβ at the incipient shmoo site prior to morphogenesis, choosing the polarity site closest to the potential mating partner, and maintaining the direction of growth (DeFlorio et al., 2013). Additionally, we showed evidence for a role of Gβ phosphorylation in gradient tracking after formation of the original mating projection through its interaction with Far1 (DeFlorio et al., 2013). We proposed that the dynamic interaction between Gβ and Far1 links the actin cytoskeleton to the receptor on the PM to update the cell on a change in a pheromone gradient, allowing the cell to track a changing gradient (DeFlorio et al., 2013). Here we propose a larger picture for Gβ and its phosphorylation in the establishment of a polarity site and gradient tracking. Gβ interacts with Yck on the up-gradient side of the cell where it protects the receptor from phosphorylation and internalization, establishing the polarity site. Yck also phosphorylates Gβ, destabilizing the interaction between Gβ and Far1. This destabilization allows the cell to be continually updated through its interaction with the receptor, allowing it to track a changing gradient.

3. Future Directions

Directional sensing plays an important role in many biological and pathological processes, but the mechanism by which cells are able to interpret a range of gradients and convert them into steeper intracellular signaling gradients still remains unclear. In this study, we proposed a novel mechanism for pheromone receptor polarity establishment in response to a gradient of pheromone and tested its different postulates. We have provided evidence that Gβ plays an important role in the establishment of receptor polarity during the pheromone response (Fig. 7). We have characterized the interaction between Gβ and a yeast casein kinase, Yck1 (Fig. 4A-C). To our knowledge, this is the first interaction between a Gβ and a casein kinase that has been reported. We also showed that a mutant form of Gβ that cannot be phosphorylated, $G\beta^{P-}$, and is defective in its interaction with Yck1 (Fig. 4A,B), is defective in establishment of receptor polarity (Fig. 7). This suggests that the interaction between Gβ and Yck1 is important for establishment of receptor polarity. Computational modeling can be a powerful tool to provide insight into complex interaction networks. We collaborated with a systems biology group to mathematically model the different interactions described in our model and to determine if they are sufficient for correct receptor polarization in a pheromone gradient. Our computational results suggest that the interactions described in our model are sufficient to correctly polarize the pheromone receptor in response to a pheromone gradient (Fig. 11F). We also added a second positive feedback loop that locally amplifies Gβ phosphorylation and resulted in faster polarization of the receptor (Fig. 11G). The results we have

presented here have provided insight into the mechanism of directional sensing during the yeast mating response, but questions still remain. Further study of the model we have proposed here will help elucidate the mechanism of directional sensing.

3.1 Gβ phosphorylation

In response to pheromone, Gβ is rapidly phosphorylated (Cole and Reed, 1991); however, the function of this phosphorylation has remained elusive. It was initially thought that Gβ phosphorylation played a role in adaptation, but $G\beta^{P-}$ cells were not found to have any defects in adaptation or signaling (Li et al., 1998). Fus3 was found to be required for full phosphorylation of Gβ (Li et al., 1998, Metodiev et al., 2002). A more recent study found that $G\beta^{P-}$ cells were defective in directional sensing, stabilization of the polarization site, and gradient tracking (DeFlorio et al., 2013). In this study, we showed that full phosphorylation of Gβ also requires the activity of the two yeast casein kinases, Yck1 and Yck2 (Fig. 4D). Using mass spectrometry, we identified Gβ phosphorylation sites (Fig. 5), some of which were also predicted by previous genetic data (Li et al., 1998). Some of the phosphorylation sites are MAPK and CKI phosphorylation motifs (Fig. 4E). Together, these results suggest that Fus3 and the yeast casein kinases phosphorylate Gβ. If Fus3 and the yeast casein kinases phosphorylate Gβ, which sites do they phosphorylate? To determine this, *in vitro* kinase assays can be conducted with Gβ and Fus3 and Gβ and the yeast casein kinases, Yck1 and Yck2. Additionally, Gβ phosphorylation can be assessed by mass spectrometry in pheromone treated cells lacking Fus3 and the yeast casein kinases.

3.2 Asymmetric Receptor internalization

A key aspect of our model is asymmetric internalization. Since the pheromone receptor is continuously trafficked to the membrane, distinguishing between activated PM receptor and newly synthesized receptor trafficked to the PM makes following receptor internalization difficult. In this study, we presented results supporting the idea of asymmetric receptor internalization using Alexa fluor 594-conjugated α-factor bound to cell surface receptors and followed receptor internalization. Using this method, in a subset of cells we were able to detect a region of receptor on the membrane that had a slower rate of internalization compared to the rest of the cell (Fig. 10A-D). This suggests that these cells are asymmetrically internalizing the receptor. It was previously published that the Alexa fluor 594-conjugated α-factor will induce pheromone-induced receptor internalization but does not induce the mating response as unconjugated α-factor does (Toshima et al., 2006). Additionally, binding of the conjugated α-factor to cell surface receptors requires a 2 hour incubation on ice in an amino acid and sugar deficient medium and also makes it impossible to examine asymmetric receptor internalization in response to a pheromone gradient. Use of a photo-convertible fluorophore would provide a more powerful way to visualize asymmetric internalization because it allows us to distinguish between the receptor that was initially on the PM (photo-converted) and receptor that was not initially on the PM (not photo-converted). It would also allow us to visualize PM receptor internalization in response to a pheromone gradient. We can use a microfluidic device that can establish linear pheromone gradients (Brett et al., 2012, DeFlorio et al., 2013), photo-convert the

receptor on the PM, and follow the internalization of the photo-converted PM receptor over time.

3.3 Computational modeling predictions

A computational model can identify key parameters and give testable predictions. Our primary goal of mathematically modeling was to determine if the interactions we described were sufficient to polarize the pheromone receptor in response to a gradient of pheromone. Using parameters taken from the literature, when possible, we were able to develop a model that polarized the receptor correctly in a gradient of pheromone, suggesting that the interactions we have described in our model are sufficient for amplification of a shallow extracellular gradient.

3.3.1 Diffusion coefficients

A secondary goal of our mathematical modeling was to determine if our computational cell would be able to overcome a default polarity site and polarize at the chemotropic site. The default site was defined as an area enriched with the receptor and G protein by 2-fold and was localized in a patch that represented 10% of the computational yeast cell. Our current networks (Network 2 and Network 3) (Fig. 11C,D) were unable overcome the default polarity site when exposed to a gradient of pheromone at a 90 degree angle from the default site. One plausible reason for the inability of our current networks to overcome default polarity is that all molecules in the networks have the same diffusion coefficient. The uniform diffusion coefficient that we are currently using was taken from a previously published study modeling yeast polarization (Chou et al., 2008). We predict that cytoplasmic proteins, peripheral membrane proteins, and integral membrane proteins will all have different diffusion

coefficients (Weiss et al., 2013). Many factors can affect the diffusion rates of the different molecules during the yeast mating response, including clustering and membrane composition (Weiss et al., 2013). Measuring the diffusion coefficients for the molecules in our network may provide critical values that will allow our computational yeast cell to overcome default polarity when responding to a gradient of pheromone.

3.3.2 Gβγ/Gβ^{P}γ affinity with Yck

Mathematical modeling of complex interaction networks can identify key parameters in the network. Many parameters in our network can be varied within a 10-fold range and have no effect on receptor polarization. However, some interaction values require a very narrow range to induce receptor polarity and are very critical parameters. One such parameter that was identified as being critical was the dissociation rate between Gβ^{P}γ and Yck (Fig. 12D). Since this is the first identified interaction between a Gβ and a casein kinase, there were no measured values in the literature to use to estimate this interaction. Since this value is critical for receptor polarity in response to a gradient, measuring the dissociation rate between Gβ^{P}γ and Yck will provide a measured value for a critical parameter in our computational model. We can measure the dissociation rate by isothermal titration calorimetry (Velazquez-Campoy et al., 2004). Identifying this value may provide the critical parameter needed for the computational yeast cell to overcome the default polarity site and more accurately mimic the biological yeast cell.

Figure 12. Key network parameters.
Polarity index is graphed as a function of the indicated parameter values. (A) The rate of Gα and Gβγ reassociation is not rate limiting; model output is insensitive to k_{gd} values in the indicated range. (B) The rate of Gα-GTP inactivation (k_{gad}) is a critical parameter. (C) Model output is insensitive to the rate of $G\beta^{P}\gamma$/Yck association (k_{ycki}) above minimal value. (D) The rate of $G\beta^{P}\gamma$/Yck disassociation (k_{ycka}) is crucial; the polarity index falls dramatically as the magnitude of this parameter increases beyond its optimal value.

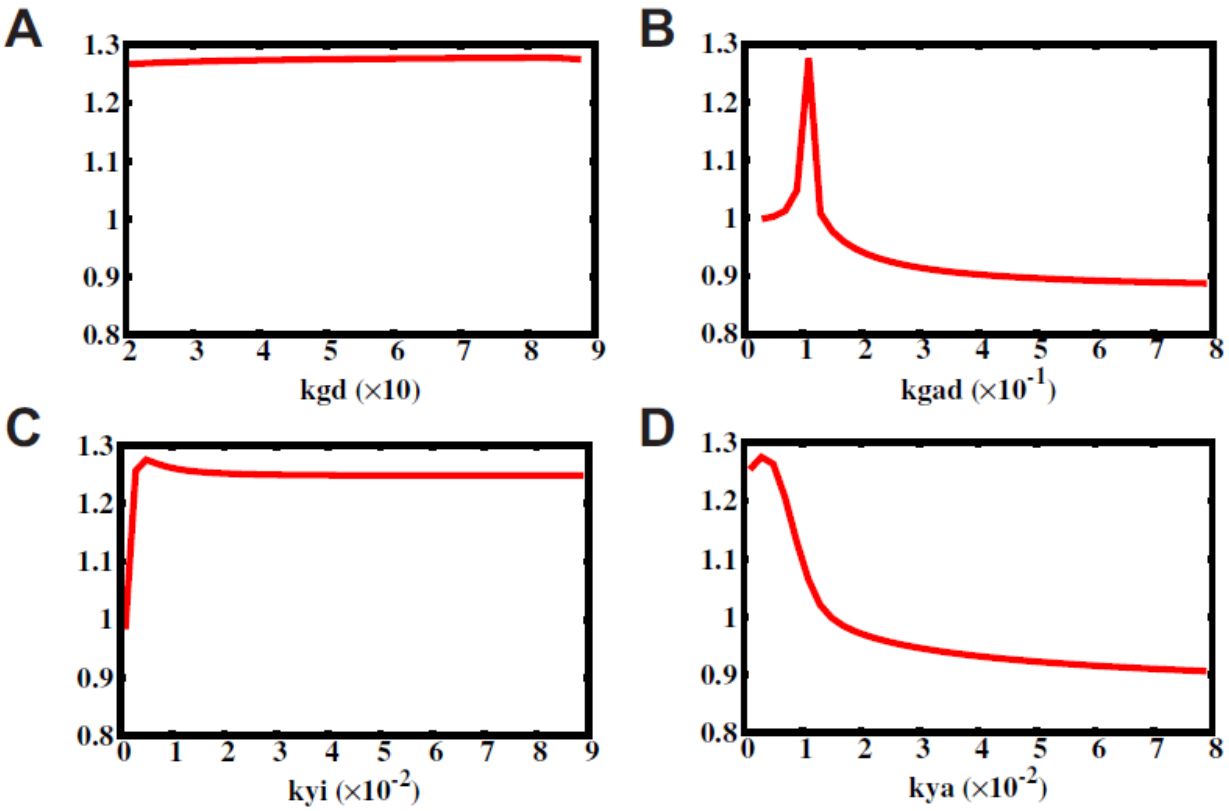
A
1.3
1.2
1.1
1
0.9
0.8
2 3 4 5 6 7 8 9
kgd (×10)
B
1.3
1.2
1.1
1
0.9
0.8
0 1 2 3 4 5 6 7 8
kgad (×10-1)
C
1.3
1.2
1.1
1
0.9
0.8
0 1 2 3 4 5 6 7 8 9
kyi (×10-2)
D
1.3
1.2
1.1
1
0.9
0.8
0 1 2 3 4 5 6 7 8
kya (×10-2)

3.3.3 Is Gβ preferentially internalized over $G\beta^P$?

The results I have presented here suggest that Gβ phosphorylation is important for pheromone induced receptor polarization (Fig. 7) and that it's the phosphorylatable form of Gβ that can interact with Yck1 to protect the receptor from Yck dependent phosphorylation and internalization. $G\beta^{P-}$ was defective in protection of the receptor from phosphorylation and polarization of the unphosphorylated receptor crescent (Fig. 6A-C). Cells expressing $G\beta^{P-}$ were also defective in 'movement' of the unphosphorylated receptor patch from the default site to the chemotropic site and receptor polarization (Fig. 6D). Therefore, it isn't surprising that the computational model also identified $G\beta^P$ internalization, and thus its degradation, as a critical parameter. We previously showed that Gβ internalization and polarization requires receptor internalization and interaction with Gα (Suchkov et al., 2010). During the mating response, Gα is activated and dissociates from Gβ. During this time, Gβ is rapidly phosphorylated (Cole and Reed, 1991). Therefore, when constructing our model, we hypothesized that it is the unphosphorylated form of Gβγ that interacts with Gα and is internalized with the receptor. To test how critical this parameter was, we constructed a network where $G\beta^P\gamma$ was also internalized with the receptor (Fig. 13A). When 0-1% of $G\beta^P\gamma$ was internalized with the receptor, the cell was still able to polarize the receptor (Fig. 13B,C). However, when as little as 3% of $G\beta^P\gamma$ was internalized, receptor polarization dramatically dropped (Fig. 13D). When 5% of $G\beta^P\gamma$ was internalized with the receptor, receptor polarization was almost completely lost (Fig. 13E). This prediction suggests that the half-life of $G\beta^P$ would be much larger than the half-life of unphosphorylated Gβ in response to pheromone. Measuring the half-life of

both Gβ and $G\beta^{P}$ would provide insight into the role of Gβ phosphorylation. Does phosphorylation stabilize Gβ and protect it from degradation? If $G\beta^{P}$ doesn't have a larger half-life than Gβ, this information will be incorporated into a new network.

Figure 13. Phospho-specific trafficking of Gβ.
(A) Hypothetical network where phosphorylated Gβγ can be internalized. In addition to the internalization of the heterotrimeric G protein, phosphorylated Gβγ is also taken away from the cell membrane with receptor with a stoichiometry ratio of θ:1. (B) When 0% of $G\beta^{P}$ is internalized (same as network 3), the receptor robustly polarizes. (C) When 1% of $G\beta^{P}$ is internalized, there is a dramatic decrease in receptor polarization. (D) When 3% of $G\beta^{P}$ is internalized, receptor polarity is almost completely lost. (E) When 5% of $G\beta^{P}$ is internalized, receptor polarity is lost.

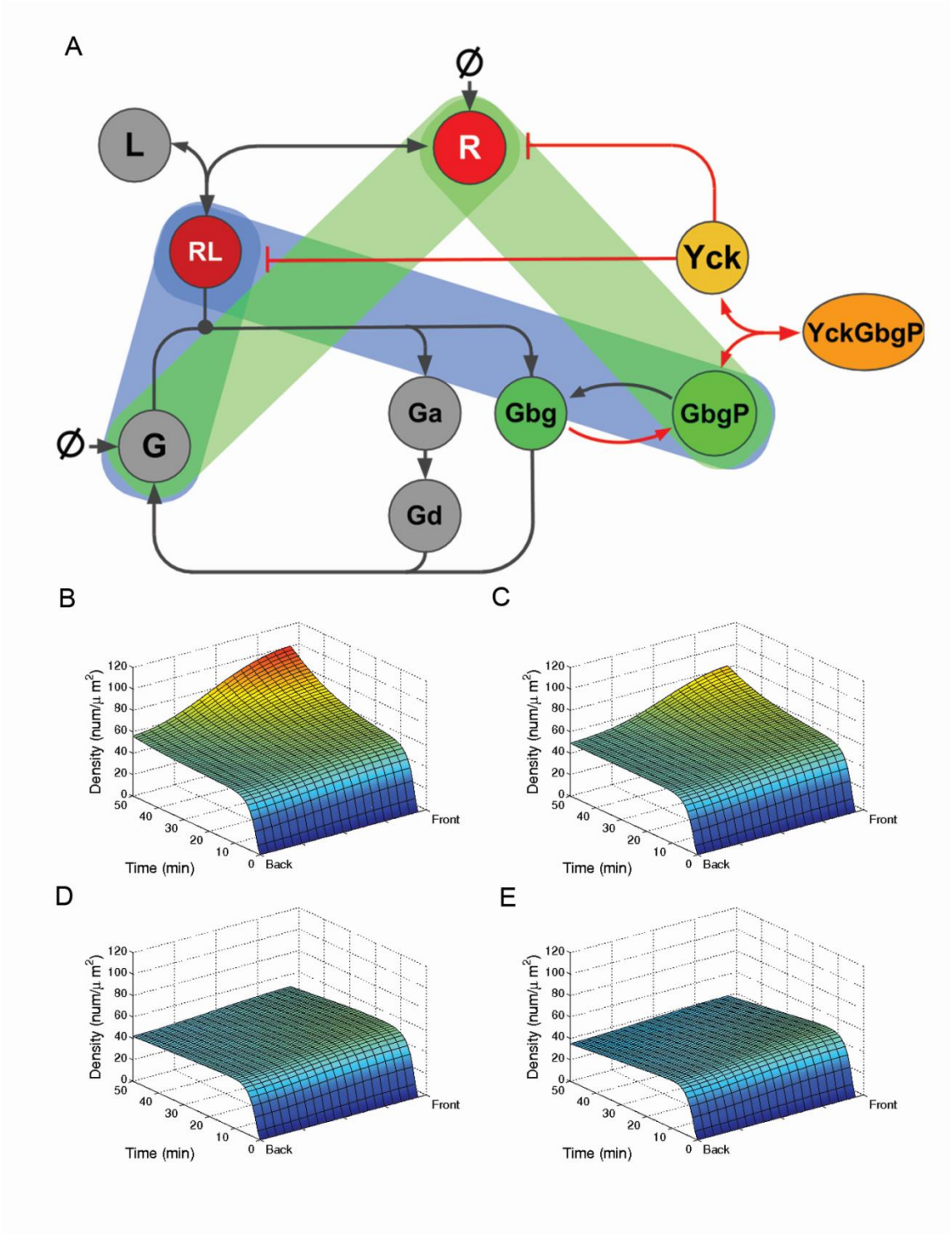
A
Ø
L
R
RL
Yck
YckGbgP
Ga
Gbg
GbgP
Ø
G
Gd
B
C
D
E
Density (num/μ m²)
Time (min)
Front
Back
0
10
20
30
40
50
0
20
40
60
80
100
120

3.3.4 Is there an inverse gradient of Gβ and $G\beta^P$?

From our molecular model, we predicted that there would be a gradient of $G\beta^P$ across the cell with an accumulation at the front, decreasing along the axis of the cell. This prediction was made from the idea that there is more activated receptor, and thus, more free Gβγ at the front of the cell to be phosphorylated. We also predicted that there would be an inverse gradient of unphosphorylated Gβ. Using Network 2, we asked the network to output the spatial and temporal dynamics of Gβ and $G\beta^P$. As predicted, there was a steep gradient of $G\beta^P$ front-to-back (Fig. 14B); however, there was a shallow gradient of Gβ also front-to-back (Fig. 14A). Surprisingly, there was more unphosphorylated Gβ across the entire axis of the cell (Fig. 14A). *In vitro* localization of the different phospho-species of Gβ would provide valuable information about the spatial dynamics of Gβ phosphorylation. Our model predicts that there is an amplification of Gβ phosphorylation on the up-gradient side of the cell and that it's this species of Gβ that preferentially interacts with Yck to protect the receptor from phosphorylation and internalization, thereby establishing the polarity site. The development of monobody probes conjugated to a fluorescent fluorophore that recognize the phosphorylated or unphosphorylated forms of Gβ would allow us to test the predictions of our networks and provide insight into the dynamics of Gβ phosphorylation.

Figure 14. Spatio-temporal dynamics of Gβ and $G\beta^{P}$.
(A) PM-localized Gβ decreases then recovers and forms a shallow front-to-back gradient. (B) PM-localized $G\beta^{P}$ increases and forms a steep front-to-back gradient.

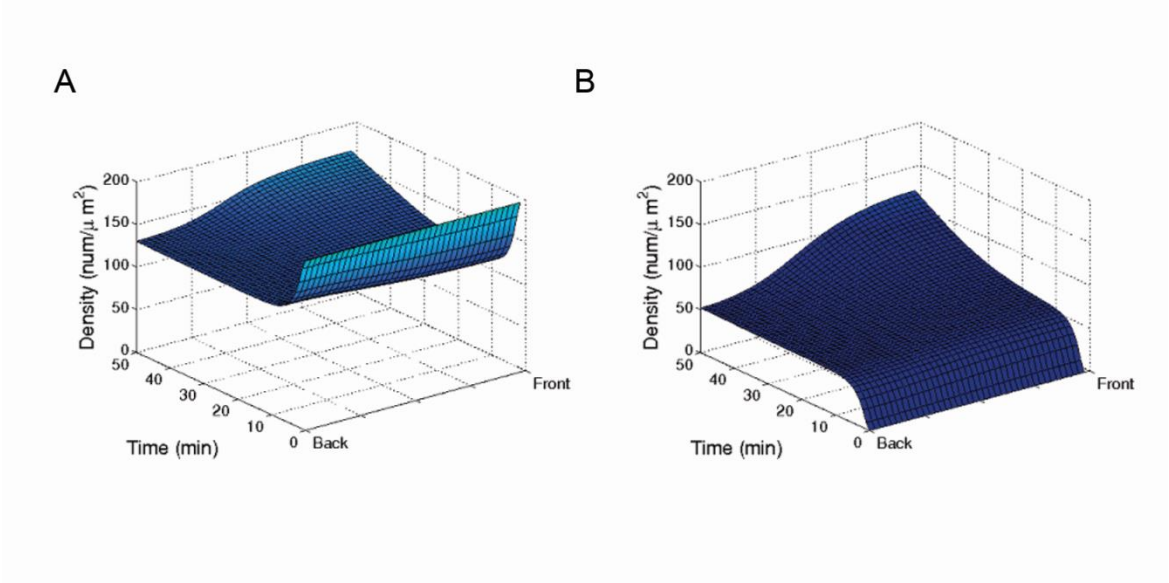
A
B
Density (num/μ m²)
200
150
100
50
0
50
40
30
20
10
0
Time (min)
Back
Front

3.3.5 Test the proposed positive feedback in Network 3

In this study, I tested the different postulates of the described model. Previous studies have published results suggesting a second positive feedback loop that amplifies Gβ phosphorylation on the up-gradient side of the cell. It has been published that full phosphorylation of Gβ requires Fus3 and the interaction between Gα and Fus3 (Li et al., 1998, Metodiev et al., 2002). A model for amplification of Gβ phosphorylation was proposed, in which activated Gα recruits the MAPK, Fus3, to the PM to phosphorylate Gβ (Metodiev et al., 2002). As there is slightly more activated receptor, activated Gα, and free Gβγ on the up-gradient side of the cell, there will be more phosphorylation of Gβ on the up-gradient side of the cell. In this study, I did not test the second positive feedback loop, but we included it in Network 3 (Fig. 11D) to see what effect it would have on receptor polarization. When we added the second positive feedback loop that amplified Gβ phosphorylation at the front of the cell, we found that Network 3 polarized faster and more robustly than Network 2 (Fig. 11G). In the previous study that proposed the Gα-Fus3 positive feedback loop, a mutant form of Gα was identified, $G\alpha^{DSD}$, that was defective in its interaction with Fus3 and exhibited decreased Gβ phosphorylation (Metodiev et al., 2002). To test the effect of this second feedback loop, receptor polarization can be examined in $G\alpha^{DSD}$ cells. Additionally, Gβ phospho-specific monobodies (described above) could be used to visualize Gβ phosphorylation in WT and $G\alpha^{DSD}$ cells.

4. Appendix I

The yeast pheromone receptor is the most upstream component of the pheromone signaling pathway. In response to pheromone, receptor internalization is up-regulated 5- to 10-fold (Jenness and Spatrick, 1986). The receptor disappears from the membrane, later reappears as a polarized crescent, and remains polarized within the mating projection (Ayscough and Drubin, 1998, Jackson et al., 1991). Pheromone binding to the receptor induces the receptor to change its conformation, allowing its C-terminus to be phosphorylated (Hicke et al., 1998). Upon phosphorylation, the receptor is ubiquitinated and internalized (Hicke and Riezman, 1996, Hicke et al., 1998). It was thought that the primary role of this rapid internalization of the receptor in response to pheromone was to down-regulate the pheromone response (Dohlman et al., 1991). However, more recent studies have linked receptor internalization to directional sensing and chemotropism. When the pheromone receptor C-terminus is deleted and the receptor cannot be internalized, the cells are defective in orienting their mating projections toward the source of pheromone (Vallier, 2002).

In Suchkov et al., 2010, we showed that the receptor is able to polarize in the absence of actin-dependent directed secretion, prior to actin polarization, and that polarization of the receptor requires its internalization (Suchkov et al., 2010). We proposed a model where the polarity site is established by asymmetric receptor internalization. When the cell is exposed to a gradient of pheromone, the receptor releases or activates a downstream component that protects the receptor from phosphorylation and internalization. This results in the receptor at the back of the cell

being phosphorylated and internalized to a greater degree. Sst2 has been shown to bind specifically to unphosphorylated receptor (Ballon et al., 2006). Using an engineered strain where the receptor was mutated so that it could not be internalized (*Ste2*^{7XR}), and therefore, cannot polarize, it was shown that Sst2-GFP polarized to the mating projection in response to pheromone (Ballon et al., 2006). This was consistent with asymmetric receptor phosphorylation, where the receptor was protected from phosphorylation and internalization at the front of the cell, which would lead to asymmetric internalization. Ballon et al., 2006 attributed the localization of Sst2-GFP within the mating projection to newly synthesized receptor that hadn't yet been phosphorylated (Ballon et al., 2006). To test this, we followed the localization of Sst2-GFP in the absence of actin-dependent directed secretion in response to pheromone. We treated the RPA strain with pheromone and LatA and followed Sst2-GFP localization over time. In response to pheromone, the receptor did not polarize, but Sst2-GFP became significantly polarized on the membrane after 45 minutes (Suchkov et al., 2010, Figure 8A,B). These results are consistent with a model where the receptor is asymmetrically phosphorylated, and thus, asymmetrically internalized.

Cited Literature

Apanovitch, D. M., K. C. Slep, P. B. Sigler & H. G. Dohlman, (1998) Sst2 is a GTPase-activating protein for Gpa1: purification and characterization of a cognate RGS-Galpha protein pair in yeast. *Biochemistry* **37**: 4815-4822.

Arkowitz, R. A., (2009) Chemical gradients and chemotropism in yeast. *Cold Spring Harbor perspectives in biology* **1**: a001958.

Ayscough, K. R. & D. G. Drubin, (1998) A role for the yeast actin cytoskeleton in pheromone receptor clustering and signalling. *Current Biology* **8**: 927-931.

Ballon, D. R., P. L. Flanary, D. P. Gladue, J. B. Konopka, H. G. Dohlman & J. Thorner, (2006) DEP-Domain-Mediated Regulation of GPCR Signaling Responses. *Cell* **126**: 1079-1093.

Bar, E. E., A. T. Ellicott & D. E. Stone, (2003) Gbetagamma recruits Rho1 to the site of polarized growth during mating in budding yeast. *The Journal of biological chemistry* **278**: 21798-21804.

Bardwell, L., (2005) A walk-through of the yeast mating pheromone response pathway. *Peptides* **26**: 339-350.

Bendezu, F. O. & S. G. Martin, (2011) Actin cables and the exocyst form two independent morphogenesis pathways in the fission yeast. *Molecular biology of the cell* **22**: 44-53.

Berzat, A. & A. Hall, (2010) Cellular responses to extracellular guidance cues. *The EMBO journal* **29**: 2734-2745.

Biber, K., M. W. Zuurman, I. M. Dijkstra & H. W. Boddeke, (2002) Chemokines in the brain: neuroimmunology and beyond. *Current opinion in pharmacology* **2**: 63-68.

Brett, M. E., R. DeFlorio, D. E. Stone & D. T. Eddington, (2012) A microfluidic device that forms and redirects pheromone gradients to study chemotropism in yeast. *Lab on a chip* **12**: 3127-3134.

Brzostowski, J. A., S. Sawai, O. Rozov, X. H. Liao, D. Imoto, C. A. Parent & A. R. Kimmel, (2013) Phosphorylation of chemoattractant receptors regulates chemotaxis, actin reorganization and signal relay. *J Cell Sci* **126**: 4614-4626.

Bukusoglu, G. & D. D. Jenness, (1996) Agonist-specific conformational changes in the yeast alpha-factor pheromone receptor. *Mol. Cell. Biol.* **16**: 4818-4823.

Butty, A. C., P. M. Pryciak, L. S. Huang, I. Herskowitz & M. Peter, (1998) The role of Far1p in linking the heterotrimeric G protein to polarity establishment proteins during yeast mating. *Science* **282**: 1511-1516.

Chang, F. & I. Herskowitz, (1990) Identification of a gene necessary for cell cycle arrest by a negative growth factor of yeast: FAR1 is an inhibitor of a G1 cyclin, CLN2. *Cell* **63**: 999-1011.

Chen, L., M. Iijima, M. Tang, M. A. Landree, Y. E. Huang, Y. Xiong, P. A. Iglesias & P. N. Devreotes, (2007) PLA2 and PI3K/PTEN Pathways Act in Parallel to Mediate Chemotaxis. *Developmental Cell* **12**: 603-614.

Chou, C. S., T. I. Moore, S. D. Chang, Q. Nie & T. M. Yi, (2012) Signaling regulated endocytosis and exocytosis lead to mating pheromone concentration dependent morphologies in yeast. *FEBS letters* **586**: 4208-4214.

Chou, C. S., Q. Nie & T. M. Yi, (2008) Modeling robustness tradeoffs in yeast cell polarization induced by spatial gradients. *PloS one* **3**: e3103.

Cicchetti, G., P. G. Allen & M. Glogauer, (2002) CHEMOTACTIC SIGNALING PATHWAYS IN NEUTROPHILS: FROM RECEPTOR TO ACTIN ASSEMBLY. *Crit Rev Oral Biol Med* **13**: 220-228.

Cismowski, M. J., M. Metodiev, E. Draper & D. E. Stone, (2001) Biochemical analysis of yeast G(alpha) mutants that enhance adaptation to pheromone. *Biochemical and biophysical research communications* **284**: 247-254.

Cole, G. M. & S. I. Reed, (1991) Pheromone-induced phosphorylation of a G protein [beta] subunit in S. cerevisiae is associated with an adaptive response to mating pheromone. *Cell* **64**: 703-716.

Comer, F. I. & C. A. Parent, (2002) PI 3-kinases and PTEN: how opposites chemoattract. *Cell* **109**: 541-544.

DeFlorio, R., M. E. Brett, N. Waszczak, E. Apollinari, M. V. Metodiev, O. Dubrovskyi, D. Eddington, R. A. Arkowitz & D. E. Stone, (2013) Phosphorylation of Gbeta is crucial for efficient chemotropism in yeast. *J Cell Sci* **126**: 2997-3009.

Dohlman, H. G., J. Song, D. Ma, W. E. Courchesne & J. Thorner, (1996) Sst2, a negative regulator of pheromone signaling in the yeast Saccharomyces cerevisiae: expression, localization, and genetic interaction and physical association with Gpa1 (the G-protein alpha subunit). *Molecular and cellular biology* **16**: 5194-5209.

Dohlman, H. G. & J. Thorner, (1997) RGS proteins and signaling by heterotrimeric G proteins. *The Journal of biological chemistry* **272**: 3871-3874.

Dohlman, H. G., J. Thorner, M. G. Caron & R. J. Lefkowitz, (1991) Model systems for the study of seven-transmembrane-segment receptors. *Annual review of biochemistry* **60**: 653-688.

Dorer, R., P. M. Pryciak & L. H. Hartwell, (1995) Saccharomyces cerevisiae cells execute a default pathway to select a mate in the absence of pheromone gradients. *J. Cell Biol.* **131**: 845-861.

Dunn, R., D. A. Klos, A. S. Adler & L. Hicke, (2004) The C2 domain of the Rsp5 ubiquitin ligase binds membrane phosphoinositides and directs ubiquitination of endosomal cargo. *The Journal of cell biology* **165**: 135-144.

Fets, L., J. M. Nichols & R. R. Kay, (2014) A PIP5 kinase essential for efficient chemotactic signaling. *Current biology : CB* **24**: 415-421.

Flotow, H., P. R. Graves, A. Q. Wang, C. J. Fiol, R. W. Roeske & P. J. Roach, (1990) Phosphate groups as substrate determinants for casein kinase I action. *J. Biol. Chem.* **265**: 14264-14269.

Flotow, H. & P. J. Roach, (1989) Synergistic phosphorylation of rabbit muscle glycogen synthase by cyclic AMP-dependent protein kinase and casein kinase I. Implications for hormonal regulation of glycogen synthase. *The Journal of biological chemistry* **264**: 9126-9128.

Franca-Koh, J., Y. Kamimura & P. Devreotes, (2006) Navigating signaling networks: chemotaxis in Dictyostelium discoideum. *Current Opinion in Genetics & Development* **16**: 333-338.

Friedl, P. & D. Gilmour, (2009) Collective cell migration in morphogenesis, regeneration and cancer. *Nat Rev Mol Cell Biol* **10**: 445-457.

Friedl, P. & B. Weigelin, (2008) Interstitial leukocyte migration and immune function. *Nature immunology* **9**: 960-969.

Funamoto, S., R. Meili, S. Lee, L. Parry & R. A. Firtel, (2002) Spatial and temporal regulation of 3-phosphoinositides by PI 3-kinase and PTEN mediates chemotaxis. *Cell* **109**: 611-623.

Gamba, A., A. de Candia, S. Di Talia, A. Coniglio, F. Bussolino & G. Serini, (2005) Diffusion-limited phase separation in eukaryotic chemotaxis. *Proc Natl Acad Sci U S A* **102**: 16927-16932.

Gartner, A., A. Jovanovic, D. I. Jeoung, S. Bourlat, F. R. Cross & G. Ammerer, (1998) Pheromone-dependent G1 cell cycle arrest requires Far1 phosphorylation, but may not involve inhibition of Cdc28-Cln2 kinase, in vivo. *Molecular and cellular biology* **18**: 3681-3691.

Ghaemmaghami, S., W. K. Huh, K. Bower, R. W. Howson, A. Belle, N. Dephoure, E. K. O'Shea & J. S. Weissman, (2003) Global analysis of protein expression in yeast. *Nature* **425**: 737-741.

Gierer, A. & H. Meinhardt, (1972) A theory of biological pattern formation. *Kybernetik* **12**: 30-39.

Gietz, R. D. & A. Sugino, (1988) New yeast-Escherichia coli shuttle vectors constructed with in vitro mutagenized yeast genes lacking six-base pair restriction sites. *Gene* **74**: 527-534.

Gordon, A., A. Colman-Lerner, T. E. Chin, K. R. Benjamin, R. C. Yu & R. Brent, (2007) Single-cell quantification of molecules and rates using open-source microscope-based cytometry. *Nature methods* **4**: 175-181.

Henchoz, S., Y. Chi, B. Catarin, I. Herskowitz, R. J. Deshaies & M. Peter, (1997) Phosphorylation- and ubiquitin-dependent degradation of the cyclin-dependent kinase inhibitor Far1p in budding yeast. *Genes & development* **11**: 3046-3060.

Hicke, L. & H. Riezman, (1996) Ubiquitination of a Yeast Plasma Membrane Receptor Signals Its Ligand-Stimulated Endocytosis. *Cell* **84**: 277-287.

Hicke, L., B. Zanolari & H. Riezman, (1998) Cytoplasmic Tail Phosphorylation of the alpha -Factor Receptor Is Required for Its Ubiquitination and Internalization. *J. Cell Biol.* **141**: 349-358.

Hoeller, O. & R. R. Kay, (2007) Chemotaxis in the Absence of PIP3 Gradients. *Current Biology* **17**: 813-817.

Iglesias, P. A., (2012) Chemoattractant signaling in dictyostelium: adaptation and amplification. *Science signaling* **5**: pe8.

Iijima, M. & P. Devreotes, (2002) Tumor Suppressor PTEN Mediates Sensing of Chemoattractant Gradients. *Cell* **109**: 599-610.

Jackson, C. L. & L. H. Hartwell, (1990) Courtship in S. cerevisiae: Both cell types choose mating partners by responding to the strongest pheromone signal. *Cell* **63**: 1039-1051.

Jackson, C. L., J. B. Konopka & L. H. Hartwell, (1991) S. cerevisiae [alpha] pheromone receptors activate a novel signal transduction pathway for mating partner discrimination. *Cell* **67**: 389-402.

Janetopoulos, C. & R. A. Firtel, (2008) Directional sensing during chemotaxis. *FEBS letters* **582**: 2075-2085.

Janetopoulos, C., T. Jin & P. Devreotes, (2001) Receptor-mediated activation of heterotrimeric G-proteins in living cells. *Science* **291**: 2408-2411.

Janetopoulos, C., L. Ma, P. N. Devreotes & P. A. Iglesias, (2004) Chemoattractant-induced phosphatidylinositol 3,4,5-trisphosphate accumulation is spatially amplified and adapts, independent of the actin cytoskeleton. *Proc Natl Acad Sci U S A* **101**: 8951-8956.

Jenness, D. D. & P. Spatrick, (1986) Down regulation of the alpha-factor pheromone receptor in S. cerevisiae. *Cell* **46**: 345-353.

Jin, T., (2011) GPCR-controlled chemotaxis in Dictyostelium discoideum. *Wiley interdisciplinary reviews. Systems biology and medicine* **3**: 717-727.

Jin, T., (2013) Gradient sensing during chemotaxis. *Current opinion in cell biology* **25**: 532-537.

Jin, T., X. Xu & D. Hereld, (2008) Chemotaxis, chemokine receptors and human disease. *Cytokine* **44**: 1-8.

Jin, T., N. Zhang, Y. Long, C. A. Parent & P. N. Devreotes, (2000) Localization of the G Protein Î²Î³ Complex in Living Cells during Chemotaxis. *Science* **287**: 1034-1036.

Jose, M., S. Tollis, D. Nair, J. B. Sibarita & D. McCusker, (2013) Robust polarity establishment occurs via an endocytosis-based cortical corralling mechanism. *The Journal of cell biology* **200**: 407-418.

Kamimura, Y. & P. N. Devreotes, (2010) Phosphoinositide-dependent protein kinase (PDK) activity regulates phosphatidylinositol 3,4,5-trisphosphate-dependent and -independent protein kinase B activation and chemotaxis. *The Journal of biological chemistry* **285**: 7938-7946.

Kamimura, Y., Y. Xiong, P. A. Iglesias, O. Hoeller, P. Bolourani & P. N. Devreotes, (2008) PIP3-independent activation of TorC2 and PKB at the cell's leading edge mediates chemotaxis. *Current biology : CB* **18**: 1034-1043.

Kavelaars, A., A. Vroon, R. P. Raatgever, A. M. Fong, R. T. Premont, D. D. Patel, R. J. Lefkowitz & C. J. Heijnen, (2003) Increased acute inflammation, leukotriene B4-induced chemotaxis, and signaling in mice deficient for G protein-coupled receptor kinase 6. *J Immunol* **171**: 6128-6134.

Kedrin, D., J. van Rheenen, L. Hernandez, J. Condeelis & J. E. Segall, (2007) Cell motility and cytoskeletal regulation in invasion and metastasis. *Journal of mammary gland biology and neoplasia* **12**: 143-152.

Koizumi, K., S. Hojo, T. Akashi, K. Yasumoto & I. Saiki, (2007) Chemokine receptors in cancer metastasis and cancer cell-derived chemokines in host immune response. *Cancer science* **98**: 1652-1658.

Krishnan, J. & P. A. Iglesias, (2004) A modeling framework describing the enzyme regulation of membrane lipids underlying gradient perception in Dictyostelium cells. *Journal of theoretical biology* **229**: 85-99.

Laird, D. J., U. H. von Andrian & A. J. Wagers, (2008) Stem cell trafficking in tissue development, growth, and disease. *Cell* **132**: 612-630.

Levine, H., D. A. Kessler & W. J. Rappel, (2006) Directional sensing in eukaryotic chemotaxis: a balanced inactivation model. *Proc Natl Acad Sci U S A* **103**: 9761-9766.

Li, E., M. J. Cismowski & D. E. Stone, (1998) Phosphorylation of the pheromone-responsive Gbeta protein of Saccharomyces cerevisiae does not affect its mating-specific signaling function. *Molecular & general genetics : MGG* **258**: 608-618.

Lohof, A. M., M. Quillan, Y. Dan & M. M. Poo, (1992) Asymmetric modulation of cytosolic cAMP activity induces growth cone turning. *J. Neurosci.* **12**: 1253-1261.

Ma, L., C. Janetopoulos, L. Yang, P. N. Devreotes & P. A. Iglesias, (2004) Two complementary, local excitation, global inhibition mechanisms acting in parallel can explain the chemoattractant-induced regulation of PI(3,4,5)P3 response in dictyostelium cells. *Biophysical journal* **87**: 3764-3774.

Maeder, C. I., M. A. Hink, A. Kinkhabwala, R. Mayr, P. I. Bastiaens & M. Knop, (2007) Spatial regulation of Fus3 MAP kinase activity through a reaction-diffusion mechanism in yeast pheromone signalling. *Nat Cell Biol* **9**: 1319-1326.

Marco, E., R. Wedlich-Soldner, R. Li, S. J. Altschuler & L. F. Wu, (2007) Endocytosis optimizes the dynamic localization of membrane proteins that regulate cortical polarity. *Cell* **129**: 411-422.

Mato, J. M., A. Losada, N. Vidyanand & T. M. Konijn, (1975) Signal Input for a Chemotactic Response in the Cellular Slime Mold Dictyostelium discoideum. *Proceedings of the National Academy of Sciences of the United States of America* **72**: 4991-4993.

Meggio, F., A. Donella-Deana & L. A. Pinna, (1979) Studies on the structural requirements of a microsomal cAMP-independent protein kinase. *FEBS letters* **106**: 76-80.

Meier-Schellersheim, M., X. Xu, B. Angermann, E. J. Kunkel, T. Jin & R. N. Germain, (2006) Key role of local regulation in chemosensing revealed by a new molecular interaction-based modeling method. *PLoS computational biology* **2**: e82.

Meinhardt, H., (1982) *Models of biological pattern formation*. Academic Press London.

Meinhardt, H., (1999) Orientation of chemotactic cells and growth cones: models and mechanisms. *J Cell Sci* **112 (Pt 17)**: 2867-2874.

Meinhardt, H. & A. Gierer, (1974) Applications of a theory of biological pattern formation based on lateral inhibition. *J Cell Sci* **15**: 321-346.

Metodiev, M. V., (2011) Applications of nanoscale liquid chromatography coupled to Tandem mass spectrometry in quantitative studies of protein expression, protein-protein interaction, and protein phosphorylation. *Methods Mol Biol* **790**: 99-113.

Metodiev, M. V., D. Matheos, M. D. Rose & D. E. Stone, (2002) Regulation of MAPK Function by Direct Interaction with the Mating-Specific Galpha in Yeast. *Science* **296**: 1483-1486.

Metodieva, G., N. C. Nogueira-de-Souza, C. Greenwood, K. Al-Janabi, L. Leng, R. Bucala & M. V. Metodiev, (2013) CD74-dependent deregulation of the tumor suppressor scribble in human epithelial and breast cancer cells. *Neoplasia* **15**: 660-668.

Mogilner, A., J. Allard & R. Wollman, (2012) Cell polarity: quantitative modeling as a tool in cell biology. *Science* **336**: 175-179.

Moore, T. I., C. S. Chou, Q. Nie, N. L. Jeon & T. M. Yi, (2008) Robust Spatial Sensing of Mating Pheromone Gradients by Yeast Cells. *PloS one* **3**.

Muller, A., B. Homey, H. Soto, N. Ge, D. Catron, M. E. Buchanan, T. McClanahan, E. Murphy, W. Yuan, S. N. Wagner, J. L. Barrera, A. Mohar, E. Verastegui & A. Zlotnik, (2001) Involvement of chemokine receptors in breast cancer metastasis. *Nature* **410**: 50-56.

Murphy, P. M., (2001) Chemokines and the molecular basis of cancer metastasis. *The New England journal of medicine* **345**: 833-835.

Nern, A. & R. A. Arkowitz, (1999) A Cdc24p-Far1p-Gbeta gamma Protein Complex Required for Yeast Orientation during Mating. *J. Cell Biol.* **144**: 1187-1202.

Nishikimi, A., H. Fukuhara, W. Su, T. Hongu, S. Takasuga, H. Mihara, Q. Cao, F. Sanematsu, M. Kanai, H. Hasegawa, Y. Tanaka, M. Shibasaki, Y. Kanaho, T. Sasaki, M. A. Frohman & Y. Fukui, (2009) Sequential regulation of DOCK2 dynamics by two phospholipids during neutrophil chemotaxis. *Science* **324**: 384-387.

Nishio, M., K. Watanabe, J. Sasaki, C. Taya, S. Takasuga, R. Iizuka, T. Balla, M. Yamazaki, H. Watanabe, R. Itoh, S. Kuroda, Y. Horie, I. Forster, T. W. Mak, H. Yonekawa, J. M. Penninger, Y. Kanaho, A. Suzuki & T. Sasaki, (2007) Control of cell polarity and motility by the PtdIns(3,4,5)P3 phosphatase SHIP1. *Nat Cell Biol* **9**: 36-44.

Overton, M. C. & K. J. Blumer, (2000) G-protein-coupled receptors function as oligomers in vivo. *Current biology : CB* **10**: 341-344.

Paquin, N., M. Menade, G. Poirier, D. Donato, E. Drouet & P. Chartrand, (2007) Local activation of yeast ASH1 mRNA translation through phosphorylation of Khd1p by the casein kinase Yck1p. *Mol Cell* **26**: 795-809.

Parent, C. A., B. J. Blacklock, W. M. Froehlich, D. B. Murphy & P. N. Devreotes, (1998) G Protein Signaling Events Are Activated at the Leading Edge of Chemotactic Cells. *Cell* **95**: 81-91.

Park, H. O., E. Bi, J. R. Pringle & I. Herskowitz, (1997) Two active states of the Ras-related Bud1/Rsr1 protein bind to different effectors to determine yeast cell polarity. *Proc Natl Acad Sci U S A* **94**: 4463-4468.

Postma, M. & P. J. Van Haastert, (2001) A diffusion-translocation model for gradient sensing by chemotactic cells. *Biophysical journal* **81**: 1314-1323.

Pruyne, D. & A. Bretscher, (2000a) Polarization of cell growth in yeast. *J Cell Sci* **113**: 571-585.

Pruyne, D. & A. Bretscher, (2000b) Polarization of cell growth in yeast. I. Establishment and maintenance of polarity states. *J Cell Sci* **113**: 365-375.

Remy, I., A. Montmarquette & S. W. Michnick, (2004) PKB/Akt modulates TGF-beta signalling through a direct interaction with Smad3. *Nat Cell Biol* **6**: 358-365.

Reneke, J. E., K. J. Blumer, W. E. Courchesne & J. Thorner, (1988) The carboxy-terminal segment of the yeast [alpha]-factor receptor is a regulatory domain. *Cell* **55**: 221-234.

Ross, E. M. & T. M. Wilkie, (2000) GTPase-activating proteins for heterotrimeric G proteins: regulators of G protein signaling (RGS) and RGS-like proteins. *Annual review of biochemistry* **69**: 795-827.

Rubel, E. W. & K. S. Cramer, (2002) Choosing axonal real estate: location, location, location. *The Journal of comparative neurology* **448**: 1-5.

Sahin, A., B. Daignan-Fornier & I. Sagot, (2008) Polarized growth in the absence of F-actin in Saccharomyces cerevisiae exiting quiescence. *PloS one* **3**: e2556.

Sasaki, A. T., C. Chun, K. Takeda & R. A. Firtel, (2004) Localized Ras signaling at the leading edge regulates PI3K, cell polarity, and directional cell movement. *The Journal of cell biology* **167**: 505-518.

Sasaki, A. T. & R. A. Firtel, (2005) Finding the way: directional sensing and cell polarization through Ras signalling. *Novartis Foundation symposium* **269**: 73-87; discussion 87-91, 223-230.

Sasaki, A. T. & R. A. Firtel, (2006) Regulation of chemotaxis by the orchestrated activation of Ras, PI3K, and TOR. *European journal of cell biology* **85**: 873-895.

Schandel, K. A. & D. D. Jenness, (1994) Direct evidence for ligand-induced internalization of the yeast alpha-factor pheromone receptor. *Mol. Cell. Biol.* **14**: 7245-7255.

Segall, J. E., (1993) Polarization of Yeast Cells in Spatial Gradients of {alpha} Mating Factor. *Proceedings of the National Academy of Sciences* **90**: 8332-8336.

Serge, A., S. de Keijzer, F. Van Hemert, M. R. Hickman, D. Hereld, H. P. Spaink, T. Schmidt & B. E. Snaar-Jagalska, (2011) Quantification of GPCR internalization by single-molecule microscopy in living cells. *Integrative biology : quantitative biosciences from nano to macro* **3**: 675-683.

Servant, G., O. D. Weiner, P. Herzmark, T. Balla, aacute, J. W. Sedat & H. R. Bourne, (2000) Polarization of Chemoattractant Receptor Signaling During Neutrophil Chemotaxis. *Science* **287**: 1037-1040.

Singh, S., Anguaraj Sadanandam and Rakesh K. Singh, (2007) Chemokines in tumor angiogenesis and metastasis. *Cancer and Metastasis Reviews* **26**: 453-467.

Skupsky, R., W. Losert & R. J. Nossal, (2005) Distinguishing modes of eukaryotic gradient sensing. *Biophysical journal* **89**: 2806-2823.

Slaughter, B. D., A. Das, J. W. Schwartz, B. Rubinstein & R. Li, (2009) Dual modes of cdc42 recycling fine-tune polarized morphogenesis. *Dev Cell* **17**: 823-835.

Suchkov, D. V., R. DeFlorio, E. Draper, A. Ismael, M. Sukumar, R. Arkowitz & D. E. Stone, (2010) Polarization of the yeast pheromone receptor requires its internalization but not actin-dependent secretion. *Molecular biology of the cell* **21**: 1737-1752.

Toshima, J. Y., J. Toshima, M. Kaksonen, A. C. Martin, D. S. King & D. G. Drubin, (2006) Spatial dynamics of receptor-mediated endocytic trafficking in budding yeast revealed by using fluorescent alpha-factor derivatives. *Proc Natl Acad Sci U S A* **103**: 5793-5798.

Turing, A. M., (1990) The chemical basis of morphogenesis. 1953. *Bulletin of mathematical biology* **52**: 153-197; discussion 119-152.

Ueda, M., Y. Sako, T. Tanaka, P. Devreotes & T. Yanagida, (2001) Single-molecule analysis of chemotactic signaling in Dictyostelium cells. *Science* **294**: 864-867.

Valdez-Taubas, J. & H. R. Pelham, (2003) Slow diffusion of proteins in the yeast plasma membrane allows polarity to be maintained by endocytic cycling. *Current biology : CB* **13**: 1636-1640.

Vallier, L., Jeffrey E. Segall Michael Snyder, (2002) The alpha-factor receptor C-terminus is important for mating projection formation and orientation in <I>Saccharomyces cerevisiae</I>. *Cell Motility and the Cytoskeleton* **53**: 251-266.

Van Haastert, P. J., (1987) Down-regulation of cell surface cyclic AMP receptors and desensitization of cyclic AMP-stimulated adenylate cyclase by cyclic AMP in Dictyostelium discoideum. Kinetics and concentration dependence. *The Journal of biological chemistry* **262**: 7700-7704.

Van Haastert, P. J. M. & P. N. Devreotes, (2004) Chemotaxis: signalling the way forward. *Nat Rev Mol Cell Biol* **5**: 626-634.

Velazquez-Campoy, A., H. Ohtaka, A. Nezami, S. Muzammil & E. Freire, (2004) Isothermal titration calorimetry. *Current protocols in cell biology / editorial board, Juan S. Bonifacino ... [et al.]* **Chapter 17**: Unit 17 18.

Vernay, A., S. Schaub, I. Guillas, M. Bassilana & R. A. Arkowitz, (2012) A steep phosphoinositide bis-phosphate gradient forms during fungal filamentous growth. *The Journal of cell biology* **198**: 711-730.

Wang, F., (2009) The signaling mechanisms underlying cell polarity and chemotaxis. *Cold Spring Harbor perspectives in biology* **1**: a002980.

Wang, Y., C. L. Chen & M. Iijima, (2011) Signaling mechanisms for chemotaxis. *Development, growth & differentiation* **53**: 495-502.

Weiner, O. D., P. O. Neilsen, G. D. Prestwich, M. W. Kirschner, L. C. Cantley & H. R. Bourne, (2002) A PtdInsP3- and Rho GTPase-mediated positive feedback loop regulates neutrophil polarity. *Nat Cell Biol* **4**: 509-513.

Weiss, K., A. Neef, Q. Van, S. Kramer, I. Gregor & J. Enderlein, (2013) Quantifying the diffusion of membrane proteins and peptides in black lipid membranes with 2-focus fluorescence correlation spectroscopy. *Biophysical journal* **105**: 455-462.

Wong, W., (2012) Focus issue: a cell's sense of direction. *Science signaling* **5**: eg3.

Xiao, Z., N. Zhang, D. B. Murphy & P. N. Devreotes, (1997) Dynamic Distribution of Chemoattractant Receptors in Living Cells During Chemotaxis and Persistent Stimulation. *J. Cell Biol.* **139**: 365-374.

Xu, J., F. Wang, A. Van Keymeulen, P. Herzmark, A. Straight, K. Kelly, Y. Takuwa, N. Sugimoto, T. Mitchison & H. R. Bourne, (2003) Divergent signals and cytoskeletal assemblies regulate self-organizing polarity in neutrophils. *Cell* **114**: 201-214.

Xu, X., M. Meier-Schellersheim, X. Jiao, L. E. Nelson & T. Jin, (2005) Quantitative imaging of single live cells reveals spatiotemporal dynamics of multistep signaling events of chemoattractant gradient sensing in Dictyostelium. *Molecular biology of the cell* **16**: 676-688.

Yesilaltay, A. & D. D. Jenness, (2000) Homo-oligomeric complexes of the yeast alpha-factor pheromone receptor are functional units of endocytosis. *Molecular biology of the cell* **11**: 2873-2884.

Yi, T.-M., S. Chen, C.-S. Chou & Q. Nie, (2007) Modeling Yeast Cell Polarization Induced by Pheromone Gradients. *Journal of statistical physics* **128**: 193-207.

Zigmond, S. H., (1977) Ability of polymorphonuclear leukocytes to orient in gradients of chemotactic factors. *J. Cell Biol.* **75**: 606-616.

VITA

NAME: Amber Ismael

EDUCATION: B.S. Biology, University of California, Irvine, Irvine, California, 2004

Ph.D. Biology, University of Illinois at Chicago, Chicago, Illinois, 2014

TEACHING EXPERIENCE: Mendelian and Molecular Genetics, Discussion
Department of Biological Sciences
University of Illinois at Chicago, Chicago, Illinois

Mendelian and Molecular Genetics, Laboratory
Department of Biological Sciences
University of Illinois at Chicago, Chicago, Illinois

Molecular Biology, Laboratory
Department of Biological Sciences
University of Illinois at Chicago, Chicago, Illinois

ABSTRACTS: Yeast Genetics and Molecular Biology Meeting. Toronto, Canada, 2008. Poster presentation: Establishment of receptor polarity.

Yeast Genetics and Molecular Biology Meeting. Vancouver, Canada, 2010. Platform presentation: Receptor phosphorylation and polarization are regulated by Gβ interaction with Yck1.

Cold Spring Harbor Yeast Meeting. Cold Spring Harbor, NY, 2011. Poster presentation: Receptor phosphorylation and polarization are regulated by Gβ interaction with Yck1.

Midwest Yeast Meeting – Northwestern University. Evanston, IL, 2011. Platform presentation: Receptor phosphorylation and polarization are regulated by Gβ interaction with Yck1.

Chicago Symposium on Cell Signaling – Northwestern University. Chicago, IL, 2012. Poster presentation: Receptor phosphorylation and polarization are regulated by Gβ interaction with Yck1.

American Society for Cell Biology Annual Meeting. San Francisco, CA, 2012. Poster presentation: Receptor phosphorylation and polarization are regulated by Gβ interaction with Yck1.

Chicago Symposium on Cell Signaling – Northwestern University. Chicago, IL, 2013. Poster presentation: Receptor phosphorylation and polarization are regulated by Gβ interaction with Yck1.

American Society for Cell Biology Annual Meeting. New Orleans, LA, 2013. Poster presentation: Gβ promotes polarization of the pheromone receptor by inhibiting its phosphorylation.

Chicago Symposium on Cell Signaling – Northwestern University. Chicago, IL, 2014. Poster presentation: Gβ promotes polarization of the pheromone receptor by inhibiting its phosphorylation.

PUBLICATIONS: Suchkov D, DeFlorio R, Draper E, Ismael A, Sukumar M, Arkowitz R, Stone D (2010) Polarization of the yeast pheromone receptor requires its internalization but not actin-dependent secretion. *Mol. Biol. Cell* **21**: 1737-1752